ENHANCEMENT OF THE RESPONSE RANGE AND LONGEVITY OF MICROPARTICLE-BASED GLUCOSE SENSORS

A Dissertation

by

SAURABH SINGH

Submitted to the Office of Graduate Studies of
Texas A&M University
in partial fulfillment of the requirements for the degree of

DOCTOR OF PHILOSPHY

May 2010

Major Subject: Biomedical Engineering

ENHANCEMENT OF THE RESPONSE RANGE AND LONGEVITY OF MICROPARTICLE-BASED GLUCOSE SENSORS

A Dissertation

by

SAURABH SINGH

Submitted to the Office of Graduate Studies of
Texas A&M University
in partial fulfillment of the requirements for the degree of

DOCTOR OF PHILOSPHY

Approved by:

Chair of Committee,	Michael J. McShane
Committee Members,	Jaime C. Grunlan
	Melissa A. Grunlan
	Kenith E. Meissner
Head of Department,	Gerard L. Cote'

May 2010

Major Subject: Biomedical Engineering

ABSTRACT

Enhancement of the Response Range and Longevity of Microparticle-Based Glucose Sensors. (May 2010)

Saurabh Singh, B.E., Pandit Ravishankar Shukla University;

M.S., Louisiana Tech University

Chair of Advisory Committee: Dr. Michael J. McShane

Luminescent microspheres encapsulating glucose oxidase and an oxygen-sensitive lumophore have recently been reported as potential implantable sensors for *in vivo* glucose monitoring. However, there are two main issues that must be addressed for enzymatic systems such as these to realize the goal of minimally-invasive glucose monitoring. The first issue is related to the short response range of such sensors, less than 200 mg/dL, which must be extended to cover the full physiological range (0-600 mg/dL) of glucose possible for diabetics. The second issue is concerning the short operating lifetime of these systems due to enzyme degradation (less than 7 days).

Two approaches were considered for increasing the range of the sensor response; nanofilm coatings and particle porosity. In the first approach, microparticle sensors were coated with layer-by-layer deposited thin nanofilms to increase the response range. It was observed that, a precise control on the response range of such sensors can be achieved by manipulating different characteristics (e.g., thickness, deposition condition, and the outermost capping layer) of the nanofilms. However, even with 15 bilayers of

poly(allylamine hydrochloride)/poly(styrene sulfonate) (PAH/PSS) nanofilm, limited range was achieved (less than 200 mg/dL). By performing extrapolation on the data obtained for the experimentally-determined response range versus the number of PAH/PSS bilayers, it was predicted that a nanofilm coating comprising of more than 60 PAH/PSS bilayers will be needed to achieve a linear response up to 600 mg/dL.

Using modeling, it was realized that a more effective method for achieving a linear response up to 600 mg/dL is to employ microparticles with higher porosity. Sensors were prepared from highly porous silica microparticles (diameter = 7 μm, porosity = 0.6) and their experimental response was determined. Not surprisingly, the experimentally determined response range of such sensors was found to be higher than 600 mg/dL.

To improve the longevity of these sensors, two approaches were employed; incorporation of catalase and increasing the loading of glucose oxidase. Catalase was incorporated into microparticles, which protects the enzyme from peroxide-mediated deactivation, and thus improves the stability of such sensors. Sensors incorporating catalase were found to ~5 times more stable than the GOx-only sensors. It was theoretically predicted, that by maximizing the loading of glucose oxidase within the microparticles, the longevity of such sensors can be substantially improved. Based on this understanding, sensors were fabricated using highly porous microparticles; response range did not vary even after one month of continuous operation under normal physiological conditions. Modeling predicts that 1 mM of glucose oxidase and 1 mM of catalase would extend the operating lifetime to more than 90 days.

TABLE OF CONTENTS

Page

Page

LIST OF FIGURES

Page

Page

LIST OF TABLES

1 INTRODUCTION

A disease is an abnormal condition in which normal bodily functions are impaired. Most often diseases are manifested in the form of biochemical imbalances. In such cases, concentrations of biochemicals present in the body can be used as an indicator of the disease. Some prime examples of such biochemicals are: (1) lactate, which is a key metabolite of the anaerobic glycolytic pathway, is constantly present in excess levels in patients suffering through ischemic conditions; (2) cholesterol, which is needed for building and maintaining of membranes, is generally observed in elevated levels in people suffering from atherosclerosis; (3) oxygen, the lack of which may indicate severe pneumonia, asthama, or other conditions; (4) glucose, whose imbalances are manifested in diabetics. For the diagnosis and management of such medical conditions, the development of sensing techniques that can result in a simple and accurate detection of biochemicals is becoming a medical priority.

Resulting from the serious drive for the development of such technologies, highly-sensitive enzyme-based sensors for these analytes (e.g., lactate, cholesterol, and glucose) have already been developed. These employ oxidoreductase enzymes, which catalyze the oxidation of such analytes in the presence of oxygen (e.g., lactate oxidase, cholesterol oxidase, glucose oxidase).[1-3] The oxygen level in the proximity of the enzyme, which is inversely related to the analyte concentration, is amperometrically detected via Clark type electrode. Thus, it can be observed that by mere switching of oxidoreductase enzyme it is possible to develop biosensors for different analytes.

This dissertation follows the style of *Analytical Chemistry*.

In this dissertation, the effort has been towards the development of a platform technology that can be used for the development of biosensors for different analytes. A prime example of a clinical need to such devices can be found in diabetes, where frequent monitoring of glucose is required for the proper management of disease. Glucose was chosen as a model analyte for which a biosensor has been developed, however, the same concept can be used for the development of biosensors for a different analyte for which oxidoreductase enzyme is known to exist.

Diabetes affects more than 20 million Americans (7%) and nearly 250 million persons worldwide in its two primary types (Type I "insulin-dependent": ~10%; Type II "insulin-resistant": ~90%), resulting in a huge economic and social burden on society.[4,5] To date there is no cure for this disease. Complications such as cardiovascular disease, stroke, hypertension, retinopathy, nephropathy, neuropathy, periodontis, gingivitis, and cataract formation are common and tend to develop with time. Clinical trials have shown that proper care and management of blood glucose levels are critical in delaying the progression of complications in both types. Therefore, diabetics share a common need of continuously monitoring and subsequently restoring their blood glucose level to euglycemic range, which is the normal glucose range (80–120 mg/dL), by injecting insulin.

The "finger-prick" test is considered as the gold-standard for the self-monitoring of blood glucose levels. The blood sample extracted by lancing the skin is placed in a portable device to determine glucose concentration using disposable test strips. Although this being a reliable method for the self-monitoring of glucose, diabetics fail to adhere to

the recommended testing frequency and cite excessive pain and inconvenience as the principal reasons for lack of compliance. Therefore, *there is an urgent necessity of a minimally invasive continuous glucose monitoring system that can assist diabetics and their physicians in making appropriate decisions regarding insulin therapy.*

To assist diabetics in managing glycemia, continuous glucose monitoring systems (CGMS) have been recently developed. CGMS based on highly selective enzyme electrodes are commercially available, such as Medtronic's Guardian® RT, DexCom's STS® Seven System, and Abbott Laboratories' FreeStyle™ Navigator, giving patients real-time access to glycemic trends. Such sensors are inserted through the skin, much like an infusion set used to deliver insulin from a pump.[6] While these systems represent major advances in technology for diabetes care, they still suffer from serious drawbacks such as poor stability/longevity (up to 7 days), a potential infection pathway resulting from the percutaneous insertion, slow response due to the macroscopic dimensions of the electrode, susceptibility to electromagnetic interference, and particularly impaired responses and unpredictable drift in the signal necessitating frequent calibration.[7,8] Such issues with these devices will plague any similar technology and, therefore, present barriers to adoption. In addition, these devices are not designed to fully replace blood-draw measurements, but are marketed as a means to track blood glucose trends. The wide variability in sensor performance within same and among different human subjects is another hurdle that must be overcome to make CGMS standard glucose monitoring devices.

In addition to commercially-available CGMS, non-invasive glucose analysis methods based on optical phenomena such as absorbance spectroscopy [9], Raman spectroscopy,[10] and polarimetry [11] have also been investigated as attractive alternatives. However, these techniques lack selectivity and also exhibit poor sensitivity, which makes them unreliable for accurate glucose predictions. Recently, sensors based on surface-enhanced raman spectroscopy (SERS), which is a near infrared (NIR) spectroscopy, have been proposed for minimally-invasive glucose monitoring.[10] Such sensors exhibit superior sensitivity and specificity compared to many other optical techniques for glucose detection. The sensors were shown to be stable up to 11 days when continuously used for glucose measurements. However, the long-term stability of such sensors must be investigated to determine their potential for *in vivo* glucose monitoring.

To overcome the problems associated with the abovementioned sensing techniques, an ideal approach would be to use optical "readout" to monitor a selective interaction between an implanted specific receptor and glucose.[12] Two possibilities have recently been reported for this by McShane et. al, both of which are based on the encapsulation or the immobilization of sensing chemistry inside microcapsules/microspheres that can be implanted in the dermis. The selective interaction between glucose and the immobilized specific receptor can be optically interrogated using luminescence techniques. Such systems have also been termed as "smart-tattoo."[12] The first possibility is to use a competitive binding assay for glucose monitoring.[13,14] In this, a glucose receptor (e.g., concanavalin A or apo-GOx) and a

competitive ligand (dextran), which can compete with glucose to bind to the receptor, are encapsulated inside microcapsules. In one prototype, apo-GOx was used as a receptor and was labeled with a fluorescence resonance energy transfer (FRET) donor and the competitive ligand was labeled with a FRET acceptor.[14] The extent of the non-radiative energy transfer occurring between the donor and the quencher thus depended on the glucose concentration. An increase in fluorescence emission intensity was observed from the sensors with increasing glucose concentration. Nevertheless, the long term stability of receptors is questionable and the stability of response of such sensors must be investigated to determine their potential for *in vivo* application.

Another possibility for "smart-tattoo" systems have been reported in the form of enzymatic luminescent microspheres.[15-20] Prototypes consist of microspheres loaded with an oxygen-sensitive luminescent indicator and an oxido-reductase enzyme, which catalyzes the oxidation of glucose to gluconic acid. The reaction results in reduced oxygen levels within the microspheres, in direct proportion to the glucose concentration in the surrounding fluid. The indicator dye then transduces the average oxygen concentration, which is inversely proportional to the glucose concentration of the surrounding fluid, to the luminescence intensity or lifetime.

Enzymatic microparticle-based glucose sensors have been shown to exhibit an excellent sensitivity (4.16%/mg/dL).[18] In addition, the response range and sensitivity of such sensors can be fine-tuned. These attributes make the microparticle-based sensing to be a very promising approach for *in vivo* monitoring of glucose.

While a microparticle-based glucose monitoring approach is very promising there are two main issues that must be addressed: first, the *response range* of such sensors must be such that it covers the entire physiological glucose range (0-600 mg/dL); second, the *longevity* of these microsphere-based sensors must be investigated to determine the viability of this sensing approach for long-term *in vivo* glucose monitoring. This dissertation focuses on addressing these two issues. The goals are to extend the response range of sensors up to 600 mg/dl and to enhance the longevity of sensors so that they remain operational up to ~3 months when exposed to physiological conditions. The response range of sensors will be extended by tuning the mass transport properties of sensors to substrates, glucose and oxygen. The longevity of sensors will be increased by achieving an increased concentration of immobilized GOx and by co-immobilizing catalase (CAT) and GOx in the sensor matrix.

The sections in this dissertation are organized to present the disseminated material in a clear and logical manner. Section 2 begins with a short description on fluorescence quenching. Subsequently, it provides a detailed description of previous prototypes of enzymatic microparticle probes. In addition, it also provides a thorough background to the problems of enzymatic glucose sensors, focusing on the issues of mass transport, enzyme kinetics, and enzyme deactivation that are critical to sensor performance and operational stability. The theory involved in the modeling of the response of enzymatic microparticle-based glucose sensors is surveyed in Section 3. The reaction-diffusion theory and the reaction and deactivation kinetics of enzyme, which will be used to predict the response and stability of sensors via mathematical modeling,

are discussed. Methods and instrumentation used to experimentally determine the response of sensors are described in Section 4. The tuning of sensitivity and response range by modulating the thickness and other characteristics of mass transport limiting films is presented in Section 5. Some of the results and the associated methods presented in this section were published in *Analytical Chemistry*.[19] In Section 6, the role of porosity of microparticle in determining the response of microparticle-based sensors is presented. Section 7 is dedicated to a study of the enhancement of the longevity of sensors using co-immobilization of CAT. The results and associated methods in this section were published in *Biosensors and Bioelectronics*.[21] Finally, conclusions are drawn and future work is proposed in section 8 that can aid in advancing this technology to the next level of long term *in vivo* studies. It is noteworthy that much of the content of this dissertation has been presented at professional meetings and has been published or submitted for publication in peer-reviewed journals.

2 BACKGROUND

Enzymatic sensors rely on the glucose concentration-dependent depletion of local oxygen, enabling the indirect optical monitoring of glucose via measurement of local oxygen levels using an oxygen-sensitive indicator dye. An ideal glucose sensor will be expected to exhibit high sensitivity and cover the entire clinical range of 40-600 mg/dL for *in vivo* monitoring.[18] To achieve the desired performance, the mass transport and enzyme kinetics must be properly designed. Furthermore, the reaction involves production of byproducts that can damage the enzyme and thereby reduce the life of sensors. Consequently, the sensors must also be properly designed to achieve stable operation. All of this involves materials–the particles, the enzyme and dye components, cross-linkers, the coatings–as well the processes required to assemble them.

This section begins with a short background on oxygen sensing using luminescent probes. After introducing the key concepts of oxygen sensing, a thorough literature review on enzymatic microparticle-based glucose sensors is provided. The review will highlight the major advances in microparticle-based glucose monitoring systems and the shortcomings that must be addressed to successfully apply such sensors for *in vivo* glucose monitoring. In addition, issues related to mass transport, enzyme kinetics, and enzyme deactivation, which are critical to sensor performance and enzyme stability will be also discussed in context.

2.1 Oxygen Sensing

Oxygen is a well-known quencher of luminescence. However, there are only a limited number of dyes that undergo significant quenching to make them useful as oxygen indicators. A variety of indicators have been used for oxygen sensing. A few of them are:[22]

Polycyclic aromatic hydrocarbons: pyrene, pyrenebutyric acid, fluoranthene, decacyclene, diphenylanthracene and benzo (g,h,i)perylene.

A variety of longwave absorbing dyes and heterocycles: perylene dibutyrate, fluorescent yellow, trypaflavin, and porphyrins.

Metal organic complexes of ruthenium, platinum, and palladium: these have metal to ligand energy transfers and normally have long-lived excited states (up to ~1 ms) which make them useful for life-time based oxygen sensing.[23]

2.1.1 Sensing principles

The luminescence of an indicator is supposed to obey the linear Stern-Volmer equation,

$$\frac{I_0}{I} = 1 + K_{sv} \cdot P_{O_2} \qquad (2.\ 1)$$

where, I_0 and I are the luminescence intensities in the absence and presence of oxygen. K_{sv} is the overall dynamic quenching constant,

$$K_{sv} = k_d \cdot \tau_0 \qquad (2.\ 2)$$

where, k_d is the diffusional bimolecular rate constant, and τ_0 is the natural lifetime of the luminophore. While τ_0 is an intrinsic property of a luminophore, k_d is a combined

property of the luminophore, quencher, and the matrix in which the lumophore is immobilized.[24] As this type of quenching is a dynamic event, involving the collision of dye and oxygen, the process is sometimes called collisional quenching. The above equation may also be written in the lifetime form

$$\frac{\tau_0}{\tau} = 1 + K_{sv} \cdot P_{O_2} \qquad (2.3)$$

where, τ_0 and τ are the decay times of luminophores in the absence and presence of oxygen.

For oxygen in liquid solvents, the P_{O_2} can be replaced by its concentration [O_2], which is related to P_{O_2} by the Henry-Dalton solubility coefficient α, so that Equation 2.3 reads

$$\frac{I_0}{I} = 1 + K_{sv} \cdot \alpha[O_2] \qquad (2.4)$$

It must be noted that K_{sv} is directly proportional to τ_0. In order to obtain high sensitivity, larger values of K_{sv} are desired. Therefore, luminophores with longer natural lifetime are expected to exhibit higher sensitivity towards oxygen.

A typical plot of luminescence intensity versus oxygen concentration as obtained in a luminescence quenching process, and the respective Stern-Volmer plot is show Figure 2.1. In this case, the slope of the blue line represents K_{sv}. Generally, K_{sv} depends on the chemical structure of the lumophore and the solvent medium in which the lumophore is dissolved.[24,25] However, lumophores are often immobilized within a matrix when sensing is the intended application. In such cases, K_{sv} depends on the chemical

structure of the lumophore and the type of the matrix in which the lumophore is immobilized. Conventionally, silicone has been a preferred matrix for the immobilization of oxygen-sensitive lumophores due to its high permeability for oxygen. For a given lumophore immobilized within a silicone matrix, it has been shown that K_{sv} increases with an increase in the plasticity of the matrix. Increased plasticity makes the matrix more flexible, thereby rendering it more permeable to oxygen, which results in an increased K_{sv}.[25]

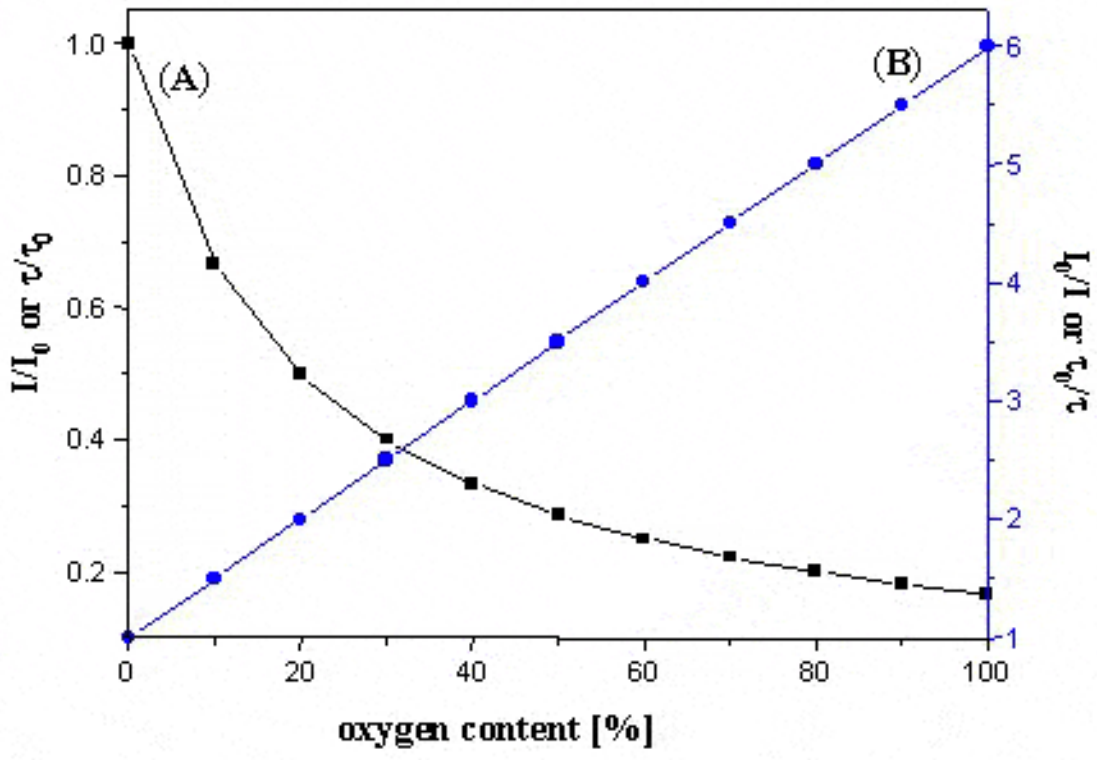

Figure 2.1 (A) Luminescence quenching in the presence of oxygen. (B) Stern-Volmer plot.[26]

2.2 Microparticle-based Glucose Sensors

To the best of the writer's knowledge, Brown et. al. first reported enzymatic microparticle-based sensors for minimally-invasive glucose monitoring.[27] Alginate microspheres with 10-20 μm size were synthesized using (water-in-oil) emulsification method.[28] GOx was immobilized via entrapment during the synthesis of microspheres. Subsequently, an oxygen-sensitive fluorescent dye, ruthenium-tris(4,7-diphenyl-1,10-phenanthroline) dichloride (Ru(dpp), λ_{ex} = 450 nm, λ_{em} = 620 nm, τ_0 = 5.34 μs),[25,29] was immobilized using insolubility-induced precipitation. Ru(dpp) was found to be homogeneously distributed inside the microspheres and no evidence of leaching was found. Finally, GOx- and Ru(dpp)-loaded microspheres were coated with four bilayers of PAH/PSS nanofilm (NF) using the layer-by-layer assembly technique. NFs are perm-selective membranes that have been used to perform the separation of molecules based on their size.[30] It had been previously shown that in NFs the diffusion of big molecules (e.g., sucrose, glucose) can be substantially reduced without significantly affecting the diffusion of small molecules (e.g, methanol, oxygen).[30] NF coatings on microparticles will impose an additional transport barrier to diffusates (glucose and oxygen) that will directly depend on their size. Therefore, it was hypothesized that the use of NF coating will substantially reduce the transport of glucose to the sensor matrix without significantly affecting the transport of oxygen, resulting in an extension of the response range of microparticle-based glucose sensors. The use of LbL NFs as a transport barrier to adjust the sensor response can be considered as a novel application of such films.

In this initial work, the PAH used for first few precursor layers was conjugated to Alexa Fluor® 488 (AF 488), which was used as a reference fluorophore to account for nonspecific signal modulations. Thus, the sensors reported in this work were *ratiometric*. The sensors were suspended in water and aliquots of concentrated glucose solution were added for response measurement at each glucose concentration. The sensors were reported to exhibit a linear response up to 400 mg/dL, after which the response plateaued. The sensors were also found to exhibit a reversible response. Nevertheless, the maximum increase in luminescence signals was reported to be ~7%, which indicate the poor sensitivity of such sensors (Figure 2.2). Also, the confidence in the glucose response measurements was poor due to the movement of sensors during intensity measurements.[27] The standard method of determining the clinical accuracy of self-monitoring blood glucose (SMBG) systems is the Clarke's error grid analysis.[31] In order to make the right therapeutic decisions, the difference between the actual and the SMBG-measured glucose concentration must be less than 20%. For all measurements, it can be observed that the standard deviation was higher than 20%, which suggests that the reading obtained from such sensors are not reliable enough for making clinical decisions.

Computational modeling was also performed to gain better insight into the performance of such sensors (Curve A, Figure 2.2). Theoretically, it was predicted that a decrease in GOx concentration and/or an increase in effective diffusivity of oxygen inside the sensor matrix can result in a linear response up to 600 mg/dL, which is the desired response range for in vivo monitoring of glucose (Curve B, Figure 2.2).

However, none of the theoretical predictions indicated that a substantial improvement in the sensitivity was achievable for these sensor prototypes.

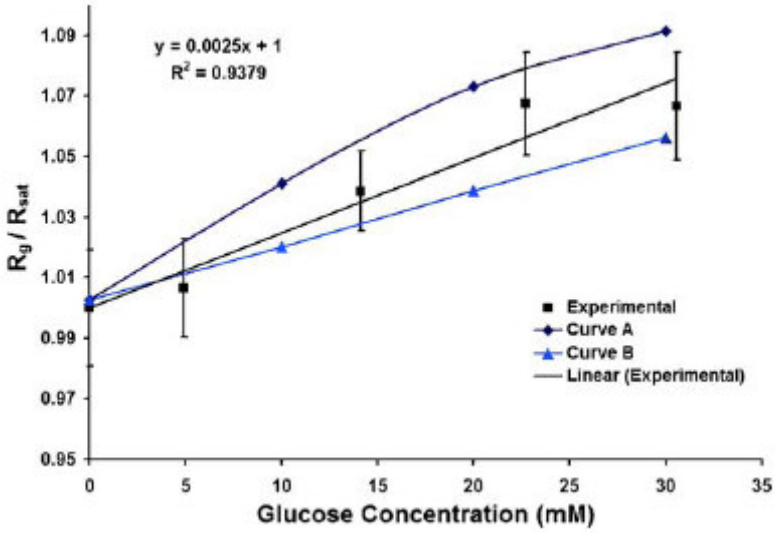

Figure 2.2 Plot of experimentally and theoretically obtained fluorescence peak ratio values.[27]

In a subsequent work, Brown et. al. measured the response of sensors for step changes in glucose concentrations by immobilizing the sensors on the glass slide and placing it inside a custom designed flow-through testing setup.[17] Due to immobilized sensors in this work, the coefficient of variation for each glucose measurement was found to be much smaller than the previous one. Sensor response was measured for random changes in the glucose concentrations up to 160 mg/dL, and the response was found to be linear throughout. However, it would have been interesting to see the response of sensors up to 600 mg/dL, which is the maximum glucose level for accepted

clinical range. In addition, the low sensitivity (*Sensitivity* = 0.018%/mg/dL) of such sensors makes them a poor candidate for making accurate measurements in vivo.

As the enzymatic microparticle-based glucose sensors relied on the reaction-diffusion kinetics of substrate and immobilized enzyme, there were seemingly endless possibilities of tailoring the response of sensors by changing one or a combination of the parameters namely, sphere size, sphere material, enzyme loading, NF thickness, NF material type, and NF deposition conditions. With the advancement that already took place in the field of microparticle synthesis and LbL films, it was possible to have a precise control over several of the abovementioned parameters and thereby tune the response of such sensors.

Brown et. al. made an important contribution towards the development of such sensors by developing a mathematical model that allowed a better understanding of the role of the size of microparticle (diameter) and the thickness of the NF coating on determining the response of such sensors. The model used a quasi-steady-state approximation, which greatly simplified the model from a system of six partial differential equations (PDEs) to a system of two PDEs. It was predicted that the response time of sensors made from alginate microparticles was less than 3 seconds. Such a short response time can be attributed to the microscopic size of the sensors. The increase in the diameter of microspheres was expected to result in an increased sensitivity and a slight increase in the linear response range. In contrast, an increase in the thickness of the NF was predicted to result in a reduced sensitivity with increased response range. It

was estimated that PAH/PSS NFs with a thickness of ~60 nm should result in sensors exhibiting linear response up to 600 mg/dL.

The role of GOx concentration was also investigated and it was predicted that an increase in enzyme concentration will result in an increase in linear response range and reduced sensitivity. These general trends were used to guide further sensor prototyping. It should be noted that one limitation of the modeling approach used is the reliance on the quasi-steady-state approximation, which only holds true when substrate levels exceed enzyme concentration.[32] The oxygen concentration inside the microspheres can range from 0-270 μM, whereas the reported immobilized GOx concentration was 0.5-1 mM. Therefore, the model based on quasi-state-approximation might not yield accurate predictions under the current situation.

Given the low sensitivity of early prototypes employing Ru oxygen indicators, subsequent efforts sought to increase the response by using more sensitive oxygen indicators. Stein et. al. employed platinum(octaethyl porphine) (PtOEP λ_{ex} = 540 nm, λ_{em} = 645 nm, τ_0 = ~90 μs) as an oxygen indicator.[18] As PtOEP is an extremely hydrophobic dye, it was not possible to immobilize it in the alginate matrix. Therefore, custom alginate-silica hybrid microparticles were used in which silica provided the hydrophobic regions for PtOEP immobilization and alginate provided the hydrophilic regions that were suitable for enzyme immobilization. Standard sol-gel process was used for the synthesis of microparticles.[18] The average diameter of alginate-silica microparticles was determined to be 14±3 μm. As natural lifetime of PtOEP is ~30X higher than Ru(dpp), it exhibits a significantly higher sensitivity towards oxygen. GOx was loaded and

covalently attached to the hybrid matrix using EDC/sulfo-NHS covalent attachment.[18] Microparticles loaded with the sensing chemistry were then coated with ten bilayers of PAH/PSS. PAH used for the first three layers was conjugated to rhodamine B isothiocyanate (RITC, λex = 540 nm, λem = 580 nm). RITC emission is nearly insensitive to oxygen concentration and, therefore, was used as a reference luminophore.

Measurement of the response towards oxygen resulted in a linear Stern-Volmer plot, indicating the homogeneous distribution of PtOEP inside the algilica matrix (K_{SV} = 0.0142 μM^{-1}). Uniform immobilization of dye and enzyme was confirmed via images obtained from confocal microscopy.

Glucose response was experimentally determined using a flow-through system controlled via a custom-designed software suite (LabVIEW, National Instruments), The experimentally determined response time was found to be ~86 s, which is more than adequate for monitoring the fluctuations in the blood glucose, which usually occur over a period of 30 min.[33] The sensors exhibited a reversible response with a sensitivity of ~4/mg dL^{-1}, which was at least one order of magnitude greater than what was previously reported for the similar systems. Nevertheless, the analytical range of sensors was determined to be 2-120 mg/dL, which did not cover the entire accepted range of 40-600 mg/dL required for self-testing systems.[34]

In a further exploration of the GOx-PtOEP in algilica matrix, Stein et. al. characterized the effect of the thickness of NF coating on sensor response.[19] Sensors with 5, 10, 15, 20, and 25 bilayers of PAH/PSS were prepared and their response was experimentally determined. Sensors with 5-25 bilayers exhibited a steady increase in

response range and a decrease in sensitivity with increasing film thickness. Sensors coated with 25 PAH/PSS bilayers were found to show a linear response up to ~225 mg/dL. Although adjusting the film thickness was found to be effective in fine tuning the range of sensors, it was realized that extending the linear response range of sensors up to 350 mg/dL will require a NF coating that consists of more than 100 PAH/PSS bilayers. Given that the deposition of each bilayer requires *ca.* 25 minutes, depositing a NF that consists of 100 bilayers will be a very labor intensive and time consuming task. Moreover, microparticles often start aggregating during LbL assembly process after the deposition of certain number of bilayers, which can drastically affect the response of sensors. From the preceding discussion, it can be understood that NFs play a crucial role in the design of microparticle-based glucose sensors. A short survey on LbL deposited NFs will assist the reader in gaining a better understanding on the role NFs in sensor design.

2.3 LbL Assembled Transport Limiting Films

As the response of such sensors relies on the delicate balance between the reaction and mass transport rates of substrates (glucose and oxygen), it will be useful to introduce the reader to the role of layer-by-layer (LbL) assembled ultrathin films in tuning the effective transport of substrates. *While several techniques are available for the formation of NF coating on planar substrates (e.g., spin coating, Langmuir-Blodgett), only the LbL method allows the formation of NF coating on substrates that have complex shapes (e.g, spherical).*[35,36] In addition, LbL assembly technique offers precise control over the film thickness, on the order of *ca.* 1 nm. LbL films are typically

formed by the consecutive immersions of a solid support into solutions containing oppositely charged species to form structures based on the electrostatic attraction between polyelectrolytes.[35] Polycations that have predominantly been used in these structure include: poly(allylamine hydrochloride) (PAH), poly(ethylene imine) (PEI), poly(dimethyldiallylammonium chloride) (PDDA), and poly(lysine) (PLL). The most commonly used polyanions are poly(styrenesulfonate) (PSS), poly(acrylic acid) (PAA), and poly(vinylsulphonate) (PVS). Film properties such as thickness, porosity, and diffusivity can be tailored by using the appropriate combination of polyelectrolytes and by adjusting the polyelectrolyte concentrations, pH of the solutions, and salt concentration.[35,37,38] LbL deposited thin films have been used for a variety of applications including microencapsulation, biosensors, bioreactosr, and separations.[14,20,30,39-41]

For the research presented in this dissertation, literature involving the application of LbL-assembled films for separations are of special interest, as the primary purpose of such films in microparticle-based glucose sensors is to act as a transport barrier. The advantage of PSS, PAH, PEI, and other polyelectrolytes is their flexible conformation, which allows them to deposit even on “defects” of the previously immobilized layer. Due to contiguous formation of the films on the support, the diffusion of macromolecules (e.g., proteins, DNA) can be significantly slowed or completely prevented, while allowing the passage of small molecules (e.g., oxygen, glucose).[42-46]

The transport of gases across LbL assembled thin films has been heavily investigated in the past.[43-45] Stroeve et. al. studied the gas-permeation properties of thin films made by the self-assembly of PAH and PSS on permeable supports; the film consisted of 40 bilayers of PAH/PSS deposited on a porous solid support.[43] Carbon dioxide and nitrogen were used as the model gases in these experiments and diffusion studies were conducted at varying temperatures. It was found that at all temperatures the permeability to carbon dioxide was approximately an order of magnitude higher than that of nitrogen. Higher solubility of CO_2 in hydrophilic polymers accounted for this observation. Levasalmi et. al. studied the diffusion of O_2, N_2, and H_2 across PAH/PSS film deposited on a solid support with carboxylate moieties that imparted negative charge to the porous solid substrate.[45] Different samples consisting of 10, 20, 50, 100, and 200 PAH/PSS bilayers were constructed. The permeability of oxygen was found to be more than an order of magnitude higher than the nitrogen permeability across the film consisting of 40 bilayers of PAH/PSS. This observation was again attributed to the higher solubility of oxygen in hydrophilic polymers when compared to nitrogen. Moreover, an increase in selectivity (O_2/N_2) was observed with an increasing number of PAH/PSS bilayers. The permeability of H_2 was found to be ~8X that of oxygen. As the solubility of hydrogen in hydrophilic polymers is lower than the solubility of oxygen, it is the smaller size of the molecule that was responsible for the increased permeability. Also, an increase in selectivity (H_2/O_2) was observed with increased film thickness. Kotov et. al. prepared aluminosilicate-PDDA composites using LbL assembly technique and studied the diffusion of oxygen and water vapor across such membranes.[44] The

permeation rate of oxygen was found to decrease 6.6 times for ca. 200 nm film, while a permeation rate of aqueous vapor did not change at all. This observation was attributed to the dominance of solution/adsorption permeation mechanism over the Knudsen diffusion. *All of these researches indicate that the transport rate of a diffusate across NF bears a direct relationship to the solubility of diffusate in the NF matrix and an indirect relationship to the size of the diffusate*.

Liu et. al. made an important contribution towards the understanding of transport in aqueous media by investigating the diffusion of uncharged molecules of varying size across multilayer polyelectrolyte membranes.[30] They chose to investigate the diffusion of methanol, glycerol, glucose, and sucrose because these molecules differ in size and yet have similar functional groups and hydrophilicities. Diffusion studies using these molecules showed that LbL films can exhibit very high size-based selectivities (glucose/ sucrose selectivity reaches 150) that depend on membrane composition; selectivity has been defined as the ratio of the flux that has been normalized with respect to the feed side concentration of the diffusate. It must be noted that sucrose is almost twice the size of glucose. The diffusion coefficient of methanol, glycerol, glucose, and sucrose in water are 1.56×10^{-9}, 0.95×10^{-9}, 0.69×10^{-9}, and 0.52×10^{-9} m^2/s, respectively. In contrast, the diffusion coefficient of methanol, glycerol, glucose, and sucrose through 7 bilayers of PSS/PAH membrane was found to be 1.6×10^{-12}, 4.84×10^{-13}, 9.87×10^{-14}, and 3.7×10^{-15} cm^2/s, respectively. Thus it was found that just 7 bilayers of PAH/PSS reduced the diffusivity of the molecules by *ca.* 1000, 2000, 7000, and 140,000 times, respectively. In addition, it was found that terminating the outer layer of LbL film with PAH instead

of PSS resulted in a decrease of glucose flux by ~7%. As PAH is more hydrophobic than PSS,[30] this results in the exclusion of water molecules from its surrounding, thereby resulting in even slower glucose transport. As PAA is more hydrophobic than PAH,[30] it was hypothesized that the application of PAA as an outer coating can result in a substantial reduction of the transport of water soluble molecules. To test this hypothesis, the transport of glucose through NFs consisting of $(PSS/PAH)_5$/PAA/PAH and $(PSS/PAH)_5$-(PAA/PAH)-PAA compositions was studied and it was found that only one additional layer of PAA, applied as an outer coating, resulted in *ca.* 20% decrease in the glucose flux.

In summary of the above discussion, the transport of glucose and oxygen into the sensor matrix can be precisely controlled by varying one of several parameters, such as the material used for the formation of LbL NF, the film thickness, film deposition conditions, and the capping layer of the NF. The ability to precisely control the transport of glucose and oxygen is very important in the manufacturing of such sensors, as their response completely depends on the intricate balance between the transport and reaction kinetics of substrates (i.e., glucose and oxygen). The next section will provide an introduction to the reaction kinetics, which play a critical role in the design of such sensors.

2.4 Enzyme Kinetics

Glucose oxidase (GOx) from *Aspergillus niger* is a well-characterized oxidoreductase enzyme, which catalyzes the oxidation of glucose to gluconolactone in the presence of oxygen.[47] It consists of two identical 80-kDa subunits with two bound

FAD co-enzymes. Each GOx molecule has one active site. GOx is a slightly elongated globular protein with an axial ratio of 2.5:1 and an average diameter of 8 nm.[48] Gibson et. al. investigated the redox reaction of glucose and oxygen catalyzed by GOx, for which the reaction scheme may be expressed as[49,50]

$$\begin{aligned} E_{ox} + G &\xrightarrow{k_1} E_{red}P_1 \xrightarrow{k_2} E_{red} + \delta\text{-gluconolactone} \\ E_{red} + O_2 &\xrightarrow{k_3} E'_{ox}P_2 \xrightarrow{k_4} E_{ox} + H_2O_2 \end{aligned} \qquad (2.\ 5)$$

where G and O_2 are the co-substrates, glucose and oxygen, respectively, E_{ox} and E_{red} are the oxidized and reduced forms of the enzymes, respectively, $E_{red}P_1$ and $E_{ox}P_2$ are the enzyme substrate complexes, and k_1, k_2, k_3, and k_4 are the rate constants of the respective reaction steps. The rate constants k_1, k_2, k_3, and k_4 at 37 °C are as follows: k_1: 10^4 $M^{-1}s^{-1}$; k_2: 0 s^{-1}; k_3: 2.1×10^6 $M^{-1}s^{-1}$; k_4: 1150 s^{-1}.[49,50]

Catalase (CAT) is a heme-containing enzyme that is present in virtually all aerobic organisms. It is a tetramer of four polypeptide chains and has a molecular weight of ~250-kDa. CAT is able to protect cells against the damaging effects of H_2O_2 by catalytically decomposing it into oxygen and water. The catalytic consumption of H_2O_2 via bovine liver CAT has been investigated by Lardinois et. al., which can be expressed as[51]

$$\begin{aligned} H_2O_2 + CAT &\xrightarrow{k_5} I + H_2O \\ H_2O_2 + I &\xrightarrow{k_6} CAT + H_2O + O_2 \end{aligned} \qquad (2.\ 6)$$

where I is the intermediate form of the enzyme, which is converted back to the native form of CAT by reacting with another peroxide molecule; k_5 and k_6 are the rate constants

of the reaction steps shown in scheme (2). The rate constants k_5, and k_6 are: k_5: 1.7×107 $M^{-1}s^{-1}$; k_6: 2.6×107 $M^{-1}s^{-1}$.

2.5 Enzyme Deactivation

Like other proteins, enzymes are susceptible to destruction and/or inhibition.[52] GOx deactivation will result in decreased reaction rates, which will result in increased oxygen concentration inside the sensor matrix. Altered oxygen concentration in the sensor matrix will be reflected as a drift in response, and it is expected that decreased sensitivity and an increased response range would be observed under such conditions. Therefore, the deactivation kinetics will determine the useful operating lifetime of such sensors. Both GOx and CAT have been widely employed in research and, as a result, a significant amount of work has been dedicated to understanding their catalytic properties and the factors affecting them.[50,53] Primarily, there are two ways by which an enzyme loses its activity. The first is spontaneous deactivation, which is caused by the denaturation of enzyme.[53] The second is peroxide-mediated hydrolytic cleavage, which depends on the hydrogen peroxide concentration.[53] As these kinds of deactivation involve different mechanisms, they can be addressed separately. For continuously-operating enzymes, peroxide-mediated deactivation has been identified as the primary source of enzyme degradation.

2.5.1 Spontaneous deactivation

Spontaneous degradation that occurs due to the unfolding or denaturing of the enzyme results in a loss of active enzyme, which is believed to be constant for a given

matrix at a particular temperature.[53] This type of deactivation follows first-order kinetics, in which the rate of enzyme degradation is proportional to its concentration. The rate equation can be expressed as

$$\frac{dE}{dt} = -k_s[E] \qquad (2.7)$$

where [E] is the concentration of enzyme, and k_s is the spontaneous deactivation rate constant. All forms of GOx and CAT immobilized in homogenous collagen membranes have been shown to be equally susceptible to spontaneous deactivation.[53] The spontaneous deactivation rate constants of GOx and CAT, k_{sGOx} and k_{sCAT}, have been determined to be 9.2×10^{-8} s^{-1} and 1.5×10^{-7} s^{-1}, respectively.[53] Using these rate constants the estimated half-life ($t_{1/2}$) of GOx and CAT is *ca.* 82 and 53 days, respectively.

It has been shown that the spontaneous deactivation can be significantly reduced by providing structural support to the enzyme.[54] Zhou et al. have shown that the pore size of the matrix plays a significant role in determining the spontaneous deactivation rate of immobilized protein.[55] Using theory, they showed that confinement of a protein in a cage that is 2-6 times larger than the protein diameter provides a drastic increase in protein stability by preventing it from unfolding and denaturing. Vamvakaki et al. examined the effect of enzyme and pore size matching by determining the spontaneous deactivation of GOx and horseradish peroxidase (HRP) in various matrices.[56] GOx and HRP have a diameter of 7 nm and 4.8 nm, respectively. Two matrices with average pore sizes of 10 nm and 30 nm were used for enzyme immobilization. In both cases, the enzyme stability was found to be higher for the matrix with 10 nm pores. In addition, it was observed that a greater stabilization was imparted to GOx than HRP when

immobilized in the 10 nm pore matrix. This was attributed to the better size matching between the diameter of GOx and the matrix pore.

2.5.2 Peroxide-mediated deactivation

Peroxide-mediated degradation follows second-order kinetics, where the rate is proportional to the product of the peroxide concentration and the concentration of the respective enzyme. The rate expression for this type of deactivation can be expressed as

$$\frac{dE}{dt} = -k_p[E][H_2O_2] \qquad (2.\ 8)$$

where $[E]$ and $[H_2O_2]$ are the concentration of enzyme and hydrogen peroxide, respectively, and k_p is the rate constant.

Kleppe et. al. found that the oxidized form of GOx is relatively insusceptible to H_2O_2, when compared to the other forms; in contrast, the deactivation of other forms of GOx is at least 100 times faster than the oxidized form.[57] Tse *et. al.* have shown that the rate of immobilized GOx degradation exponentially increases with glucose and peroxide concentration.[53] The proportionality constants, also referred to as rate constants, are k_7 for the complex form of GOx and k_8 for the reduced form. The rate constants k_7 and k_8 are: k_7: 0.76 $M^{-1}s^{-1}$; k_8: 0.02 $M^{-1}s^{-1}$.[53] Tse et. al. also investigated the peroxode-mediated deactivation of immobilized CAT. All forms of CAT were found to equally susceptible to peroxide.[53] The rate constant for immobilized CAT deactivation via peroxide, k_9, was determined to be 0.015 $M^{-1}s^{-1}$.

In summary, oxygen sensing, mass transport through NFs, enzyme kinetics, and enzyme deactivation kinetics were discussed in this section that lay the foundation of

enzymatic microparticle-based glucose sensors. The knowledge available on the transport of glucose and oxygen through NFs, and reaction kinetics can be utilized to model the response of sensors. Moreover, the variation in response of sensors with time can be predicted by incorporating deactivation kinetics. The mathematical model that can be used to simulate the sensor response is known as a reaction-diffusion model for which a detailed discussion has been provided in the next section.

3 THEORY

In Section 2, theories related to oxygen-sensing, mass transport, enzyme kinetics, and enzyme deactivation kinetics were presented. The goal of this section is to develop a predictive model by combining all those theories. The mathematical model can be used to simulate the response of enzymatic microparticle-based glucose sensors.

Microparticle-based sensors described in this dissertation are very similar to microreactors, with immobilized indicator dye as an additional component to transduce the oxygen concentration to luminescence intensity or lifetime. Figure 3.1 is a simplified model for the microparticle-based glucose sensing scheme. The model consists of a microsphere of radius r with a nanofilm coating of thickness t on it. The sensing chemistry, indicator dye and enzyme, is immobilized within the microsphere. For ease of understanding, sensors incorporating only one enzyme (GOx) have been considered initially; inclusion of a second the enzyme (CAT) renders the reaction scheme more complicated; more complicated models that incorporate both enzymes, are described in Section 7. In addition, no enzyme degradation has been considered here for the sake of simplicity for the reader to develop an appreciation for the basic model. More complicated models, which can model the response of sensors incorporating two enzymes while considering enzyme deactivation, maybe implemented by a slight modification of the reaction terms of the simplified model described here.

When sensors are exposed to bulk glucose and oxygen, these two substrates diffuse inside the sensor matrix and trigger the reaction shown by Equation 2.5. After some time of exposure to bulk substrate levels, steady state is attained within the

microspheres, after which the internal substrate concentrations depend on the delicate balance between reaction and diffusion rates. For a fixed bulk oxygen level, the rate of glucose diffusion and the corresponding consumption rate of oxygen inside the sensors primarily depend on bulk glucose concentrations. Thus, with increased bulk glucose levels, we expect to observe proportionally higher reaction rates, resulting in proportionally lower oxygen levels inside microspheres; as the transduction mechanism is based on quenching of luminescence by oxygen, *increased emission intensity and lifetime will be observed for increased glucose levels.*

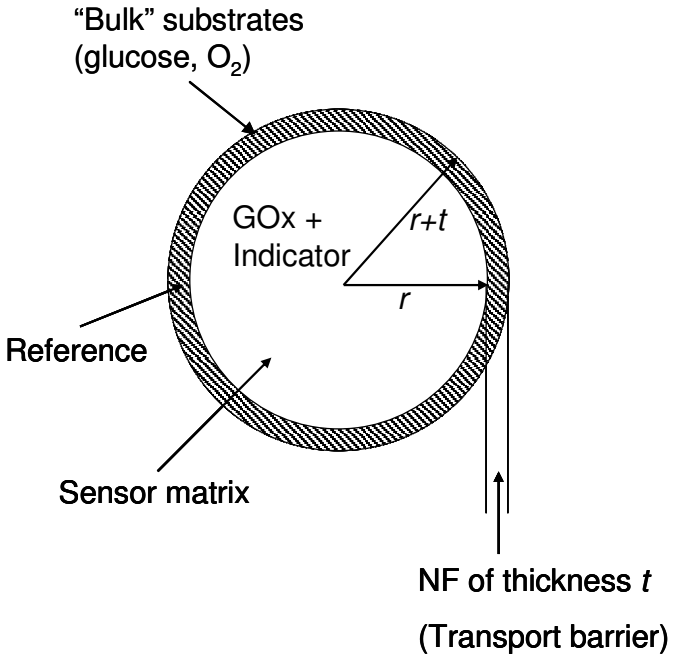

Figure 3.1 Schematic of microsphere sensors.

The mathematical equation describing such phenomena is known as a reaction-diffusion model.[58] For modeling purposes, Equation 2.5 results in a system of six

coupled partial differential equations (PDEs) that describe the behavior of the system in time and space for each individual species. There are six reactive species, glucose, oxygen, and four forms of GOx, each requiring one PDE to describe its behavior. If we assume that the boundary conditions for the sensor are constant and uniform throughout the surface of the microparticle sensor, then the solution will only depend on the radial coordinate (r). The general PDE used to model this system can be written as

$$\frac{\partial C_i}{\partial t} + \frac{1}{r^2}\frac{\partial}{\partial r}\left(-D_i r^2 \frac{\partial C_i}{\partial r}\right) = R_i \qquad (3.\ 1)$$

where i is the subscript denoting one of the six reactive species, G, O_2, E_{ox}, $E_{red}P_1$, E_{red}, $E_{ox}P_2$. D_i and R_i represent the diffusivity and reaction rates of the respective species involved in the reaction scheme. The concentration of all reactive species (six, one of which is oxygen) can be obtained by simultaneously solving the system of equations given by Equation 3.1. It must be noted that the solution gives concentration over time and space coordinates. To convert the predicted oxygen level to an estimate of relative luminescence, the Stern-Volmer equation can be applied at each point within the particle:

$$\frac{I_0}{I} = 1 + K_{SV} \cdot [O_2] \qquad (3.\ 2)$$

In this equation, I_0 is the luminescence intensity in the absence of oxygen, I is the luminescence intensity in the presence of oxygen, $[O_2]$ is the oxygen concentration, and K_{SV} is the Stern-Volmer constant. Thus, the expected luminescence intensity for a certain bulk glucose level can be predicted. To allow estimation of the response of sensors over a range of glucose levels, the luminescence intensity predicted for zero glucose is

considered as the baseline and the percentage increase in luminescence for each glucose level can then estimated to obtain a predicted response profile.

3.1 Methods to Solve Reaction-diffusion Equations

The linear reaction-diffusion equation, in which the reaction terms are of first order or less than that, can be solved by implicit methods, giving an exact solution of the problem.[59] However, the non-linear reaction-diffusion equation, in which the reaction terms are of second or higher order, can only be solved by using explicit methods. Moreover, when a PDE is coupled to other PDEs of the system, it becomes almost impossible to obtain an exact solution by using an implicit method. From Equation 2.5, which describes the glucose oxidation catalyzed by GOx, it can be observed that the reaction terms for all six reactive species are of second order. Therefore, the system of equation used to model the response of glucose sensors fall under the category of non-linear PDEs, which requires the use of explicit methods in this case.

Although several explicit methods are available that can provide the approximate solution for a PDE (e.g., finite difference, finite volume, finite element method), the finite element method (FEM) is generally preferred over other methods. This is especially true when the domain has a complex shape or when the solution lacks smoothness as other methods often fail to yield a solution. In the research presented in this dissertation, COMSOL 3.5a (COMSOL, Inc, Burlington, MA), was used to perform the simulations, which estimates the approximate solution using FEM.[60]

3.2 Solution Scheme

The system of equations given by Equation 3.1 consists of six PDEs, which models the concentration of each reactive species in space and time. As the equations are coupled, they must be solved simultaneously to model the response of sensors. From Equation 3.1, it can be inferred that the system of equations has two independent variables, which represent space (r) and time (t), and six dependent variables, representing the concentration of one of the six reactive species (C_i). There are several steps in the modeling process, which have been detailed below.

3.2.1 Drawing and meshing

The first step in any FEM modeling is to specify the geometry of the model. In a 1-D spherical coordinate system, the model for our system can be represented by a straight line as shown in Figure 3.2. The model consists of subdomains 1 and 2, representing the microparticle and NF, respectively. The lengths of subdomains 1 and 2 are proportional to the radius of the microparticle and the thickness of the NF, respectively. The left and the right node in the model represent the center of the microparticle and the surface of the NF, respectively.

After specifying the geometry of the model, each subdomain is then broken down into several smaller elements. This process of space discretization is termed as *meshing* in FEM. A node is used to connect two adjacent elements. Subdomain 1 and 2 were divided into 48 and 4 elements, respectively, using a free mesh generator. The size of each element is determined by the free mesh generator. Generally, mesh is finer in near-boundary regions.

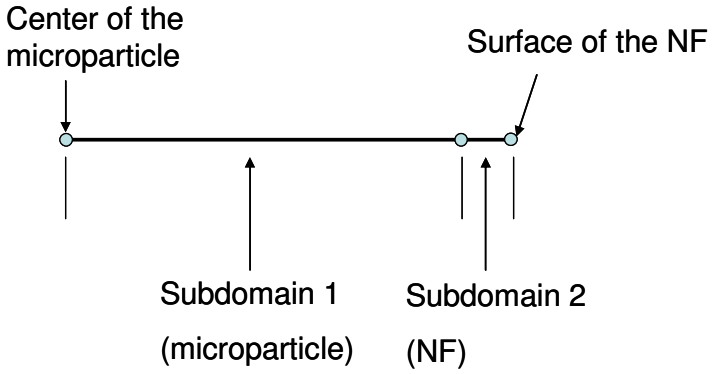

Figure 3.2 Model of the microparticle-based glucose sensor in 1-D spherical coordinate system.

3.2.2 Initial and boundary conditions

After meshing the geometry, the next step is to specify the initial (ICs) and boundary conditions (BCs). The ICs are specified by assigning the concentration of all the six reactive species in the entire domain. For example, the oxidized form of GOx is one of the six reactive species, for which the IC in subdomain 1 is the experimentally-determined concentration of immobilized GOx. In subdomain 2, which represents the NF, the IC for the oxidized GOx is set to zero, because there is no enzyme in the NF. IC for the other reactive species was set according to the varying aspects of studies that were conducted. For specific cases, ICs are tabulated in Table 6.1 and Table 7.1.

The BCs are specified by assigning a certain value or situation to the concentration of reactive species at the left and right node, representing the center of the microparticle and the surface of the NF, respectively. It must be noted that only left and right nodes represent the boundaries of the system. Due to spherical symmetry, the BC at the left boundary is always the same, which is zero flux at that boundary. The BC for the

right boundary is specified in terms of concentration of each reactive specie at the surface of the NF. The concentration of all reactive specie except glucose and oxygen is fixed at zero; GOx present on the surface of the NF that represents the right boundary. The concentration of glucose and oxygen in the solution, for which we intend to predict the response, can be specified as the right BC.

Once the IC and BC have been specified, the model can then be solved using a direct solver, which is based on the Gauss-elimination method. Depending on the IC, the solution will evolve with time, finally reaching a steady-state after which the solution will not change with time if the bulk concentrations of substrates are constant and no degradation of enzyme is assumed. For these simulations, it has been observed that the solution reaches a steady-state within 3 seconds.

3.2.3 Response prediction

The model described is designed to predict the response of enzymatic sensors when exposed to certain glucose and O_2 concentrations. The solution scheme used to accomplish this is illustrated as a flowchart shown in Figure 3.3. It was assumed that at $t=0^-$ substrate concentration inside the sensors (i.e., microsphere + film) is equal to the bulk, providing the IC for glucose and oxygen. The IC for the native enzyme concentration has to be specified, which is usually an experimentally-determined concentration of the immobilized enzyme. The ICs for the reduced and the complexed forms of the enzyme are zero concentration. As the left boundary represent the point of symmetry within a sphere, the BC for left boundary for all species is of zero flux. For the right boundary, BC is specified in terms of concentration of all reactive species. The

concentration of all forms of enzyme is set to zero as there is no enzyme on the surface of NF. The concentration of bulk oxygen is always kept constant at a value for which the response has to be predicted. At t=0, the reaction is "turned on," and the diffusion-reaction process is solved for t=20 seconds. Assuming no enzyme degradation, the solution reaches a steady-state in *ca.* 3 seconds and, therefore, at $t=20$ seconds, it is certain that the time evolution of the solution is completed. The steady-state solution is then used to predict the internal oxygen concentration distribution ($[O_2]_r$) inside the sensor, which is then converted to luminescence (I_r) using the Stern-Volmer equation (SVE). A typical data showing $[O_2]_r$ and I_r is shown in Figure 3.4. The volume averaged luminescence (I_{av}) is then estimated using an equation shown in Figure 3.3. Finally, the sensor response to glucose is estimated by calculating the percent increase in luminescence, taking luminescence intensity at zero glucose level as the baseline. The same procedure is repeated for different glucose concentrations to obtain a simulated response profile of glucose sensors. To predict glucose response profile of a sensor, all settings remain same in each simulation, except the BC for glucose on the right boundary, which is bulk the glucose concentration for which the response has to be determined.

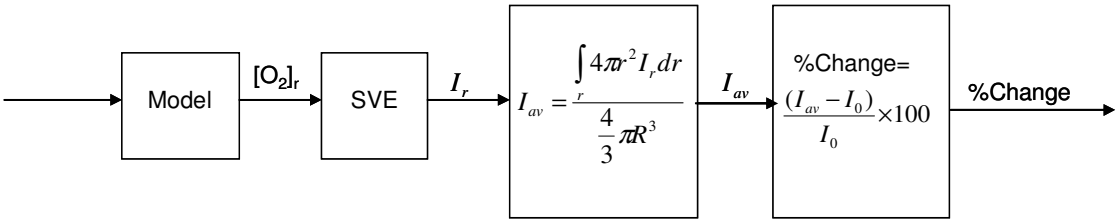

Figure 3.3 Schematic depicting the solution scheme used to predict the sensor response to glucose.

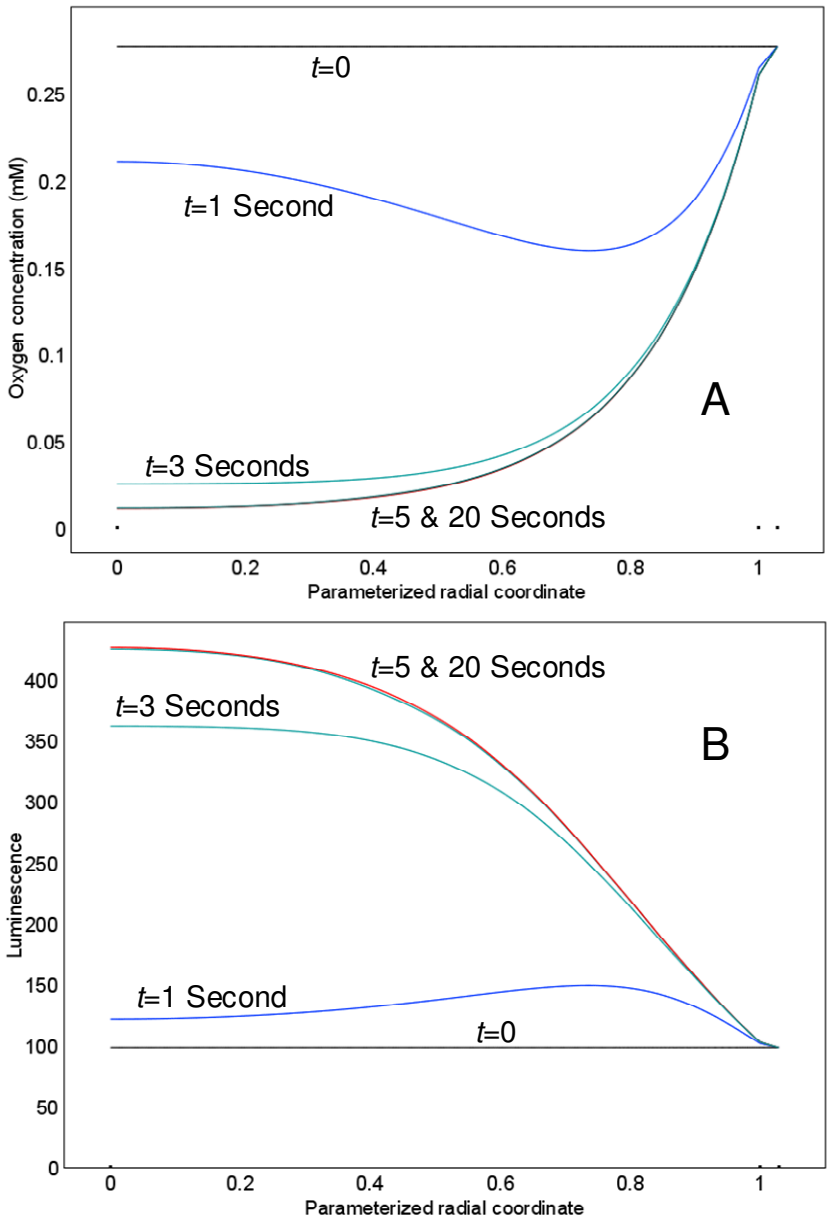

Figure 3.4 Time evolution of $[O_2]_r$ obtained by solving Equation 3.1 (A). Time evolution of luminescence obtained by substituting $[O_2]_r$ in Equation 3.2 (K_{SV} = 0.0142 µM-1) (B) .

In this section, the general reaction-diffusion equation has been described that can be solved to predict the concentration of reactive species and products within the microparticle-based sensors, and further convert oxygen concentration to luminescence intensity. The process of building a simple model to predict the response of sensors has been described, which will help the reader in gaining a better understanding of the mathematical modeling involved in this research. The model presented in this section can be used to gain a better understanding on the effects of particle size, matrix and NF diffusivities, enzyme concentration, and NF thickness on the response of sensors.

In this research, modeling has been used a tool for the design of sensors. Nevertheless, experimental validation of a model is always required to establish its reliability. Instrumentation employed for measuring the experimental response of sensors has been described in the next section. In addition, the methods used to characterize the response of sensors in terms of sensitivity and response range are discussed.

4 INSTRUMENTATION AND DATA PROCESSING

After the sensors have been designed and fabricated, the next step is to experimentally determine the response of sensors. For this, a flow-through set up has been constructed to test the dynamic response of sensors.[18] The testing apparatus allows precise control over the substrate concentrations required for obtaining accurate calibration curves.[18] In the dynamic testing apparatus, a custom-designed software suite (LabVIEW, National Instruments) is used as an interface to control and monitor real-time changes in sensor response. A schematic of the dynamic testing apparatus is shown in Figure 4.1.

Peristaltic pumps allow the mixing of buffer and glucose solutions, yielding various user-defined glucose concentrations through modulation of the flow rates. Similarly, mass flow controllers connected to nitrogen and oxygen tanks are used to adjust the dissolved oxygen concentration to the desired level. Bulk oxygen concentrations are measured using a Clark-type microelectrode. The reaction chamber consists of a custom-machined plastic flow channel that accepts a microscope slide on which sensors can be immobilized. The procedures used to immobilize sensors on the glass slide are described in the later sections. The reaction chamber has inlet and outlet ports for the test solution.

The bottom part of the chamber has a port for an optical fiber. An optical fiber bundle consists of 78 200 µm optical fibers (NA=0.22) organized into input (37 fibers) and output arms (41 fibers), combined into a single probe end. The input arm of the bundle connects to a LED light source (518 nm), and the output arm to a spectrometer

(USB2000, OceanOptics®). Tubing was selected for low oxygen permeability (Norprene® for pumps; PTFE for other sections).

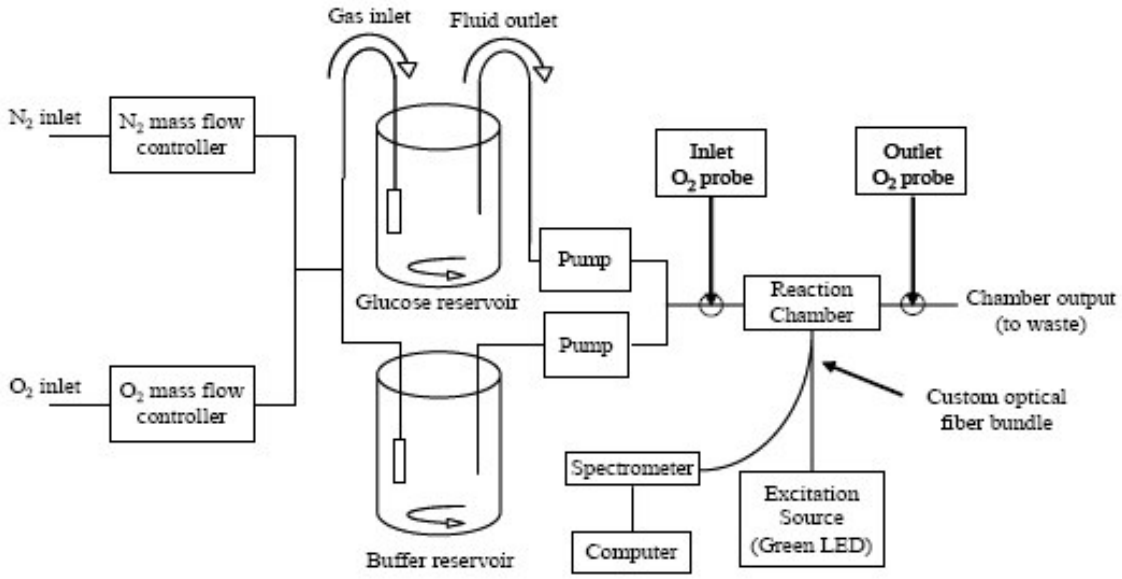

Figure 4.1 Schematic of dynamic testing apparatus.

Sample data obtained from this experimental setup are shown in Figure 4.2. The sensors used in this case consist of PtOEP as an indicator dye, with RITC as a reference dye.[61] Peak emission intensities of the indicator and reference are recorded in real-time using a spectrometer (Figure 4.2 (top)). The ratio of indicator to reference intensity is also estimated in real-time (Figure 4.2 (bottom)). In general, a constant oxygen concentration in glucose and buffer reservoirs is maintained throughout the course of experiment, though that can be changed as desired. Step changes in glucose concentrations are made after a certain interval, such that the response has reached a steady-state. Sensors are exposed to several different glucose concentration steps as desired.

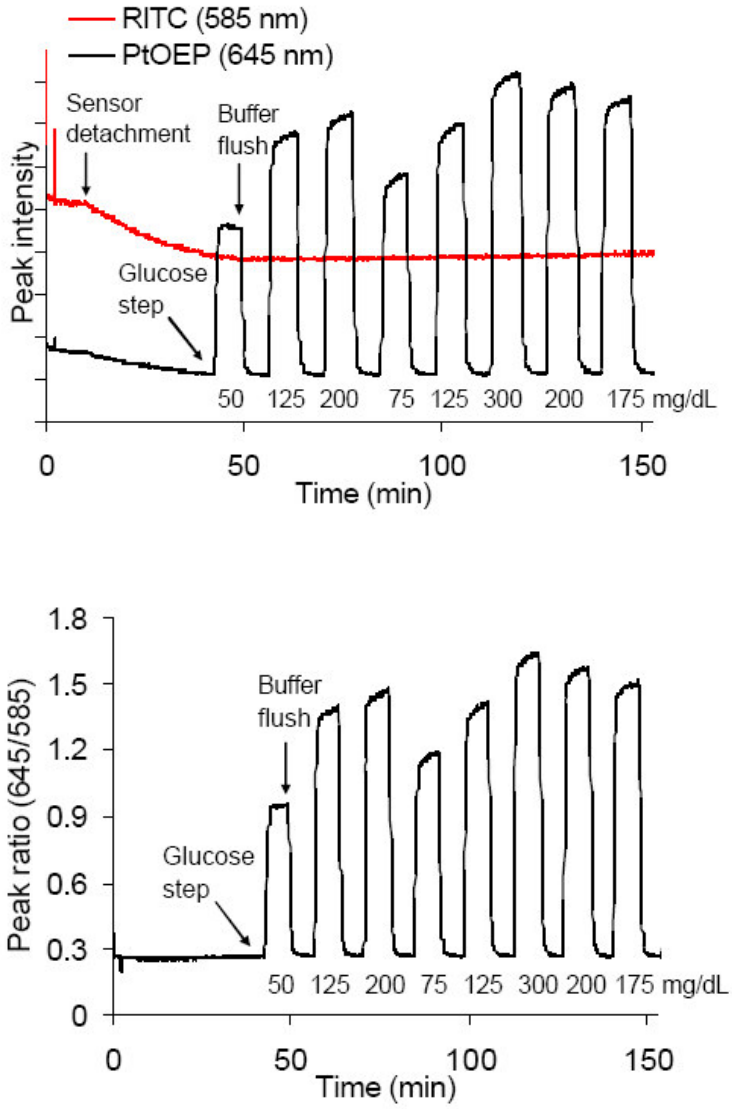

Figure 4.2 Raw data (top) and ratio data (bottom) obtained from dynamic testing setup under continuous excitation.[61]

The sensors were constantly excited to obtain the data shown in Figure 4.2. To minimize the photobleaching of luminophores, a special software suite was designed which turned on the light source only for a short duration in which data was to be

collected. The raw and ratio data obtained from this advanced setup are shown in Figure 4.3. To collect these data, sensors were exposed to each concentration step for one hour, and the data was collected during the last 5 minutes of each exposure.

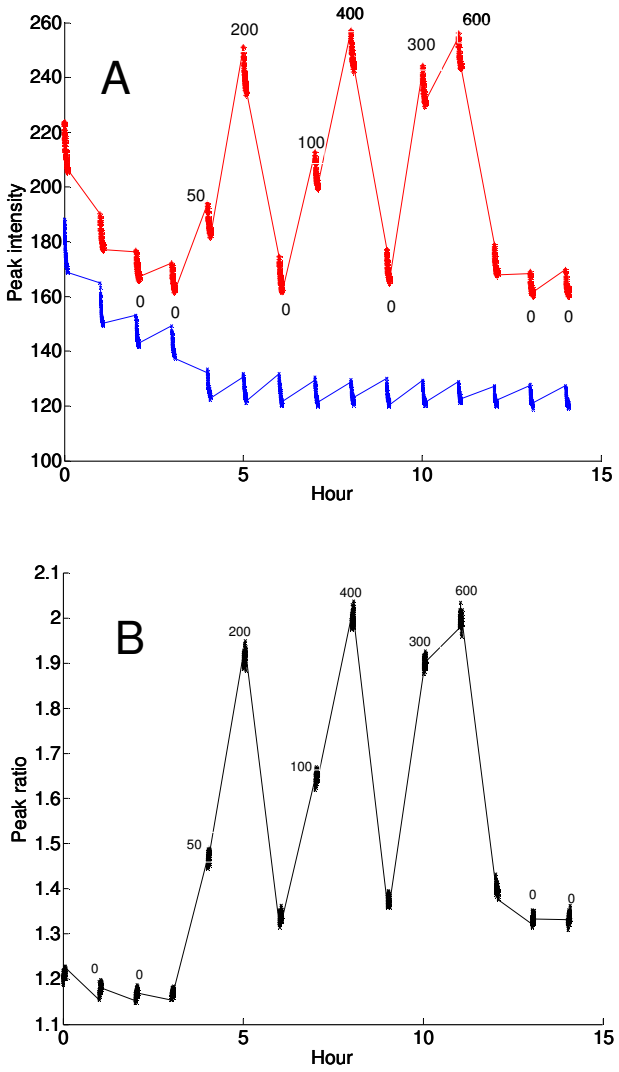

Figure 4.3 Raw data (A) and ratio data (B) obtained from dynamic testing setup under intermittent excitation.

Once the step response has been recorded for multiple glucose concentrations, the next step is to construct the response profile from the obtained ratio data. A sample response profile constructed from the step response data is shown in Figure 4.4. The drift in the baseline signal is calculated by performing a linear regression on the ratio data obtained for zero glucose concentrations; drift in the baseline occurs due to a difference in the photobleaching rates of indicator and reference dyes. Drift in the baseline is evident in Figure 4.3. To construct the response profile, the percentage change in the peak ratio for each glucose concentration is calculated by taking the ratio at zero glucose concentration as the baseline signal. The percent change in peak ratios are pooled together for each individual glucose concentration, after which the mean and standard deviation are calculated. The response profile is then constructed by plotting the mean percent change in the peak ratio versus glucose concentration, with error bars indicating the standard deviation for each measurement.

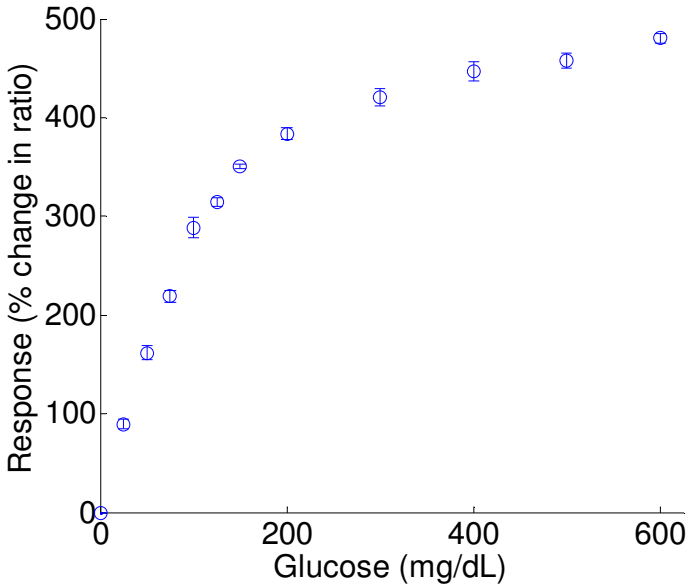

Figure 4.4 Example of response profile constructed from the data in Figure 4.2.

Once the response profile has been constructed, the next step is to characterize the response of sensors using figure of merits (FOMs) that allow the quantification of response characteristics. There are several such FOMs that are used characterize the response of sensors such as: sensitivity, response range, response time, reversibility, and drift in the response. These sensors have been shown to be completely reversible and they exhibit a very short response time (86 seconds *in vitro* when sensors are immobilized on pressure-sensitive adhesive).[18] In this dissertation, the focus in on extending the response range and longevity of sensors; therefore, sensitivity and the response range are of primary interest. The change in these FOMs over time is also of interest. Therefore, drift in these FOMs with time will be studied in experiments where

the response stability is investigated. To calculate the sensitivity and range from the response data, two primary methods have been used.[18,40]

4.1 Method 1

The processing of data to calculate the response range and sensitivity is illustrated in Figure 4.5.[18] The best fit for the response data is obtained using the equation

$$I = I_{\max}\left(1 - e^{-k[glucose]}\right) \qquad (4.1)$$

where [*glucose*] and *I* are the glucose concentration and the response (% change in ratio) at that particular glucose concentration, respectively. I_{max} and *k* are estimated using the method of nonlinear least squares analysis (Levenberg-Marquardt algorithm) in MATLAB.[21] The response fit is shown by a blue dashed line. Sensitivity—defined as the slope of the linear response—is estimated by performing a simple linear regression on the first few data points such that $R^2 \geq 0.95$. Range is defined as the glucose concentration at which the response fit deviates from linearity by 10%. The slope of the black line represents sensitivity and the abscissa of the red vertical line represents response range of sensors. Using this method, the experimentally-determined sensitivity and response range for this particular set of data are 2.3% /(mg/dL) and 189 mg/dL, respectively.

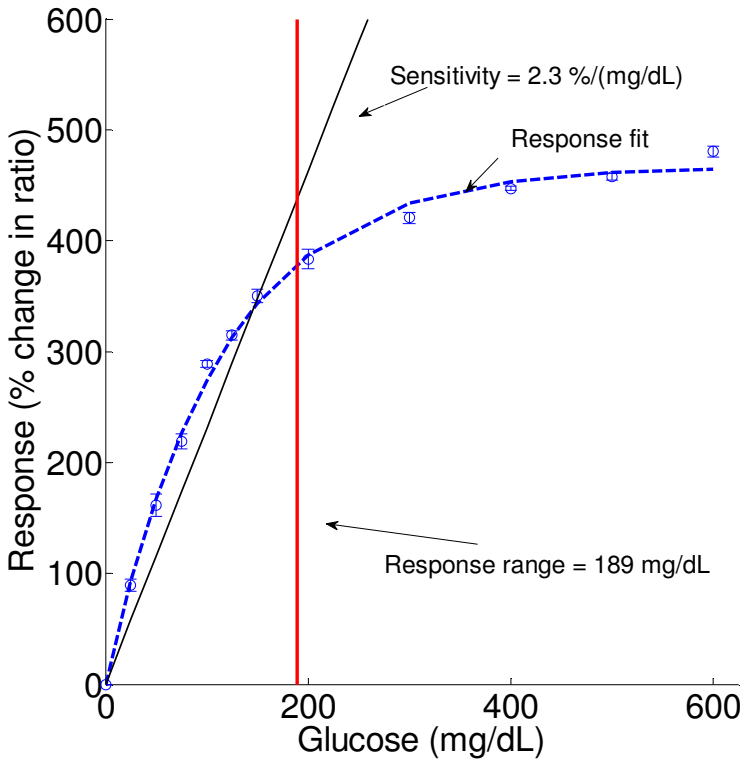

Figure 4.5 Data processing to calculate the response range and sensitivity.

4.2 Method 2

An alternative method that can be used for the processing of data has been illustrated in Figure 4.6.[40] In this case, the best fit for the response data will be obtained using the equation

$$I = \frac{I_{\max}}{1 + e^{a(K_{app} - [glu\cos e])}} \qquad (4.2)$$

where c and I are the glucose concentration and the response at that particular glucose concentration, respectively. I_{max}, a and K_{app} are estimated using the method of nonlinear

least squares analysis (Levenberg-Marquardt algorithm). Equation 4.2 is a form of sigmoidal fit and has been shown to be very effective for modeling enzyme kinetics. It can be observed from the equation that K_{app} is the glucose concentration at which the response (I) is half of the maximum possible response (I_{max}). Also, it can be noticed that at glucose concentration equal to K_{app}, the slope of the response curve is maximum; this implies that twice of K_{app} is the minimum glucose concentration up to which the sensors will exhibit response. Therefore, in this case, the range is defined as twice of K_{app}. Sensitivity can be estimated using the following Equation 4.3. It must be noted that the type of fit used in this method works very well for predicting the response when the glucose concentration lies between 25 mg/dL and the response range, which is two times K_{app}. For blood glucose measurements, the minimum glucose concentration than a sensor must be able to measure is 40 mg/dL.[19] Therefore, the fact that the sigmoidal fit does not work well for extremely low glucose levels, less than 25 mg/dL, is not a problem in this case.

$$Sensitivity = \frac{I_{\max}}{2 \times K_{app}} \qquad (4.3)$$

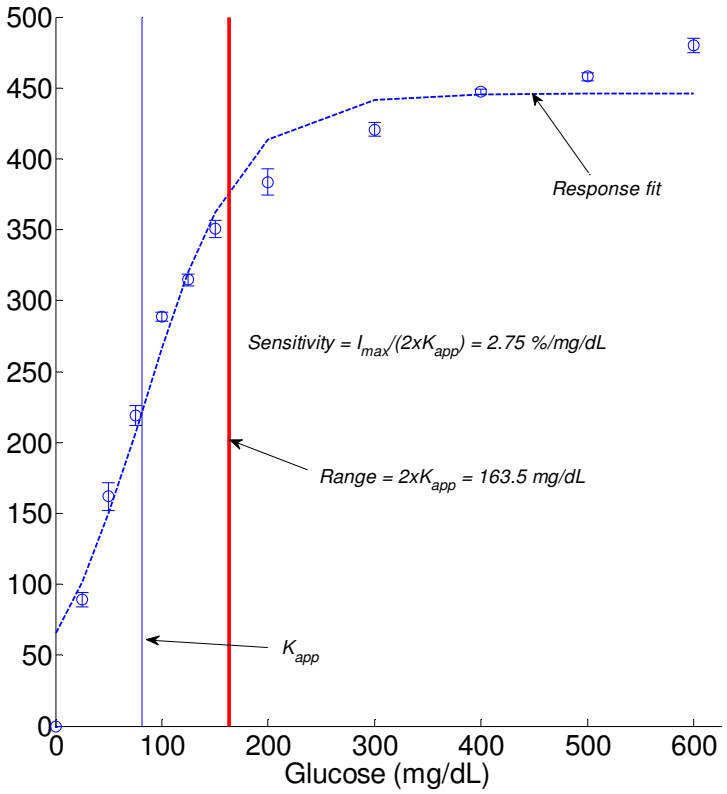

Figure 4.6 Alternative method for data processing to estimate range and sensitivity.

It can be noticed that even though the same data were used in each example, the two methods of data processing result in slightly different values for sensitivity and response range. In this dissertation, Method 1 is mostly used to characterize the response of sensors because it resulted in a good fit ($R^2 \geq 0.95$) in most cases. However, in few cases where Method 1 does not yield a good fit, Method 2 has been used. With the aid of modeling, it has been observed that with increasing GOx concentration the response profile begins to take a sigmoidal shape from exponential. Thus, an exponential profile is an indicative of a reaction-limited sensing scheme, whereas a sigmoidal profile indicates

that the sensing scheme is relatively more diffusion-limited. Interestingly, the sensors exhibiting an exponential response profile when immobilized on a pressure-sensitive adhesive, were observed to exhibit a sigmoidal response when immobilized within a PEG-gel. It must be noticed that the gel imposes an additional barrier to the transport of substrates and, therefore, the sensing scheme is relatively more diffusion-limited when sensors are immobilized within a gel instead of being immobilized on an adhesive. The two methods can also be applied to the theoretical data to obtain an estimate of the predicted range and sensitivity. These methods have been extensively used in subsequent sections to characterize and quantify the experimental and theoretical response data.

In summary, this section contains the description of instrumentation that was employed to experimentally measure the response of sensors. Also, the FOMs that are used to quantify the response of a sensor were described, which will enable quantitative comparison of different sensor prototypes in later sections. Detailed description of the methods for calculating response range and sensitivity were provided.

5 RESPONSE MODULATION BY CHANGING FILM PROPERTIES*

5.1 Introduction

As enzyme-based sensors rely on the direct measurement of oxygen, optimum sensor performance can only be attained when the ratio of glucose to oxygen concentration is less than 1 inside microparticles. When this is not the case, which is generally true *in vivo* (the normoglycemic glucose concentration is ~5.5 mM, whereas the oxygen concentration can range from 90 μM to 277 μM [62]), the lack of oxygen renders the reaction scheme oxygen-limited, and the sensors do not cover the entire physiological glucose range (0-600 mg/dL). In this situation, the sensors respond only up to a certain level of glucose, which is lower than 600 mg/dL, and no change in response is observed for higher glucose levels. This problem can potentially be addressed by coating the microparticles with a perm-selective membrane. An ideal membrane would be such that it presents a minimal barrier to oxygen transport while substantially reducing the transport of glucose.

*Parts of this section have been reprinted with permission from "Microscale enzymatic optical biosensors using mass transport limiting nanofilms. 2. Response modulation by varying analyte transport properties" by Stein, E. W.; Singh, S.; McShane, M. J. *Analytical Chemistry* **2008**, *80*, 1408-1417, Copyright [2008] by American Chemical Society, DOI: 10.1021/ac701738e

Toward controlling the range of sensors, the application of perm-selective nanofilms (NFs) formed using layer-by-layer (LbL) technique has been proposed to increase the range of microscale sensors.[16,18] The advantage of using this technique is that film characteristics such as thickness and diffusivity can be easily fine-tuned by choosing the right material composition, polyelectrolyte deposition conditions, and the outermost layer.[30] Such NFs have been reported to substantially reduce the transport of relatively bigger molecules (e.g., glucose) without significantly affecting the transport of smaller molecules (e.g., oxygen).[30] The NF permeability for a substrate can be tailored by adjusting the film thickness, deposition conditions, and outermost layer.[30] In this study, the effect of thickness and deposition conditions of NFs, on the response range and sensitivity of microparticle-based sensors was investigated. In addition, the affect of outermost layer, which is also termed as a "capping layer," on the range and sensitivity of sensors has also been investigated.

5.2 Experimental

5.2.1 Chemicals

Sodium alginate (low viscosity, 250 cps, MW 12-80 kDa), (3-glycidyloxypropyl)trimethoxysilane (GPTS), and ammonium hydroxide were obtained from Sigma and used for the synthesis of mesoporous alginate-silica particles. PtOEP (Frontier Scientific), tetrahydrofuran (THF, Fluka), GOx (type VII from Aspergillus niger, 198k units/g of solid, Sigma), N-(3- dimethylaminopropyl)-N'-ethylcarbodiimide hydrochloride (EDC, Fluka), N-hydroxysulfosuccinimide sodium salt (NHSS, Toronto Research Chemicals Inc.), and sodium acetate (Sigma) were used to prepare

PtOEP/GOx-doped alginate-silica particles. Poly(allylamine hydrochloride) (PAH, MW 70 kDa, Aldrich), poly(sodium 4-styrenesulfonate) (PSS, MW) 70 kDa, Aldrich), and sodium chloride (Sigma) were used during the deposition of multilayer thin films. Additionally, rhodamine B isothiocyanate (RITC, Aldrich) was conjugated to PAH and used in thin film deposition. β-D-glucose (MP Biomedicals, Inc.). Fluorescein isothiocynate (FITC) was conjugated to GOx using standard amine labeling protocol to confirm the immobilization of GOx in to the algilica matrix. O_2 and N_2 gas (Praxair Inc.), and phosphate-buffered saline (PBS, Sigma) were used during dynamic testing. All necessary pH adjustments were performed using titrations of 1.0 M HCl and 1.0 M NaOH (Fluka). All chemicals listed above were reagent grade and used as received. Throughout all experimental procedures, ultrapure water with a resistivity of greater than 18 MΩ was used. Unless otherwise stated, all experimental processes were conducted at room temperature.

5.2.2 Preparation of "algilica" microparticles

Alginate-silica ("algilica") particles were prepared using a procedure detailed in previous papers from the group.[18] Briefly, the precursor was prepared by stirring a solution comprised of 1.5 wt% aqueous alginate solution and glycidyl silane (GPTS) in a 1:1 volumetric ratio for at least 4 hours, resulting in an alginate-modified silanol. While stirring, 2 mL of the precursor silanol was added to 3 mL of water. To initiate the sol-gel process, 1.25 mL of 10 M NH_4OH was added dropwise and stirred for 20 min, followed by the addition of 10 mL of water and an additional stirring time of 40 min. An extra 40 mL of water was added and the suspension stirred for at least an additional

12 hours. The resulting particle suspension was rinsed with DI water using four sequential centrifugation cycles and diluted to a total aqueous suspension volume of 1.5 mL. A particle size analyzer (Elzone 540, Micromeritics®) equipped with a 190 μm aperture was used to measure the concentration and size distribution of microparticles. Dried microparticles were also sent for surface area and pore size analysis (Delta Lab, North Huntington, PA).

5.2.3 Preparation of PtOEP and GOx-doped algilica particles

Approximately 250 μL of stock particle suspension was placed in a microcentrifuge tube and dried under streaming N_2, followed by adding 750 μL of a 750 μM PtOEP solution prepared in THF. PtOEP contains eight ethyl groups, which makes the dye extremely hydrophobic (Figure 5.1). The container was sealed to prevent volatilization of THF and stirred for 30 min, after which 20 μL of water was added and the suspension stirred for an additional 30 min. The water added to the suspension initiated a solvent-mediated controlled precipitation of PtOEP into the mesoporous particles, a technique used in previous reports to aid in the immobilization of desired molecules.[43] The suspension was subsequently rinsed with DI water four times. Following the last rinse cycle, the supernatant was removed and 250 μL of 35 mg/mL GOx prepared in 50 mM pH 4 sodium acetate buffer was added. The pH value was selected based on experimental results from previous work, allowing the maximum loading of GOx into the algilica matrix due to electrostatic attraction.[5] The suspension was stirred for 4 hours, followed by two rinsing cycles with DI water. The supernatant was subsequently removed and replaced with 250 μL of solution comprised of EDC (50

mg/mL) and NHSS (50 mg/mL) in 50 mM sodium acetate (pH = 6.0) to catalyze amide bond formation between amine and carboxylic acid functionalities on GOx and alginate, respectively.[44] Finally, the suspension of PtOEP/GOx-doped particles was stirred for 2 hours then rinsed two times with DI water.

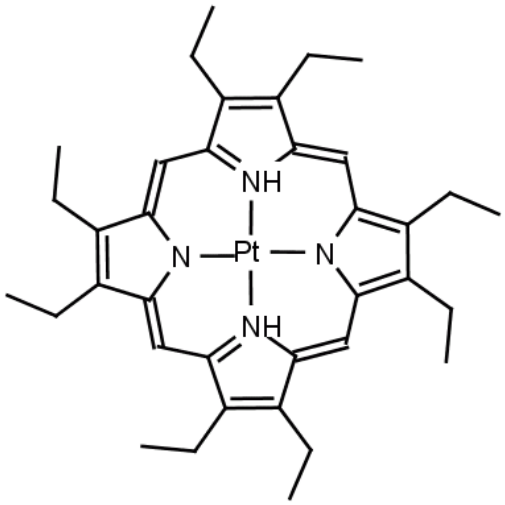

Figure 5.1 Structure of PtOEP.

5.2.4 Adsorption of NF surface coatings

RITC was conjugated to PAH (PAH-RITC) according to a standard amine conjugation protocol.[45] Prior to multilayer film deposition, solutions of PSS, PAH, and PAH-RITC were prepared at a concentration of 2 mg/mL with 0.2 M NaCl. The supernatant of the PtOEP/GOx-doped particles was removed and the particles resuspended in PAH-RITC. Following a 15 min adsorption period, during which the particles were continuously vortexed and protected from light with aluminum foil, the particles were rinsed three times with DI water and subsequently resuspended in PSS

solution. It was previously determined that three bilayers of PAH-RITC and PSS (denoted $[PAH\text{-}RITC/PSS]_3$), was required to obtain a PtOEP emission maxima (645 nm) that was approximately 75% of the RITC emission maxima (585 nm), thus all coated sensors received a base film of $[PAH\text{-}RITC/PSS]_3$. To investigate the effect of nanofilm thickness on response properties, sensors coated with 5, 10, and 15 PAH/PSS bilayers were prepared and resuspended, such that particle concentrations across all samples were equivalent. To study the effect of assembly solution ionic strength and capping layer on sensor performance, additional sensors were prepared with 5, 10, and 15 PSS- or PAH-capped nanofilms assembled with solutions without added NaCl.

5.2.5 Dynamic glucose sensitivity testing

The sensor response was experimentally determined using the flow-through system described in Section 4. The solutions in buffer and glucose reservoirs were prepared in 10 mM PBS (pH = 7.4) to maintain a physiological pH. A fixed dissolved oxygen concentration (277 μM) was achieved by aerating the solution. The method for sensor immobilization on the glass slide has been described elsewhere.[18] Briefly, ~10^7 microsensors were immobilized by pipetting 10 μL of a suspension of 10^8 particles/mL on to a double-sided pressure-sensitive adhesive attached to a glass slide and dried under a mild stream of nitrogen. The slide was then mounted inside a custom-designed plastic reaction chamber. Sensors were exposed to 0, 25, 50, 100, 150, 200, and 300 mg/dL. Step changes for glucose concentration were randomized, and each step lasted for 20 minutes and was repeated twice. The real-time data were converted to response profile (% change vs. [glucose]) and the sensitivity and response range were estimated using

Method 1 described in Section 4. Briefly, Equation 4.1 was used to fit the response. Sensitivity – defined as the slope of the linear response – was estimated by performing a simple linear regression on the first few data points such that $R^2 \geq 0.95$. Range was defined as the glucose concentration at which the response deviates from the linearity by 10%.

5.3 Results and Discussion

5.3.1 Sensor characterization

The number size distribution of algilica particles is shown in Figure 5.2. The particles exhibited a relatively broad size distribution, with a volume-average diameter of *ca.* 12 μm. The average pore size of algilica particles determined using porosimetry was *ca.* 18 nm, which is much larger than the size of GOx, which is 8 nm. Unfortunately, the porosity for algilica was found to be extremely low *ca.* 0.005. The low porosity can limit the maximum amount of enzyme that can be immobilized in the matrix. In addition, the matrix with low porosity is also expected to exhibit a reduced response range, which will be discussed in detail in Section 6.

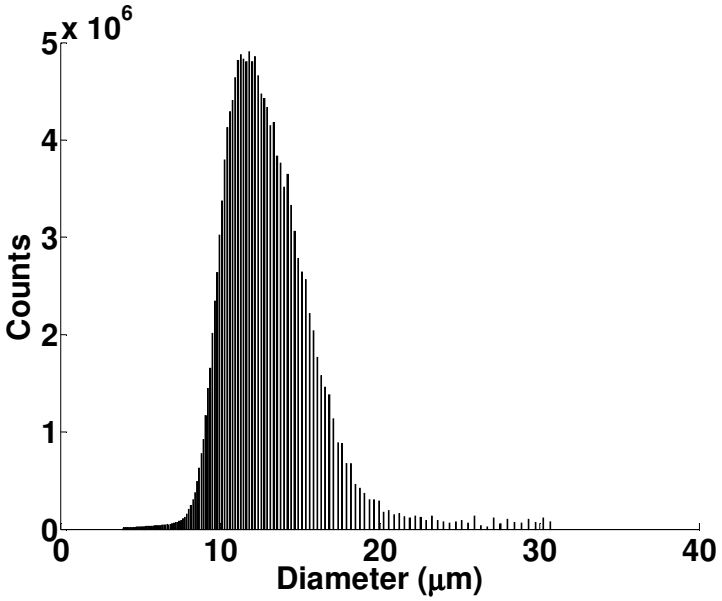

Figure 5.2 Size distribution algilica microparticles.

5.3.2 Effect of NFs on sensor response

As noted in earlier sections, successful realization of analyte-sensitive enzymatic smart tattoos relies on a delicate balance of substrate reaction-diffusion kinetics.[8,50] Surface-adsorbed polyelectrolyte nanofilms were employed to precisely modulate glucose flux relative to that of oxygen (J_G/J_O) into the sensor, allowing sensor response characteristics to be tuned. Brown et. al. theoretically predicted that J_G/J_O can be reduced by increasing the film thickness, thereby resulting in increased response range and reduced sensitivity.[16] In addition, previous work has shown that film thickness, ionic strength of assembly conditions, and the capping polymer (terminal layer) could have a drastic effect on molecular transport.[33,39] This could afford precise control on the level of response tunability.

To investigate the ability to modulate sensor response metrics by varying the film thickness, by changing the electrolyte concentration in the polyelectrolyte solution, and by varying the capping polyelectrolyte, multilayer nanofilms of 5, 10, and 15 bilayers were assembled from solutions of 0 M NaCl or 0.2 M NaCl with the capping polyelectrolyte being PAH or PSS. Following dynamic testing of each sensor configuration, steady-state glucose response profiles were obtained. The sensitivity and analytical range were extracted, and the values for each film composition were plotted for comparison (Figure 5.3).

First, it is obvious that the general trend of decreasing sensitivity and increasing range with increasing film thickness is present for all architectures. The changes in sensitivity are significant (P<0.05) for all cases except for PAH-terminated 10.5 and 15.5 films constructed with (P=0.065) and without added salt (identical values, P=1). Increases in range with increasing film thickness are significant (P <0.05) in all cases of coatings constructed with salt, whereas significant differences are only present when comparing the thinnest (5/5.5) and thickest (15/15.5 bilayers) constructed without added salt. Second, when comparing films constructed without added salt, there is also a significant difference between the response properties when films are terminated with PSS and PAH. Specifically, sensors coated with PAH-capped nanofilms are significantly less sensitive (P<0.001) and have significantly wider range (P <0.02) than the counterpart films with PSS final layers, regardless of the number of layers deposited; in these cases the difference increases with thickness. Since these comparisons are for films varying only by one added layer of PAH, these results suggest that PAH presents a

substantial reduction in J_G/J_O. This observation is likely due to the fact that PAH is more hydrophobic than PSS, which reduces the transport of glucose. This observation also matches previous reports, which have noted that the capping nanofilm layer can drastically affect molecular permeabilities; specifically, it was shown that glucose flux through nanofilms terminated with PAH is approximately 20% less than those terminated with PSS.[33] Adding one additional layer of PAH to 5 bilayers results in a film thickness increase of only 10%; however, this small modification leads to a substantial decrease in sensitivity (83%) and an even greater relative increase of the analytical range (138%). Similarly, for 10 and 15 bilayers, the addition of one PAH layer results in decreases of 88% and 84% in sensitivity and increases in range of 108% and 44%, respectively. It can be noted that the percentage increase in range is smaller for higher number of bilayers, which is generally expected as the diffusion barrier increases for increased number of layers.

In contrast, when salt is added to the assembly solutions, two important trends are evident. First, when comparing films assembled without salt to identical architectures constructed with added salt, the sensitivity decreases and increases for PSS and PAH, respectively, while the range values are inversely related. These differences in sensitivity are significant (P <0.005) for all cases except 5-bilayer PSS-terminated films (P=0.44); for range, the differences are significant (P <0.05) except for the thickest films (15 and 15.5 bilayers, P>0.2) and the 5-bilayer PSS-terminated films (P=0.96). Secondly, the differences are much less pronounced when comparing films with different terminal materials that were deposited from salt-containing solutions than those

deposited without salt; in fact, no significant difference (P <0.05) was obtained in any case.

These observations suggest some interesting influences of the nanofilms on glucose transport. First, it is noteworthy that films assembled with 0.2 M NaCl have been reported to possess a 25% increased thickness–from 2 nm to 2.5 nm for each bilayer–than those assembled in the absence of NaCl;[39,41,55] therefore, if the changes were purely related to film thickness (i.e. not changes in film density), the relative flux would be expected to decrease with added salt. This explanation could arguably match the observations for PSS-terminated films, excluding the 5-bilayer case; this latter case could be a special situation where the 5-bilayer films without salt did not yet arrive at homogeneous coverage. The expected trend of decreased sensitivity due to relative increase in film thickness is observed when 10 and 15 PSS-capped nanofilm bilayers assembled without salt and with 0.2 M NaCl are adsorbed to the sensor surface.

On the contrary, when comparing response characteristics of films capped with PAH layers, the opposite trend is observed: a significant *increase* in sensitivity is seen when salt is added. A change in thickness with added salt cannot explain this behavior; a decrease in film density with salt would match these results, but this explanation would fall short for PSS-terminated films. Thus, neither of these phenomena can explain the observations in every case.

A final comparison suggests a third possible reason for the observed behavior. When comparing films constructed from solutions with added salt, the differences between films terminated with different materials are much less substantial than in the

no-salt case. The range values are not significantly different when comparing films of the same number of coating cycles, and the sensitivity values vary little. In fact, if we consider the no-salt cases to represent films with a "purer" outer surface of the terminal material, the trend that is observed when salt is added is the films "look" more like the other material present in the film. In other words, the addition of salt appears to blend the contributions of the materials present, effectively averaging the individual effects and thereby reducing the significance of the capping layer in determining the overall glucose flux. This concept is supported by other reports on the increasing interdigitation of nanofilm layers with thickness and adsorption solution ionic strength.[41,55,56,63]

In brief, added counterions screen charges along the polyelectrolyte chains, resulting in increasing coiling and folding of molecules. Films assembled using more coiled molecules have more looping and protruding regions, and are less dense, which means they are thicker, lower density have less internal compensation (pairing of ionized moieties with those from previously adsorbed molecules), and allow more penetration from adsorbing molecules. Thus, the materials have less discrete boundaries (this is why they have been called "fuzzy")[35] and therefore the contributions of the individual layers are less discrete as well. While additional work on direct measurements of glucose flux and diffusion coefficients through various film architectures are currently in progress, these findings suggest several different means of tuning nanofilm transport properties to precisely engineer sensor response characteristics: thickness, adsorption conditions, composition and terminal layer.

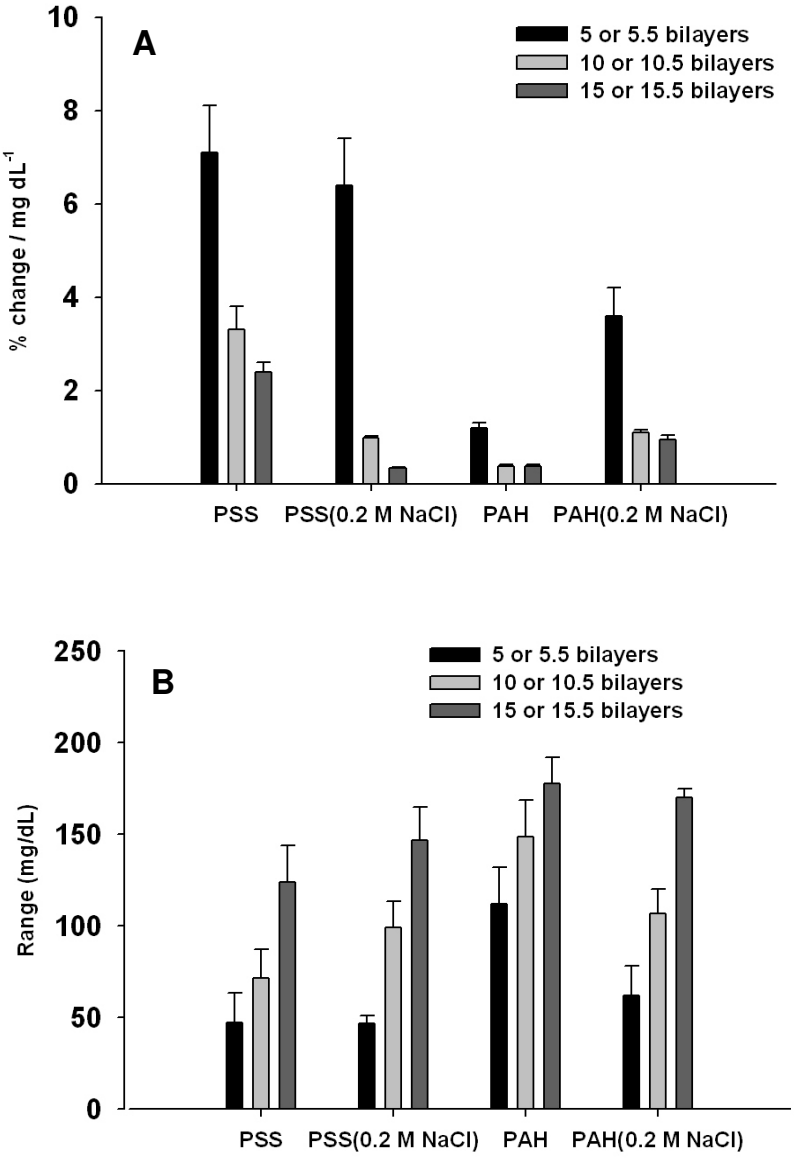

Figure 5.3 Sensor response characteristics for sensor configurations (A: sensitivity; B: range) based on different capping polyelectrolytes (PAH or PSS), assembly ionic strength (0 or 0.2 M NaCl), and number of nanofilm bilayers (5/5.5, 10/10.5, or 15/15.5) adsorbed to the sensor surface. Note that PSS-terminated films had an integer number of bilayers, whereas PAH-capped films had half-bilayer final values.

5.4 Conclusion

Highly sensitive microparticle enzymatic sensors with tunable response properties have been demonstrated using glucose as a model analyte. These sensors rely on optical transduction of oxygen levels within microscale sensors to indirectly determine bulk glucose levels. To obtain glucose-limited oxygen concentrations within the sensors, mass transport-limiting nanofilms were adsorbed to the sensor surface. By simply adjusting film assembly conditions, device sensitivity could be tuned to pinpoint hypo- (0-80 mg/dL), normo- (80-120 mg/dL), and hyperglycemic levels (>120 mg/dL). Nevertheless, the maximum linear range achieved with 15 bilayers was less than 200 mg/dL, whereas an ideal glucose sensor is expected to exhibit a linear response up to mg/dL. By extrapolating the results obtained, it is estimated that the sensors will have to be coated with *ca.* 60 bilayers of PAH/PSS in 0.2 M NaCl to obtain a linear response up to 600 mg/dL. Depositing 60 bilayers of polyelectrolyte on microparticle will be a labor-intensive and time-consuming task. Moreover, an increased tendency of microparticle aggregation is observed with increasing number of bilayers, which is extremely undesirable for the purpose of quality control. Also, the extension of response range by increasing the thickness of NF coating is always accompanied with a penalty, which is a decrease in sensitivity. Therefore, while these results suggest one pathway to achieving the goal, there is a need to investigate other effective ways of increasing the response range of such sensors.

6 ROLE OF POROSITY IN TUNING THE RESPONSE RANGE

6.1 Introduction

To address the problem of limited oxygen and resulting limited response range, use of perm-selective nanofilms was discussed in Section 5. The application of nanofilm significantly reduced the influx of glucose without substantially affecting the transport of oxygen. This resulted in an increase in the ratio of oxygen to glucose concentration inside the sensors, thereby extending the response range of sensors. However, the fabrication of sensors that exhibit a linear response range up to 600 mg/dL is not practical using only PAH/PSS nanofilms.

The other approach to addressing the problem is to increase the influx of oxygen into the matrix. It was hypothesized that the ratio of glucose to oxygen concentration can be reduced by *increasing the porosity of microspheres*, which will result in an improved oxygen transport and thereby lead to an extended response range. In this case, the effective transport of glucose will be minimally affected as it is mostly controlled by the outer NF coating. This hypothesis may be explained by calculating the effective diffusivity for glucose and oxygen through a semi-infinite plate shown in Figure 6.1, which consists of two different regions of thickness d_1 and d_2. In this case, Region 1 can be assumed as a perm-selective NF (d_1=65 nm), and Region 2 can be assumed as the sensor matrix (d_2=3 μm), which could be either of extremely low porosity (0.005) or very high porosity (0.6). It must be noted that Region 1 is same for both figures; whereas, Region 2 differs in porosity.

For our initial modeling purposes, it has been assumed that both matrices had the same tortuosity. Based on the known diffusivities of substrates through the given materials,[21] the effective diffusivity ($D_{e,i}$) can be estimated using:[64]

$$D_{e,i} = \frac{d_1 + d_2}{\frac{d_1}{D_{1,i}} + \frac{d_2}{D_{2,i}}} \qquad (6.1)$$

where $D_{1,i}$ and $D_{2,i}$ are the diffusivities of a substrate in Region 1 and 2, respectively. In this case, glucose and oxygen are the substrates. Diffusivities of glucose and oxygen in Region 1, which is PAH/PSS NF, are already known. [21,30] For Region 2, the diffusivities of substrates can be estimated by multiplying the diffusivity of substrates in water to the porosity of the matrix.[21] For the matrix with extremely low porosity with NF on its left (left figure), the effective diffusivity of glucose and oxygen can be estimated using Equation 6.1, they were calculated to be 1.4×10^{-8} and 1.01×10^{-8} cm^2/s, respectively; therefore, the ratio of glucose to oxygen diffusivity for algilica matrix is *ca.* 1.4. In contrast, for the matrix with high porosity, the estimated ratio is ca. 0.0075. This illustrates how the ratio of glucose to oxygen transport rate can be manipulated by varying the porosity of the sensor matrix. In this example a semi-infinite geometry was considered for simplicity, however, this general explanation will also hold true for other geometries.

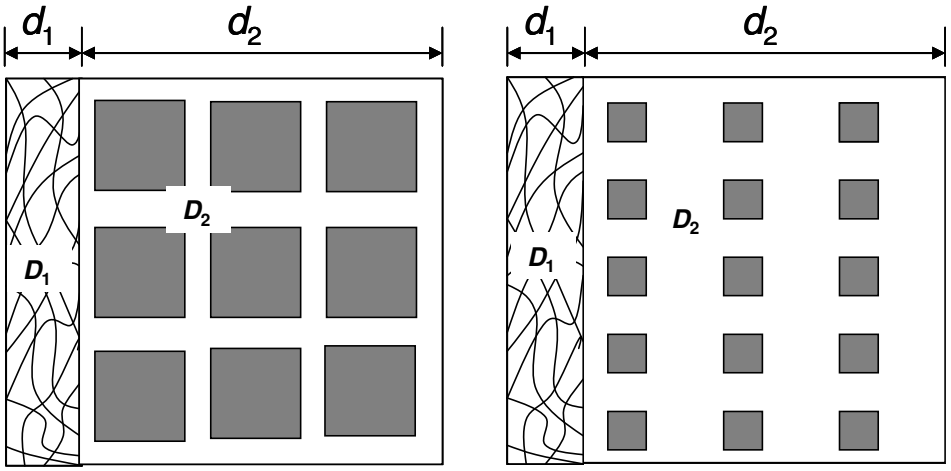

Figure 6.1 Semi-infinite plate model for a low-porosity matrix (porosity = 0.005) of thickness, d_2, with PAH/PSS NF of thickness, d_1, on its left side (left). Semi-infinite plate model for a high porosity matrix (porosity=0.6) with similar dimensions and NF on its left side (right). White space represents voids/pores in the matrix through which diffusion can occur. No transport can occur through the solid blocks.

In this work, the effect of microsphere porosity on the predicted sensor response was studied using a mathematical model, which was validated through experiments. It has been shown that by tailoring the porosity of microspheres, sensors exhibiting a linear response up to 600 mg/dL of glucose can be designed.

6.2 Experimental

6.2.1 Chemicals

Amine functionalized Zorbax® microspheres with average diameter and porosity of ~5.5 µm and 0.6, respectively, were obtained from Agilent. Pt(II) octaethylporphine (PtOEP, Frontier Scientific), Pt(II) meso-Tetra (4-carboxyphenyl) porphine (PtP, Frontier Scientific), dimethyl sulfoxide (DMSO, Aldrich), glucose oxidase (GOx, EC 232-601-0, Sigma), *N*-(3-dimethylaminopropyl)-*N´*-ethylcarbodiimide hydrochloride

(EDC, Fluka), *N*-hydroxysulfosuccinimide sodium salt (NHSS, Toronto Research Chemicals Inc.), and sodium acetate (Sigma) were used to prepare PtOEP/GOx-doped "algilica" and PtP/GOx-doped Zorbax® microspheres. BCA™ protein assay kit was acquired from Thermo Scientific to determine the protein loading. Poly-(allylamine hydrochloride) (PAH, MW 70 kDa, Aldrich), poly-(sodium 4-styrenesulfonate) (PSS, MW 70 kDa, Aldrich), and sodium chloride (Sigma) were used during the deposition of multilayer thin films. Additionally, rhodamine B isothiocyanate (RITC, Aldrich) was conjugated to PAH (PAH-RITC), which was also used in LbL NF deposition. β-D-glucose (MP Biomedicals, Inc.), oxygen and nitrogen gas (PraxAir), and PBS (Sigma) were used during dynamic testing. All necessary pH adjustments were performed using titrations of 1.0 M HCl and 1.0 M NaOH (Fluka). All chemicals listed above were reagent grade and used as received. Ultrapure water with a resistivity greater than 18 MΩ-cm was used to prepare all aqueous solutions. All experiments were conducted at ~25 °C and the oxygen concentration in the glucose and buffer reservoirs was maintained at 277 μM (air saturated) by aeration.

6.2.2 Sensor preparation and characterization

Hybrid alginate-silica "algilica" microspheres were synthesized using a protocol detailed elsewhere.[18] Dried algilica and Zorbax® microspheres were sent to an external lab for surface area and pore size analysis (Delta Lab, North Huntingdon, PA). A particle size analyzer (ElZone 540, Micromeritics®) was used to measure the concentration and size distribution of the microspheres. Algilica microspheres were loaded with PtOEP and

GOx, and subsequently coated with nanofilms comprising [PAH-RITC/PSS]$_2$-[PAH/PSS]$_{23}$-PAH nanofilms using LbL technique.[19]

As PtOEP is extremely hydrophobic, it was not possible to immobilize it into the Zorbax® microparticles using insolubility induced precipitation. A different type of platinum porphyrin dye (PtP) was employed as an indicator dye. PtP has four carboxyl moieties, which can be coupled to the amine moieties on the surface of Zorbax microparticles® (Figure 6.2). To prepare Zorbax®-based glucose sensors, amine-functionalized Zorbax® microspheres were suspended in a phosphate buffered solution (pH = 9.0) containing 50 mg/mL of both EDC and NHSS. PtP in DMSO was added to a final concentration of 50 μM and the mixture was vortexed for ~2 hours. Dye-labeled microspheres were rinsed twice in deionized (DI) water, and then suspended in EDC/NHS solution (50 mg/mL) in actetate buffer (pH = 5) to activate the free caboxylate moieties of PtP. Subsequently, GOx (35 mg/mL) dissolved in bicarbonate buffer was added to the dye-labeled microspheres and the solution was vortexed for one hour, which led to the coupling of amines moieties of GOx to the carboxylate moieties of PtP. Finally, the microspheres were rinsed with DI water and coated with [PAH-RITC/PSS]$_2$-[PAH/PSS]$_{23}$-PAH NFs using LbL technique. Thus the two batches of sensors comprised of microspheres that have significantly different porosity, however, same NF coating.

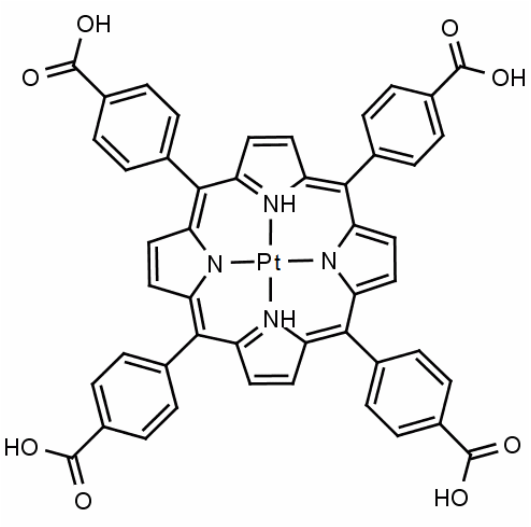

Figure 6.2 Structure of PtP.

Zorbax® microspheres doped with PtP were also separately loaded with RITC-GOx and were imaged using confocal microscopy (Leica TCS SP5) to determine the homogeneity of PtP and GOx distribution inside the microspheres. A 63X oil objective with pinhole set to 1 Airy was used for imaging.

Separate batches of indicator (i.e., PtOEP or PtP) and GOx-loaded algilica and Zorbax® microspheres were prepared without NF coating to determine the concentration of immobilized GOx using BCA protein assay.[65] The sensor response was experimentally determined using a flow-through system controlled via a custom-designed software suite (LabVIEW, National Instruments).[18] Briefly, ~10^7 microspheres were immobilized using double-sided pressure-sensitive adhesive attached to a glass slide, which was mounted inside a custom-designed reaction chamber made from Delrin containing a rubber gasket. A bifurcated optical fiber bundle was coupled into the bottom of the reaction chamber to excite the sensors and collect the emitted

fluorescence. A green LED with emission peak at ~518 nm was used as an excitation light source. Emission signals were monitored using a charge-coupled device array detector (USB 2000, OceanOptics). Emission intensity was recorded at 580 and 645/675 nm, corresponding to the emission maxima for RITC and PtOEP/PtP, respectively. The reaction chamber was placed inside an incubator at 37°C and all solutions were prepared in phosphate-buffered saline (PBS) to maintain physiological conditions.

Method 1 described in Section 3 was used to estimate sensitivity and range from the experimental data.[19] Sensitivity and range were estimated similarly for the theoretically predicted data.

6.2.3 Theory

The redox reaction of glucose and oxygen catalyzed by GOx is given by reaction scheme described in Section 2 (Equation 2.5). Figure 6.3 depicts the model for the glucose sensing scheme. When sensors are exposed to bulk glucose and oxygen, these substrates diffuse inside the sensor matrix and trigger reaction (Equation 2.5). Within a few seconds, steady state is attained within the microspheres, after which the substrate spatial and average concentrations depend on the delicate balance between reaction and diffusion rates. The reaction-diffusion model has been used to describe such phenomena (Equation 3.1).[58] As bulk oxygen is assumed to be fixed, the diffusion rate of glucose, and consequently the consumption rate of oxygen inside the sensors primarily depend on bulk glucose concentrations. With increased glucose level, we expect to observe higher reaction rates, resulting in depleted oxygen levels inside microspheres; as the

transduction mechanism is based on quenching of luminescence by oxygen, increased emission intensity will be observed for increased glucose levels.

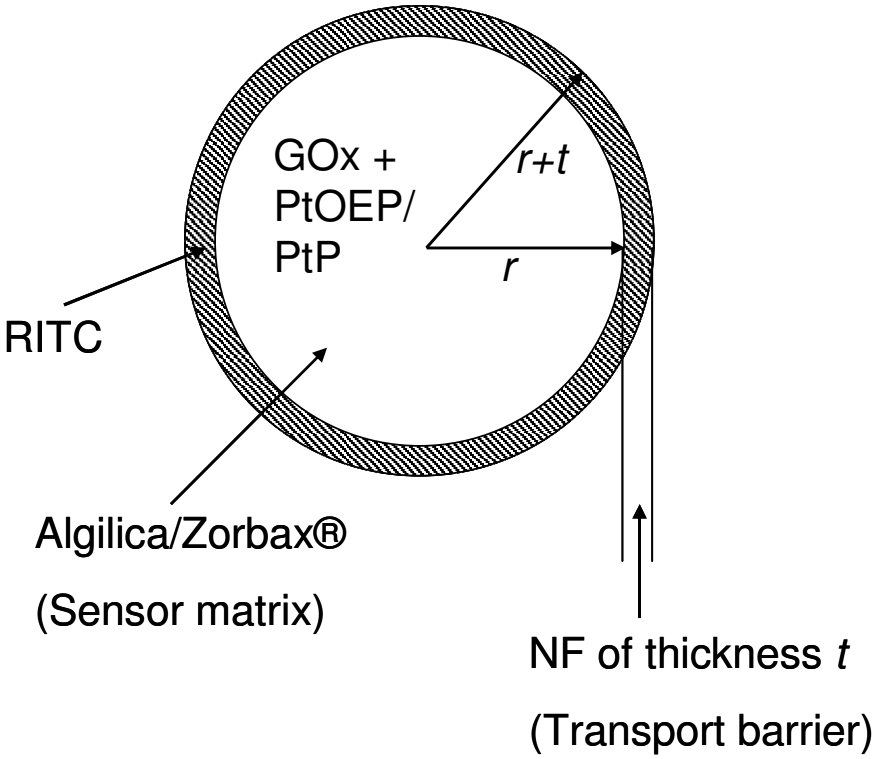

Figure 6.3 Schematic of microsphere sensors with dimensions used in the model.

For modeling purposes, reaction scheme (Equation 2.5) results in a system of six coupled partial differential equations (PDEs) that describe the behavior of the system in time and space for each individual particle. In this case the system of equation consists of six equations, where each equation gives the solution for one of the six reactive specie (i), which are: G, O_2, E_{ox}, $E_{red}P_1$, E_{red}, $E_{ox}P_2$. D_i and R_i represent the diffusivity and reaction rates of the respective species involved in the reaction scheme.

For PtOEP immobilized in the algilica matrix, the previously determined value of 14,200 M^{-1} [18] was used for K_{SV}. As the phosphorescence lifetimes of PtOEP and PtP are similar – 95 and 90 µs, respectively [23] – the K_{SV} of PtP immobilized in Zorbax® was also assumed to be 14,200 M^{-1} for simulation purposes. Percentage increase in luminescence at each glucose level was then estimated by taking luminescence at zero glucose as the base signal.

Later, K_{SV} for PtP immobilized in Zorbax® was experimentally-determined to be 10,900 M^{-1}. Using this value of K_{SV} would have resulted in ~9% decrease in the predicted percent change in luminescence intensity values.

6.2.4 Simulations

The model was used to predict the effect of porosity and microsphere size on sensor response. In addition, the response of sensors made from algilica and Zobrax® were also simulated to test the validity of model. Table 6.1 contains the value of diffusion coefficients for all reactive species in both matrix as well as nanofilm. Diffusivities of glucose and oxygen in water are 3.94×10^{-6} and 2×10^{-5} cm^2/s, respectively, which were estimated using Wilke-Chang equation.[66] The diffusivity for glucose in PAH/PSS nanofilms was 9.87×10^{-10} cm^2/s.[30] Under the assumption that diffusion occurs through water in the pores of the nanofilms and matrix, the diffusivity of oxygen in the NF was estimated by multiplying its diffusivity in water to the ratio of glucose diffusivity in NF and water. Using this process oxygen diffusivity in the nanofilm was determined to be 2.52×10^{-7} cm^2/s. Diffusivities in microspheres were estimated by multiplying the porosity of the matrix with the diffusivity of substrate in

water.[67,68] As a result, the diffusivity of glucose in algilica and Zorbax were estimated to be 1.97×10^{-8} and 2.36×10^{-6} cm^2/s, respectively. Likewise, the diffusivity of oxygen in algilica and Zorbax was estimated to be 1×10^{-7} and 1.2×10^{-5} cm^2/s, respectively. It must be noted that the effect of tortuosity in the matrix was not considered, as we do not currently have a realistic estimate for this value. Since the calculation of effective diffusivity involves a ratio of porosity to tortuosity, a large value for tortuosity could further reduce the calculated values for effective diffusivity.

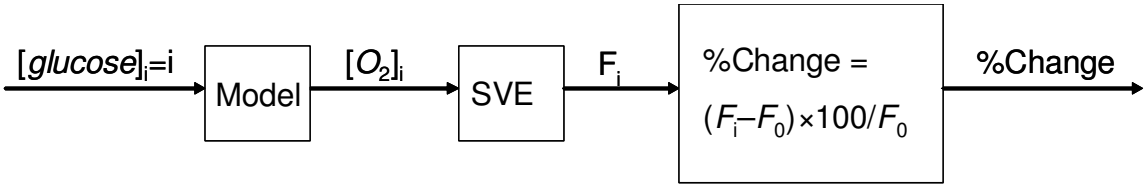

i = 0-33 mM in 1.5mM steps

Figure 6.4 Solution scheme for modeling the response of sensor.

A number of key assumptions were made to simplify the modeling, and consideration of these is necessary to properly interpret the results of the simulations and their relationship to the experimental situation. The model only predicts the response of a single sensor, whereas the experimental response was obtained by immobilizing ~107 sensors in a spot of ~2 mm diameter. The sensor was assumed to be 12 μm algilica microsphere to simulate the response of algilica sensor, which was the number averaged size of the particles produced, as determined through size analysis. In all experiments, microspheres were coated with [PAH-RITC/PSS]2-[PAH/PSS]23-PAH NF. Therefore, the thickness of the NF coating was assumed to be 65 nm as it has been shown that the thickness of a single PAH/PSS bilayer deposited under similar condition was ~2.5 nm. 38,69 It was assumed that GOx and PtOEP are homogenously distributed inside the microspheres, which was confirmed via confocal microscopy 18. It was assumed that NFs and spheres are homogeneous and have unique, but constant, diffusivity for glucose, oxygen, and peroxide. The initial (ICs) and the boundary conditions (BCs) used for each chemical species has been tabulated in Table 6.1.

The flux at the center of the microsensor was assumed to be zero because of axial symmetry, resulting in zero concentration gradient. A constant concentration of each reaction species was used as the surface BC.

Table 6.1 Parameters used in modeling the response of microsphere sensors.

Chemical Specie (*i*)	**D_i (m^2/s) Alginate/Zorbax Microsphere and NF**	**R_i**	**IC Microsphere and NF**	**BC Center (*r=0*) Surface (*r=R+t*)**
Glucose	$1.97\times10^{-12}/236.40\times10^{-12}$ 9.87×10^{-14}	$-k_1[E_{ox}][G]$	C_G [a]	No flux C_G [a]
O_2	$1.00\times10^{-11}/120.00\times10^{-11}$ 2.52×10^{-11}	$-k_3[E_{red}][O_2]$	277 µM	No flux 140 µM
E_{ox}	0 0	$-k_1[E_{ox}][G]+$ $k_4[E_{ox}P_2]$	E_{GT} [b]	No flux 0
$E_{red}P_1$	0 0	$k_1[E_{ox}][G]-$ $k_2[E_{red}P_1]$	0	No flux 0
E_{red}	0 0	$k_2[E_{red}P_1] -$ $k_3[E_{red}][O_2]$	0	No flux 0
$E_{ox}P_2$	0 0	$k_3[E_{red}][O_2]-$ $k_4[E_{ox}P_2]$	0	No flux 0

[a] C_G was varied from 0 to 33 mM at increments of 1.5 mM.

[b] E_{GT} = 0.2 mM and 1 mM for algilica and Zorbax microspheres, respectively .

6.3 Results and Discussion

The size distribution of algilica microspheres was shown in Figure 5.2. It has also been previously confirmed that the protocol used for PtOEP and GOx immobilization results in a homogeneous distribution of both within the algilica microparticles. The concentration of immobilized GOx within algilica microparticles was found to be *ca.* 0.2 mM. The average porosity and pore size for algilica matrix was found to be 0.005 and 18

nm, respectively. For proper perspective, it must be noted that the average diameter of GOx is *ca.* 8 nm.

The size distribution of Zorbax® microspheres is shown in Figure 6.5. The number-weighted average particle diameter for Zorbax® was found to be *ca.* 5.5 µm. The concentration of immobilized GOx in the Zorbax® microspheres was found to be 1 mM, which is 5 times higher than the concentration of GOx in algilica. Using porosimetry, the average porosity and pore size of Zorbax® matrix was determined to be 0.6 and 8.8 nm, respectively.

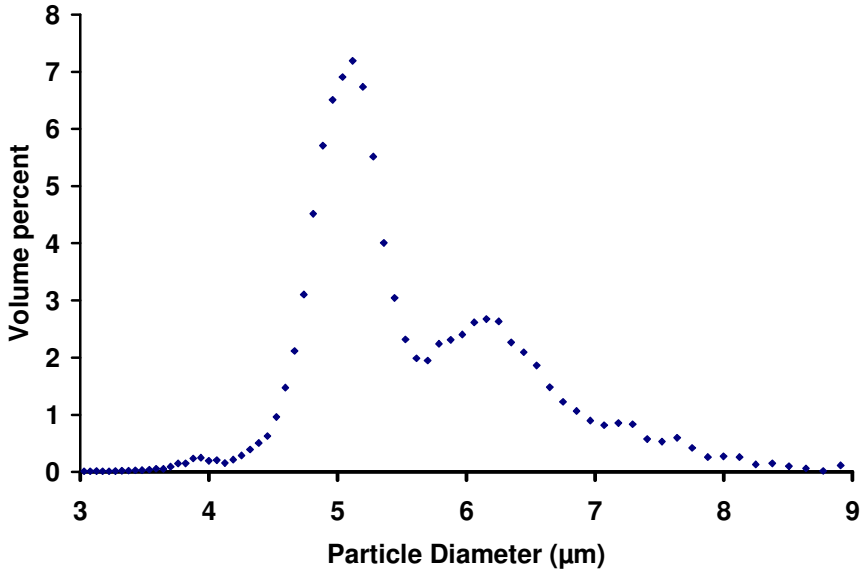

Figure 6.5 Size distribution of Zorbax® microparticles

Micrographs depicting the distribution of PtP and RITC-GOx within Zorbax® microspheres have been shown in Figure 6.6, which indicates that the distribution of PtP and GOx is nearly homogeneous.

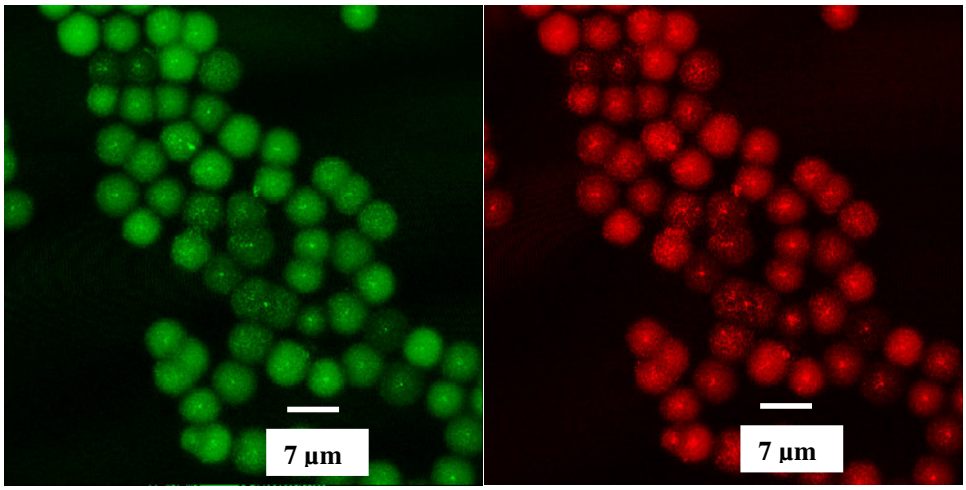

Figure 6.6 Confocal micrographs of Zorbax® microparticles loaded with GOx-RITC (left) and PtP (right).

Figure 6.7 (top) contains a graph of the theoretically-predicted response of 12 µm microsphere sensors, with varying microsphere porosity, coated with 65 nm NFs. The increased porosity results in an expected increase in the response range accompanied by reduced sensitivity. This trend is due to increased oxygen transport. Algilica microspheres, for which the average porosity was experimentally determined to be 0.005, are expected to exhibit a linear response up to approximately 200 mg/dL. In contrast, microspheres of the same size with higher porosities are expected to exhibit a linear response over the entire physiological glucose range (0-600 mg/dL) due to

improved oxygen transport. The penalty for achieving a higher range, however, is greatly reduced sensitivity. The ratio of sensitivities of sensors made from microspheres of porosity 0.005 to the sensors made from microspheres of porosity 0.6 is estimated to be approximately 18. These data lead to the inference that microspheres with porosity somewhere in between 0.01 and 0.1 can be used to make sensors that exhibit linear response up to 600 mg/dL with maximized sensitivity.

The effect of microsphere size on the sensor response, assuming microsphere porosity and NF thickness are held constant at 0.005 and 65 nm, respectively, is shown in Figure 6.7 (bottom). An increased particle size is expected to result in an improved sensitivity, as well as an increased response range. In smaller particles, lower consumption of oxygen and glucose is expected; therefore, it is reasonable to expect an increase in sensitivity with increasing size of the microspheres, as sensitivity is directly proportional to the difference between the average oxygen concentration in the bulk and inside the microspheres. In addition, the increase in particle size results in an increase in net transport resistance to substrates, which further leads to an increased response range. The sensitivity of sensors comprising of 12 μm spheres is estimated to be approximately 1.5X the sensitivity of the sensors comprising of 6 μm spheres.

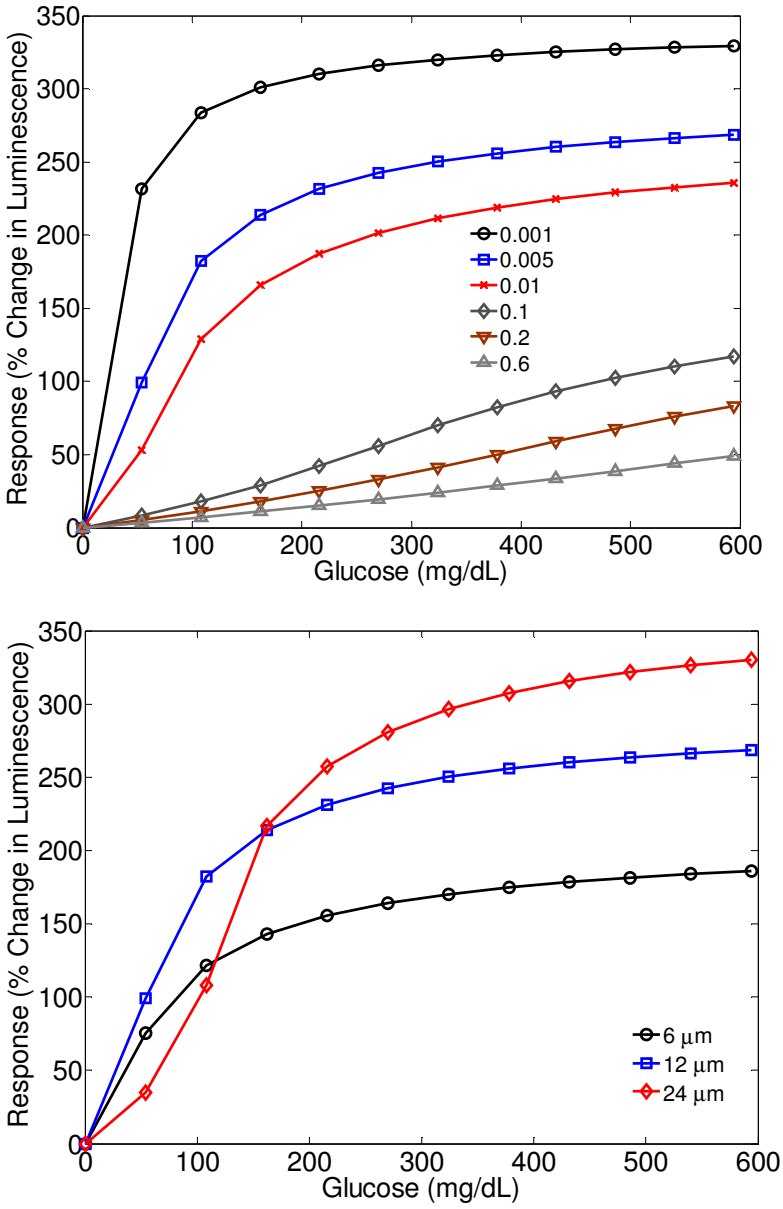

Figure 6.7 The effect of porosity on the response of 12 µm particles (top), and the effect of particle size on the response of microspheres with average porosity of 0.005 (bottom).

Figure 6.8 (top) contains the theoretically-predicted response of algilica (diameter = 12 μm, porosity = 0.005) and Zorbax® (diameter = 7 μm, porosity = 0.6) microsphere sensors. From these predictions, the algilica-based sensors are expected to exhibit a response range of approximately 200 mg/dL, while the Zorbax®-based sensors are predicted to demonstrate a highly linear response throughout the entire physiological glucose range. However, the estimated sensitivity of Zorbax®-based sensors is also approximately 24 times lower than the sensitivity of algilica-based sensors.

Figure 6.8 (bottom) is a graph of the experimentally-determined response profile of both sensor types. Interestingly, the mrasured trends in range and sensitivity match very well with the theoretical predictions; however, the sensitivity values were higher than the values predicted from modeling. This discrepancy might be explained in part by the fact that experimental measurements consider the response of an entire population of sensors, which are in close proximity to one another; therefore, some sensors are exposed to average oxygen levels lower than 277 μM, which was used as a surface boundary condition in the modeling. Thus, the actual depletion of oxygen is perhaps even higher than the depletion predicted via modeling, which explains why a higher sensitivity might be observed in experiments. The experimental response determined for sensors made from Zorbax® microspheres exhibited a linear correlation with glucose (R^2>0.90) throughout the entire physiological glucose range (0-600 mg/dL).

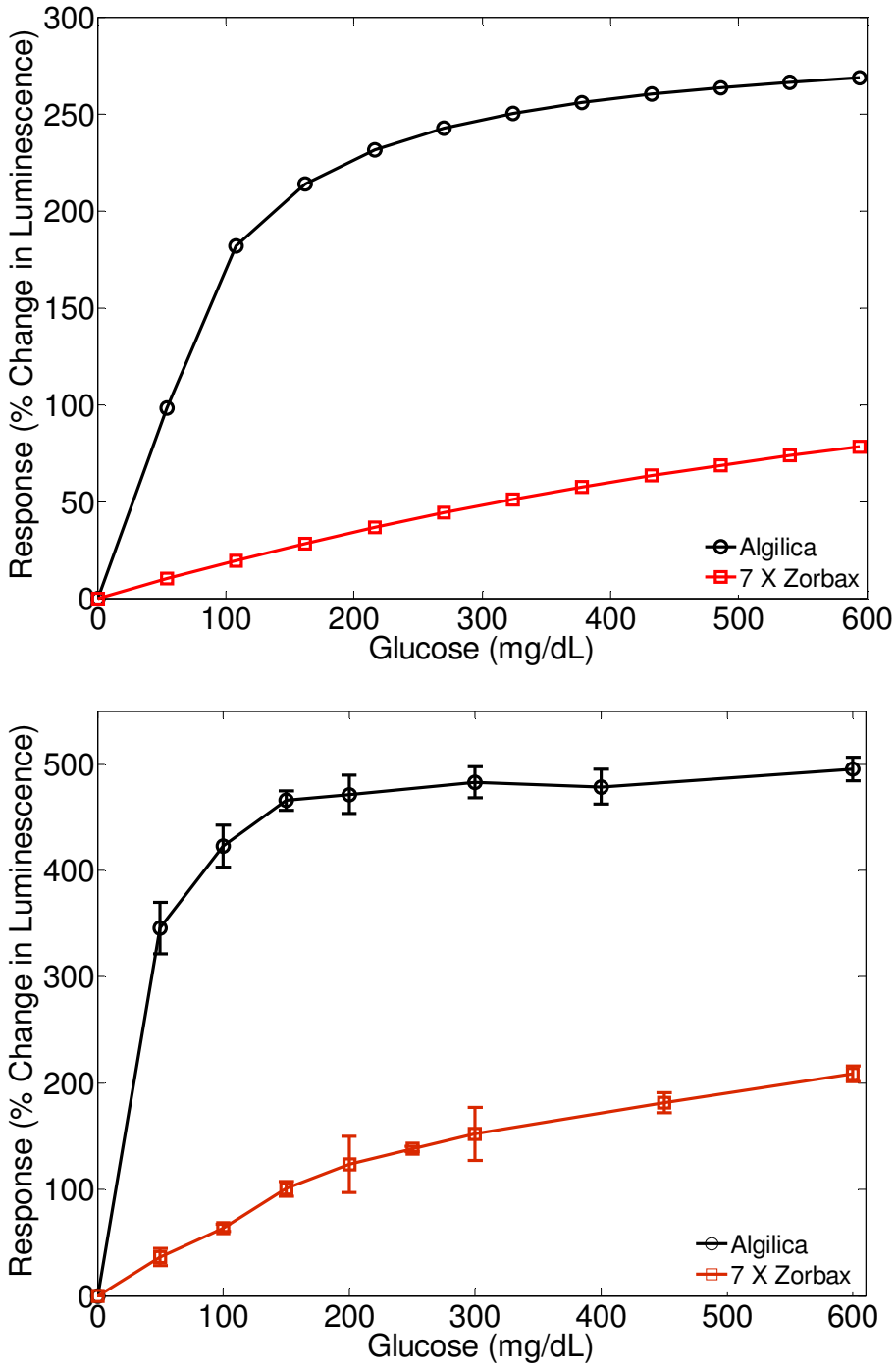

Figure 6.8 Theoretical (top) and experimental (bottom) response of algilica and Zorbax® microspheres coated with 65 nm PAH/PSS NF. The error bars indicate one standard deviation obtained from three replicate measurements at different time points.

6.4 Conclusion

This research demonstrates that, in addition to changing the NF thickness and its deposition conditions, porosity and size of the microsphere matrix can also be varied to tailor the response range and sensitivity. This provides additional options for sensor fabrication because amine- or carboxylate-functionalized microspheres with user-specified size distribution, porosity, and pore volume can be produced using a standard sol-gel method.[70] From the modeling we predict that sensors constructed from ~12 μm microspheres having an effective porosity between 0.01 and 0.1 with ~65 nm PAH/PSS LbL coatings would respond over the entire physiological glucose range with maximized sensitivity.

In summary of Section 5 and 6, it is evident that the sensitivity and response range of microparticle-based glucose sensors can be fine-tuned to fit any desired application by controlling the thickness, composition and the deposition conditions of the nanofilm, and porosity of the microsphere. Such sensors exhibit very high sensitivity and selectivity as compared to enzyme-based electrochemical sensors, which makes them highly promising for *in vivo* glucose monitoring. Nevertheless, there is still a concern about the operational lifetime of such sensors due to the use of sensitive proteins. Therefore, the longevity of such microparticle-based enzymatic sensors must be investigated to determine the viability of this sensing approach for long-term *in vivo* glucose monitoring.

7 ENHANCING THE LONGEVITY OF MICROPARTICLE-BASED GLUCOSE SENSORS*

7.1 Introduction

The aforementioned microparticle-based sensors exhibit very high sensitivity and selectivity with a response time of less than one minute *in vitro*. In addition, we have shown that the response range and sensitivity can be tailored by adjusting the thickness, composition, and conditions of the nanofilm (NF) deposition, which can be precisely controlled using the layer-by-layer (LbL) assembly technique, as well as the porosity of the matrix.[19,30,71] While these findings make the sensing approach very promising, there is a need to maximize the operational lifetime to make long-term *in vivo* glucose monitoring viable.

To understand the factors that contribute to sensors lifetime, previous work on electrochemical biosensors was reviewed. Glucose sensors based upon the amperometric detection of oxygen concentration have been extensively investigated, [3,53,72-77] and it is clear that the peroxide produced in the oxidation reaction is the primary cause of enzyme destruction. It has also been demonstrated that the longevity of GOx-based sensors can be substantially improved via incorporation of a second enzyme, catalase (CAT).

---

*Parts of this section have been reprinted with permission from "Enhancing the longevity of microparticle-based glucose sensors towards one month continuous operation" by Singh, S.; McShane, M. *Biosensors and Bioelectronics* **2010**, *25*, 1075-1081, Copyright [2010] by Elsevier, DOI: 10.1016/j.bios.2009.09.026

Hydrogen peroxide, which deactivates GOx via hydrolytic cleavage of peptide bonds, is a substrate for CAT; therefore, the incorporation of CAT minimizes the exposure of GOx to peroxide, resulting in sensors that exhibit enhanced stability.[53] Since our optical probes employ GOx as the catalyst, we hypothesized that the longevity of our sensors can be similarly improved by coimmobilizing GOx and CAT into the sensor matrix. Accordingly, the goal of this study was to assess the stability of microsphere-based glucose sensors with and without CAT. For this, a mathematical model was created to estimate the effect of immobilized enzyme (GOx and CAT) concentrations on the stability of sensor responses, and prototype sensors were then prepared and the models were validated through experimentation. The findings of this study point the way forward in the development of stable microparticle-based glucose sensors for *in vivo* application.

7.2 Experimental

7.2.1 Chemicals

Sodium alginate (low viscosity, 250 centipoise, MW 12-80 kDa), (3-glycidyloxypropyl)trimethoxysilane (GPTS), and ammonium hydroxide were obtained from Sigma and used for the synthesis of mesoporous alginate-silica microspheres. Pt(II) octaethylporphine (PtOEP, Frontier Scientific), tetrahydrofuran (THF, Fluka), glucose oxidase (GOx, EC 232-601-0, 198 units/mg of solid, Sigma), catalase (CAT, EC 232-577-1, 2950 units/mg of solid, Sigma), *N*-(3-dimethylaminopropyl)-*N´*-ethylcarbodiimide hydrochloride (EDC, Fluka), *N*-hydroxysulfosuccinimide sodium salt (NHSS, Toronto Research Chemicals Inc.), and sodium acetate (Sigma) were used to

prepare PtOEP/GOx-doped algilica particles. Poly-(allylamine hydrochloride) (PAH, MW 70 kDa, Aldrich), poly-(sodium 4-styrenesulfonate) (PSS, MW 70 kDa, Aldrich), and sodium chloride (Sigma) were used during the deposition of multilayer thin films. Additionally, rhodamine B isothiocyanate (RITC, Aldrich) was conjugated to PAH (PAH-RITC), which was also used in LbL NF deposition. β-D-glucose (MP Biomedicals, Inc.), oxygen and nitrogen gases (PraxAir), and phosphate-buffered saline (PBS) (Sigma) were used during dynamic testing. All necessary pH adjustments were performed using titrations of 1.0 M HCl and 1.0 M NaOH (Fluka). All chemicals listed above were reagent grade and used as received. Ultrapure water with a resistivity of greater than 18 MΩ-cm was used to prepare all aqueous solutions. A fixed dissolved oxygen concentration was achieved by aerating the solution with a gas mixture of nitrogen and oxygen. All experiments were conducted at 37°C and the oxygen concentration in the glucose and buffer reservoirs was maintained at 140 μM to mimic skin environment.[62]

7.2.2 Sensor preparation and characterization

Algilica microspheres were synthesized using a protocol detailed elsewhere.[18,19] Briefly, alginate and GPTS were mixed in water, and ammonium hydroxide was added to the mixture to initiate microsphere formation. Dried microspheres were sent for surface area and pore size analysis (Delta Lab, North Huntingdon, PA). A particle size analyzer (ElZone 540, Micromeritics®) was used to measure the concentration and size distribution of the microspheres. The indicator dye, PtOEP, was loaded into the microspheres via insolubility-induced precipitation.[18,19] Subsequently, two batches of

PtOEP-loaded microspheres (~10^8 microspheres/batch) were incubated in a 250 µL acetate buffer solution (pH 4) containing enzyme. The first batch was incubated in a 0.2 mM GOx solution and the second batch in a GOx and CAT solution in which the concentration of each enzyme was 0.1 mM. A UV-Vis spectrophotometer (Lambda 45, Perkin Elmer) was used for absorbance measurements to determine enzyme uptake into microspheres.[78] The dye loaded microparticles were also loaded with RITC-GOx and FITC-CAT using the same protocol that was used for GOx and CAT loading. The distribution of RITC-GOx and FITC-CAT was determined using confocal microscopy. All images were obtained using a 63X oil objective with pin hole set to 1 Airy.

After four hours of incubation with enzyme, particles were rinsed with water and incubated in 50 mg/mL of EDC and NHS solution for two hours for covalent coupling of protein amines to alginate carboxylate moieties. After rinsing, the particles were coated with [PAH-RITC/PSS]$_2$-[PAH/PSS]$_{23}$-PAH NFs using the LbL technique.[18] The NFs act as a transport barrier, allowing for the tailoring of the response range and sensitivity.[19] As before, the reference dye, RITC, was conjugated to PAH using a standard amine labeling protocol.

The sensor response was experimentally determined using a flow-through system controlled via a custom-designed software suite (LabVIEW, National Instruments), which has been described elsewhere.[18] Precise control over dissolved oxygen concentration was attained via mass flow controllers connected to oxygen and nitrogen supplies. Briefly, ~10^7 microsensors were immobilized using double-sided pressure-sensitive adhesive attached to a glass slide, which was mounted inside a custom

designed plastic reaction chamber. Emission was recorded at 580 and 645 nm, corresponding to the emission maxima for RITC and PtOEP, respectively. The reaction chamber was placed inside an incubator at 37°C and all solutions were prepared in PBS to maintain physiological conditions.

7.2.3 Theory

The redox reaction of glucose and oxygen catalyzed by GOx has already been described in Section 2 (Equation 2.5). The catalytic consumption of H2O2 via CAT has also been described in Section 2 (Equation 2.6). If we combine the two reactions, it can be observed that glucose and oxygen are the consumed substrates. Also, it can be observed that in total there are nine reactive species, which are: glucose, oxygen, hydrogen peroxide, four forms of GOx, and two forms of CAT. Figure 7.1 depicts the model for the glucose sensing scheme. When sensors are exposed to bulk glucose and oxygen, these substrates diffuse inside the sensor matrix and trigger reaction (1) and, subsequently, reaction (2). In a few seconds, steady state is attained within the microspheres, in which the substrate spatial and average concentrations depend on the delicate balance between reaction and diffusion rates. The reaction-diffusion model has been used to describe such phenomena.58 It is important to notice that the above scheme assumes constant concentrations of enzymes, which may not be a realistic assumption.

Enzymes, like any other protein molecules, undergo degradation via different mechanisms, which has already been described in Section 2. All forms of GOx have been considered to be equally susceptible to spontaneous deactivation, which is given by first-order rate kinetics with rate constant denoted as ksGOx.53 Likewise, all forms of

CAT are equally susceptible to spontaneous deactivation with rate constant ksCAT. In addition to spontaneous deactivation, GOx and CAT are susceptible to peroxide-mediated degradation that occurs via hydrolytic cleavage of peptide bonds. The oxidized form of GOx is insusceptible to H2O2, but other forms are degraded by peroxide. This type of degradation follows second-order kinetics, where the rate is proportional to the product of the peroxide concentration and the concentration of the respective enzyme. The proportionality constants, also referred to as rate constants, are k7 for the complex form of GOx and k8 for the reduced form. Likewise, both forms of CAT undergo second-order peroxide-mediated deactivation, with rate constant k9.53,75,79 Both forms of deactivation have been considered in determining the rate expression shown in Table 7.1.

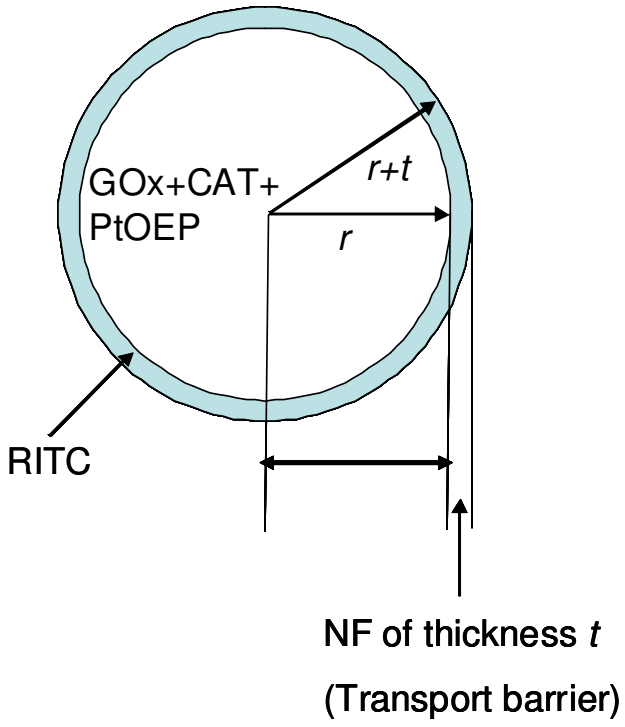

Figure 7.1 Schematic of microsphere sensors with dimensions used in the model.

The two reaction schemes can be combined together, resulting in a system of nine coupled PDEs that describe the behavior of the system in time and space. In the reaction-diffusion equation, i is the subscript denoting one of the nine reactive species, G, O_2, E_{ox}, $E_{red}P_1$, E_{red}, $E_{ox}P_2$, H_2O_2, I, and CAT. D_i and R_i represent the diffusivity and reaction rates of the respective species involved in the reaction scheme. To convert the predicted O_2 level to luminescence, the Stern-Volmer equation (Equation 3.2) was applied. For PtOEP immobilized in the algilica matrix, a previously-determined value for Stern-Volmer constant, K_{SV}, was used (14,200 M^{-1}).[18]

The rate constants k_1, k_2, k_3, k_4, k_5, k_6, k_{sGOx} and k_{sCAT} were obtained from the literature as follows: [49,51,53] k_1: 10^4 $M^{-1}s^{-1}$; k_2: 6000 s^{-1}; k_3: 2.1×10^6 $M^{-1}s^{-1}$; k_4: 1150 s^{-1}; k_5: 1.7×10^7 $M^{-1}s^{-1}$; k_6: 2.6×10^7 $M^{-1}s^{-1}$; k_{sGOx}: 9.2×10^{-8} s^{-1}; k_{sCAT}: 1.5×10^{-7} s^{-1}.

Table 7.1 contains the value of diffusion coefficients for all reactive species in algilica matrix as well as NF. Diffusivity of glucose, oxygen, and hydrogen peroxide in water was estimated using the Wilke-Chang equation.66 Diffusivity, D, for glucose in PAH/PSS nanofilms was obtained from literature.30 Under the assumption that diffusion occurs through water in the pores of the nanofilms and matrix, the diffusivity of oxygen and peroxide in the NF were estimated by multiplying their diffusivity in water to the ratio of glucose diffusivity in NF and water. The diffusivity in algilica was estimated by multiplying the porosity of the matrix (measured fractional porosity=0.005) with the diffusivity of substrate in water.[67,68] It must be noted that the effect of tortuosity in the matrix was not considered, as we do not currently have a realistic estimate for this value. Since the calculation of effective diffusivity involves a ratio of porosity to tortuosity, a

large value for tortuosity could further reduce the calculated values for effective diffusivity.

A number of key assumptions were made to simplify the modeling, and consideration of these is necessary to properly interpret the results of the simulations and their relationship to the experimental situation. The model only predicts the response of a single sensor, whereas the experimental response was obtained by immobilizing ~10^7 sensors in a spot of ~2 mm diameter. The sensor was assumed to be a 12 μm algilica microsphere, which was the number-averaged size of the particles produced, as determined through size analysis. In all experiments, microspheres were coated with [PAH-RITC/PSS]$_2$-[PAH/PSS]$_{23}$-PAH NF. Therefore, the thickness of the NF coating was assumed to be 65 nm, as it has been shown that the thickness of a single PAH/PSS bilayer deposited under similar conditions was ~2.5 nm.[38,69] Peroxide concentration at the surface of NF was assumed to be infinitesimally small, as there is no peroxide in the buffer and glucose solutions. It was assumed that GOx, CAT, and PtOEP are homogenously distributed inside the microspheres, which was confirmed via confocal microscopy.[18] It was assumed that NFs and spheres are homogeneous and have unique, but constant, diffusivity for glucose, oxygen, and peroxide. The initial (ICs) and the boundary conditions (BCs) used for each chemical species has been tabulated in Table 7.1. The flux at the center of the microsensor was assumed to be zero because of axial symmetry, resulting in zero concentration gradient. A constant concentration of each reaction species was used as the surface BC.

Table 7.1 Parameters used in modeling the response and longevity of microsphere sensors.

Chemical Specie (*i*)	D_i (m^2/s) Alginate Matrix and NF	R_i	IC Alginate Matrix and NF	BC Center (*r=0*) Surface (*r=R+t*)
Glucose	1.97×10^{-12} 9.87×10^{-14}	$-k_1[E_{ox}][G]$	C_G [a]	No flux C_G
O_2	1.00×10^{-11} 2.52×10^{-11}	$-k_3[E_{red}][O_2]+ k_6[H_2O_2][I]$	140 μM	No flux 140 μM
H_2O_2	7.00×10^{-12} 1.05×10^{-11}	$k_4[E_{ox}P_2]-k_5[CAT][H_2O_2]-k_6[I][H_2O_2]$	0	No flux 0
E_{ox}	0 0	$-k_1[E_{ox}][G]+ k_4[E_{ox}P_2]-k_{sGOx}[E_{ox}]$	E_{GT} [b]	No flux 0
$E_{red}P_1$	0 0	$k_1[E_{ox}][G]-k_2[E_{red}P_1]-k_7[E_{red}P_1][H_2O_2]-k_{sGOx}[E_{red}P_1]$	0	No flux 0
E_{red}	0 0	$k_2[E_{red}P_1] -k_3[E_{red}][O_2]-k_8[E_{red}][H_2O_2]- k_{sGOx}[E_{red}]$	0	No flux 0
$E_{ox}P_2$	0 0	$k_3[E_{red}][O_2]- k_4[E_{ox}P_2]-k_7[E_{ox}P_2][H_2O_2]-k_{sGOx}[E_{ox}P_2]$	0	No flux 0
CAT	0 0	$-k_5[CAT][H_2O_2]+k_6[I][H_2O_2]-k_9[CAT]-k_{sCAT}[CAT]$	E_{CT} [c]	No flux 0
I	0 0	$k_5[CAT][H_2O_2]-k_6[I][H_2O_2]-k_9[I]- k_{sCAT}[I]$	0	No flux 0

[a] C_G = 5.5 mM for longevity simulations; For sensor response profile simulations, C_G was varied from 0 to 33 mM at increments of 1.5 mM.

[b] E_{GT} = Concentration of total active GOx.

[c] E_{CT} = Concentration of total active CAT.

7.2.4 Simulations

The model described herein was designed to predict the enzymatic loss that occurs within microspheres when exposed to certain glucose and O_2 concentrations. To do this, it was assumed that at $t=0^-$ substrate concentration inside the sensors (algilica+film) was equal to the bulk. The bulk glucose and O_2 concentration were set to 5.5mM (100 mg/dL) and 140 μM, respectively, which are close to the physiological substrate level in normoglycemia.[62] At $t=0$, the reaction was "turned on," and the diffusion-reaction process was modeled to predict the loss of GOx and CAT with time. The system of equation was solved for t = 30 days, and enzyme concentrations were extracted for intermediate time points t = 0, 4, 7, 15, and 30 days. The enzyme distributions at different time points for different kinds of sensors were plotted together to estimate the enzyme degradation that can be expected to occur after implantation.

The response of these sensors depends on the reaction-diffusion kinetics, which is expected to vary with time because of enzyme degradation. Therefore, the system of equations was also used to predict the corresponding drift in the response profile. For this, the bulk glucose concentration was varied from 0 to 33 mM (0-600 mg/dL) in increments of 1.5 mM (20mg/dL). This provides 23 data points that were used in curve fitting using nonlinear least-squares analysis. In these predictions, the pseudo-steady-state solution—the steady state solution at a given moment, considering no enzyme deactivation—was attained within three seconds; therefore, the solution at t=20 sec after each glucose step was taken as the steady-state sensor response. Finally, the response profile was constructed by plotting the percentage increase in luminescence versus

glucose concentration, where luminescence intensity at zero glucose concentration was taken as the baseline. For these simulations, the initial condition for enzyme distribution was obtained from the longevity of simulations, where the enzyme distribution at each intermediate time point was predicted. In these simulations, glucose concentration was represented in SI units (molar); however, clinical units (mg/dL) for glucose measurements were used to show results (1 mM = 18.0 mg/dL).

The sensor model was solved numerically using diffusion mode in COMSOL 3.5a (COMSOL, Inc, Burlington, MA), which estimates the approximate solution using the finite element method. The solution of the model was obtained using parameters and assumptions that have been stated in the theory section. The output solution was plotted using COMSOL or was exported as a matrix file and imported into MATLAB (Mathworks, Natick, MA) workspace for further analysis.

7.2.5 Sensitivity and range calculations

Method 1 described in Section 4 was used to calculate range and sensitivity from the experimental data. Briefly, the data obtained from dynamic testing experiments were analyzed using a MATLAB script file, where the last 20 data points at each concentration step were taken to calculate the mean and standard deviation of the steady-state response. The percent increase from the baseline (0 mM glucose) was calculated at each concentration step. Finally, the response was plotted by taking the global average (average of three steady-state % increase in luminescence) for each concentration. Equation 4.1 was fitted to the response curve, where I_{max} and k were estimated using the method of nonlinear least-square analysis (Levenberg-Marquardt algorithm).

Sensitivity—defined as the slope of the linear response—was estimated by performing a simple linear regression on the first few data points such that $R^2 \geq 0.95$. Range was defined as the glucose concentration at which the response deviates from linearity by 10%.

7.3 Results and Discussion

7.3.1 Sensor characterization

Figure 7.2 depicts the confocal images of microparticles loaded with enzyme, enzyme distribution within microparticles, and the size distribution of algilica microparticles. The mean diameter of the particles as measured with the Coulter method was ~12 μm (Figure 7.2 D). For the microparticles loaded with GOx only, the enzyme concentration was found to be ~0.2 mM using UV-Vis absorption measurements. In the case of microparticles loaded with both GOx and CAT, the individual enzyme concentration was determined to be ~0.1 mM of each. Furthermore, it is known that a significant loss in enzyme activity can occur during immobilization of enzyme and, therefore, the concentration of the active immobilized enzyme will be less than the experimentally-determined concentration, also referred as total enzyme concentration. The enzyme distribution, as determined via confocal microscopy, was found to be nearly homogeneous homogeneous, matching previous observations (Figure 7.2 A, B, and C).[18]

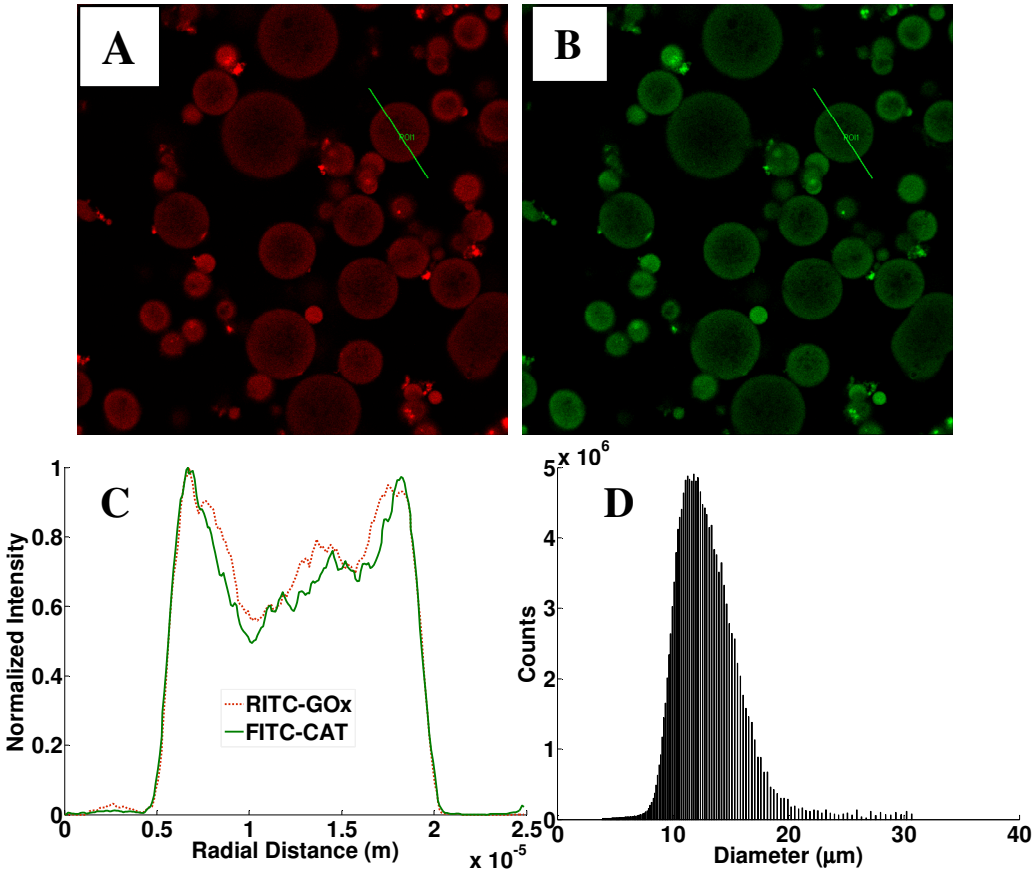

Figure 7.2 Confocal images depicting the distribution of RITC-GOx (A) and FITC-CAT (B) within algilica microparticles, obtained with sequential excitation at 543 and 488 nm. C is the intensity line scan of GOx and CAT loading along the green line shown in A and B. D is the microspheres size distribution obtained using ElZone.

7.3.2 Estimated enzyme deactivation

The system of nine PDEs was used to model the enzyme degradation occurring inside microsensors during exposure to physiological levels of glucose and oxygen. Figure 7.3 (top) contains the predicted active GOx concentration and its radial distribution at different time points, assuming sensors initially loaded with 0.2 mM GOx. It is obvious that a higher GOx degradation rate was estimated in the central region compared to the surface region. Peroxide-mediated deactivation was estimated to be

slower in the surface region, because the surface boundary condition assumed zero peroxide concentration. Moreover, it has been shown that the oxidized from of GOx is not subjected to peroxide-mediated deactivation, while all other forms are strongly affected.[57] The higher O_2 concentration in the near surface region results in an increased percentage of GOx to be present in the oxidized state, consequently slowing down the net deactivation rate of GOx. Overall, almost 70% of the total GOx is lost within 4 days of continuous operation; this increases to more than 95% loss after 15 days.

In comparison, Figure 7.3 (bottom) shows the active GOx concentration for sensors loaded with 0.1 mM GOx and 0.1 mM CAT. It is obvious that the degradation of GOx is expected to be much more uniform when CAT has been co-immobilized within the same matrix. The turnover rate of CAT is very high, which results in an immediate consumption of peroxide upon production; the effect on GOx, then, is a slower and more homogenous degradation by peroxide. Furthermore, only ~2% of the total GOx is lost within 4 days of continuous operation, with an increase to ~11% loss after 15 days. This theoretical analysis suggests a major impact on GOx stability with the inclusion of catalase.

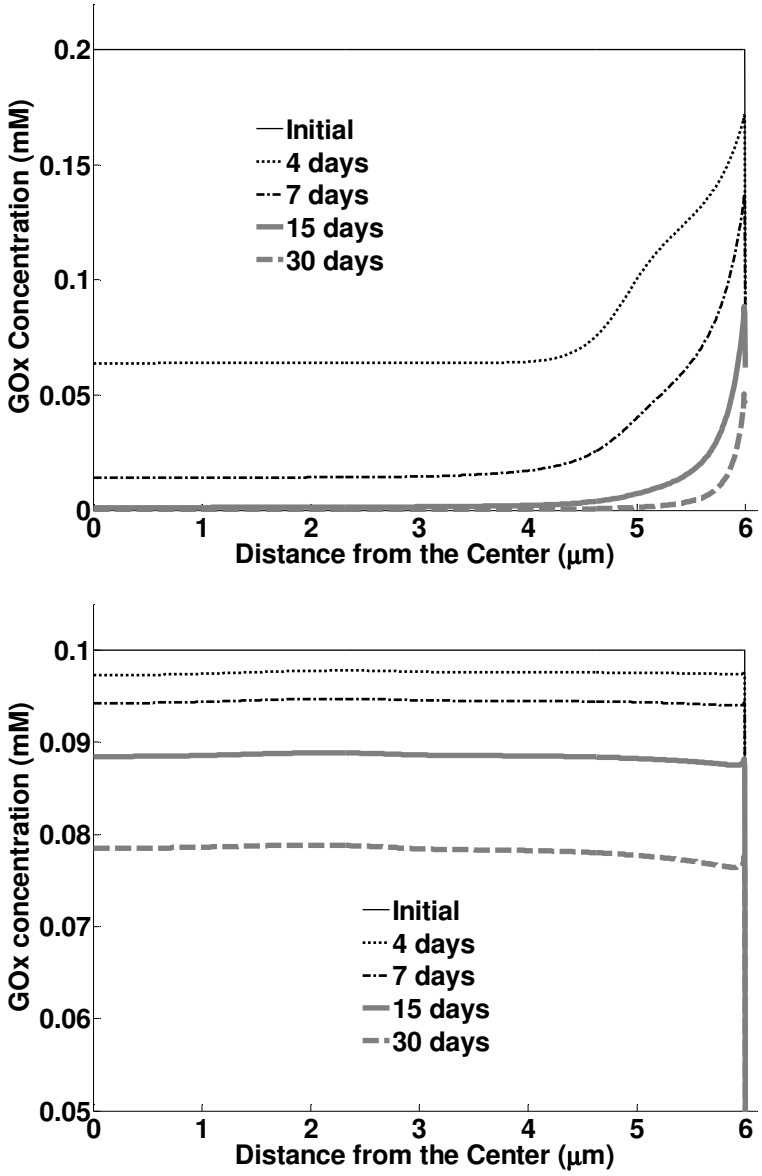

Figure 7.3 Theoretical estimation of the radial distribution of GOx inside microsphere sensors at different time points during constant operation. (top) predicted active GOx concentration for microspheres loaded with GOx only. (bottom) predicted active GOx concentration for microspheres loaded with both GOx and CAT.

Figure 7.4 shows the volume average concentration of active GOx or CAT present at any given time in both types of sensors. For sensors having no CAT, it is apparent that the average active GOx degradation follows an exponential decay profile. However, in the presence of CAT, the average active GOx concentration follows a more linear trend. The decay profile of CAT was predicted to be linear as well. The linear decay trend is due to the fact that peroxide-mediated deactivation of both enzymes is minimized in the presence of CAT. Under these conditions, nearly all deactivation occurs via spontaneous denaturation, a process exhibiting a first-order decay with infinitesimally small rate constants (k_{sGOx} and k_{sCAT}). Although first-order deactivation is expected to result in an exponential decay trend, one month is a very short time to observe the entire decay profile in this case and, therefore, the deactivation appears to be linear for the first month. As the spontaneous deactivation rate of CAT is almost twice of GOx, a faster deactivation of CAT was estimated for sensors containing both GOx and CAT. In addition, CAT is even more susceptible to the peroxide-mediated deactivation than GOx ($k_9 > k_8$) and the oxidized form of GOx is not deactivated by peroxide, whereas all forms of CAT are equally susceptible to peroxide.

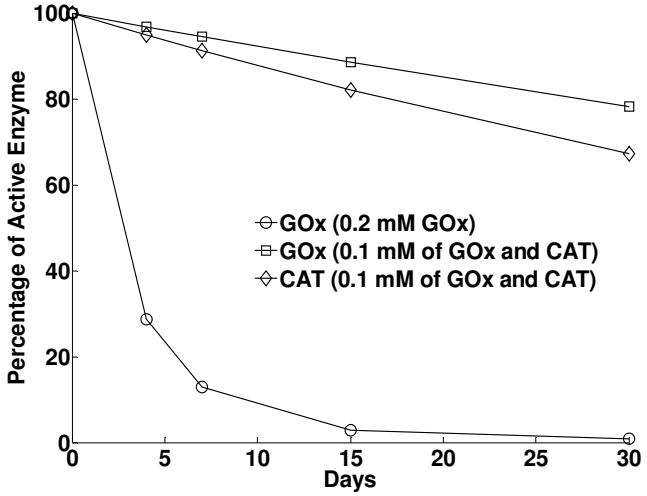

Figure 7.4 Predicted volume average of the active enzyme concentration during constant operation for sensors loaded with GOx only and for sensors loaded with both GOx and CAT.

7.3.3 Estimated calibration shift

As noted in the discussion of Figure 7.3, the loss of active enzyme is not always uniform throughout the microsphere. A changing enzyme distribution can influence the overall reaction-diffusion kinetics of the system, altering the sensor response. Therefore, when predicting the sensor response profile over different bulk glucose levels at different time points, the calculated enzyme distribution at that particular time was used for the response prediction. Figure 7.5 (A) contians the predicted response of sensors loaded with 0.2 mM of active GOx. Although approximately 90% loss in active GOx was estimated for the first 7 days, it seems that the response profile of the sensor was not proportionally affected. A decrease in sensitivity of only ~9% was predicted, along with no significant variation in response range. This latter observation leads to the interpretation that if the active GOx concentration is higher than 0.02 mM, the sensing

scheme will be primarily diffusion-limited. Therefore, in this situation, the effect of decreased enzyme concentration on the response was not significant. However, when the average GOx concentration in the microsphere falls below 0.02 mM, the predicted response was severely affected. At such low GOx concentration, a linear relationship between GOx decay and sensitivity loss can be noticed. This suggests that the sensing scheme at lower GOx concentrations (<0.02 mM) becomes reaction-limited. As long as the GOx concentration is such that the sensing scheme is not reaction-limited, we will not expect a significant change in the sensor response.

Figure 7.5 (B) contains the predicted response of sensors loaded with 0.1 mM GOx and 0.1 mM CAT. Comparing the initial response of these two types of sensors (Figures 7.5 (A) and 7.5 (B), without and with catalase, respectively), it can be noticed that the sensors with CAT are expected to exhibit lower sensitivity than sensors without CAT. This observation can be attributed to the fact that the overall consumption rate of oxygen is lower for sensors with CAT; from equations (1) and (2) we can observe that one O_2 molecule is produced for every two O_2 molecules consumed. One may also observe that sensors containing both GOx and CAT exhibit less than 10% variation in the response range and sensitivity, even when continuously exposed to 100 mg/dL glucose for one month. As approximately 85% active GOx ([GOx] > 0.02 mM) is present even after a month, the sensing scheme is predicted to remain diffusion-limited and, therefore, a stable response can be expected.

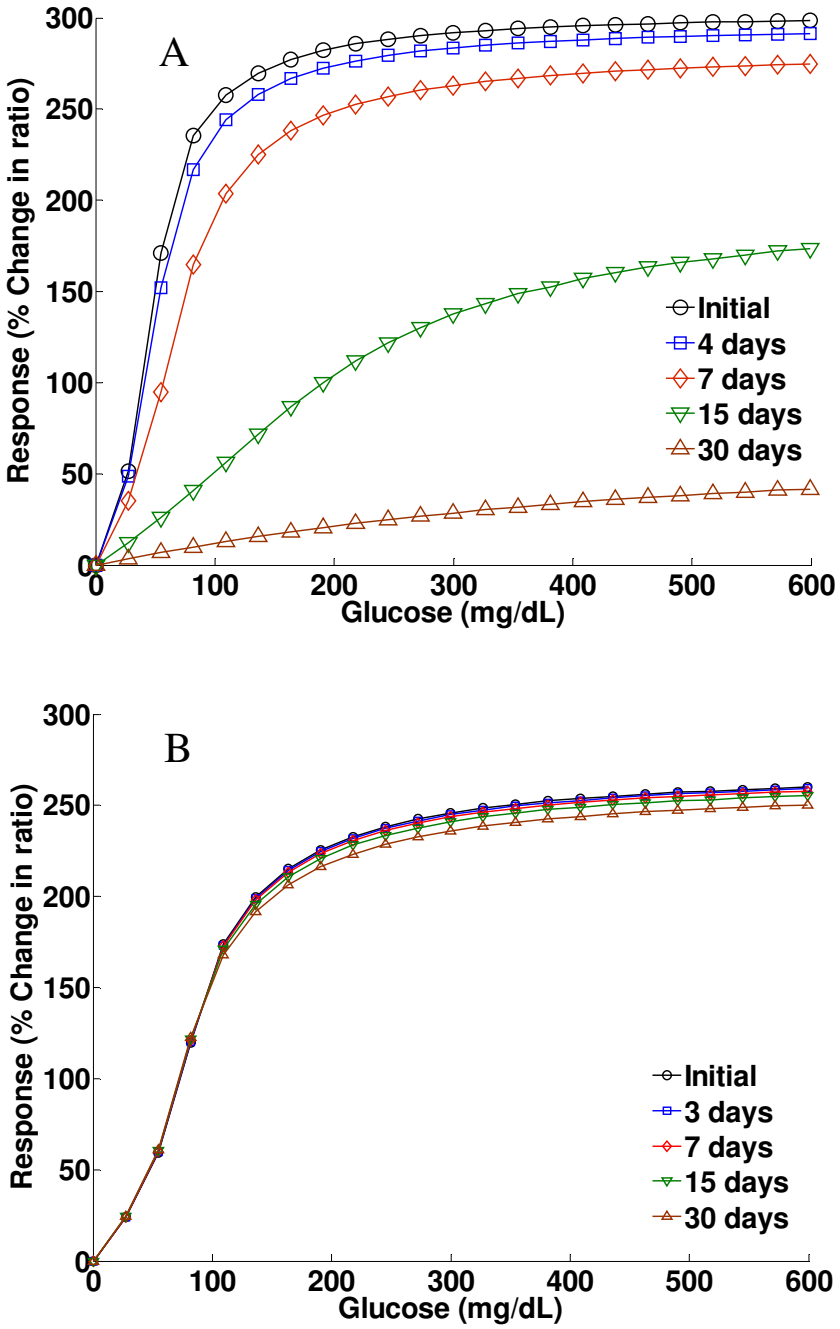

Figure 7.5 Theoretically predicted response of two types of sensors if they are continuously exposed to 5.5 mM glucose and 140 µM O_2 at 37 °C. (A) response of sensors that are loaded with 0.2 mM GOx and (B) response of sensors that are loaded with 0.1 mM GOx and 0.1 mM CAT.

7.3.4 Measured calibration shift

To validate the modeling results that predict an enhancement in stability with the inclusion of catalase, experiments were performed to compare the response of sensors with and without catalase over time. Figure 7.6 contains the measured response profiles for both sensor types. The initial response was measured for each sensor type immobilized inside the reaction chamber, after which the responses were measured after 4 and 7 days of continuous operation. The response of the fresh sensors was recorded under physiological conditions by exposing them to step changes in glucose concentration. Subsequently, the sensors were incubated in 100 mg/dL glucose for 4 days, after which the response was tested using the same procedure. After the second response measurement the sensors were again incubated in 100 mg/dL glucose for an additional 3 days, and finally the response profile was measured for the third time.

Figure 7.6 (A) shows the response of sensors (without CAT) that was measured initially, after 4 days, and after 7 days. Approximately 40% loss in sensitivity was observed for the measurements performed after 4 days. For comparison, the model predicted less than 5% loss in activity for sensors loaded with 0.2 mM active GOx. Approximately 65% loss in sensitivity can be observed after seven days. The percentage loss in sensitivity was almost uniform throughout the testing period, which suggests that the sensing scheme for these sensors was reaction-limited right from the very beginning. Therefore, it seems that the experimental conditions did not match the simulations.

It is possible that >90% loss in the enzyme activity occurred because of immobilization. The discrepancies between theoretical and experimental data are likely due to the fact that the enzyme immobilization via covalent attachment results in a significant loss of enzyme activity. Therefore, the concentration of the active enzyme immobilized in the microspheres is expected to be less than the value determined with spectrophotometric measurements. Since only total protein concentration can be measured via absorption measurements, and activity assays are confounded by transport resistance, accurate direct measurements of active enzyme are not possible.

Figure 7.6 (B) shows the measured response of sensors that were loaded with both GOx and CAT. Using spectrophotometric absorption measurements, the concentration of GOx and CAT was determined to be 0.1 mM each. It can be noticed that the sensitivity values obtained from initial experiments were significantly lower than the measured sensitivities for sensors without CAT, as predicted from modeling. For these concentrations, modeling predicted almost no change in sensor response over 7 days of continuous operation. However, we observed ~8% and ~11% losses in sensitivity after 4 and 7 days, respectively, in experimental measurements. This again is likely due a significant loss in enzyme activity during the immobilization process. Therefore, the initial active enzyme concentration could be less than the one-tenth of the total immobilized enzyme concentration predicted using absorption measurements.

Regardless of inaccurate values for active enzyme, a significant improvement in the stability of sensor response was still observed with the coimmobilization of CAT with GOx. For a 7-day period, the sensitivity loss was reduced from 65% (no CAT) to 11% (with CAT), which can be considered as a substantial improvement in the stability of sensors. The loss in sensitivity can be attributed to the loss in active GOx resulting from the spontaneous and peroxide-mediated deactivation of enzyme. It is noteworthy that, the other reaction byproduct, gluconalactone, will induce a drop in the local pH. It has been reported that the spontaneous deactivation rate of GOx exhibit pH dependency [48]. GOx has been shown to be most stable at around pH 5. Below pH 2 and above pH 8 catalytic activity is rapidly lost. When sensors are exposed to high substrate concentrations, high levels of peroxide and gluconalactone will be produced; this will result in faster enzyme deactivation thereby making the sensors less stable. Neverthless, the general response trends predicted via modeling matched the trends that were experimentally-determined.

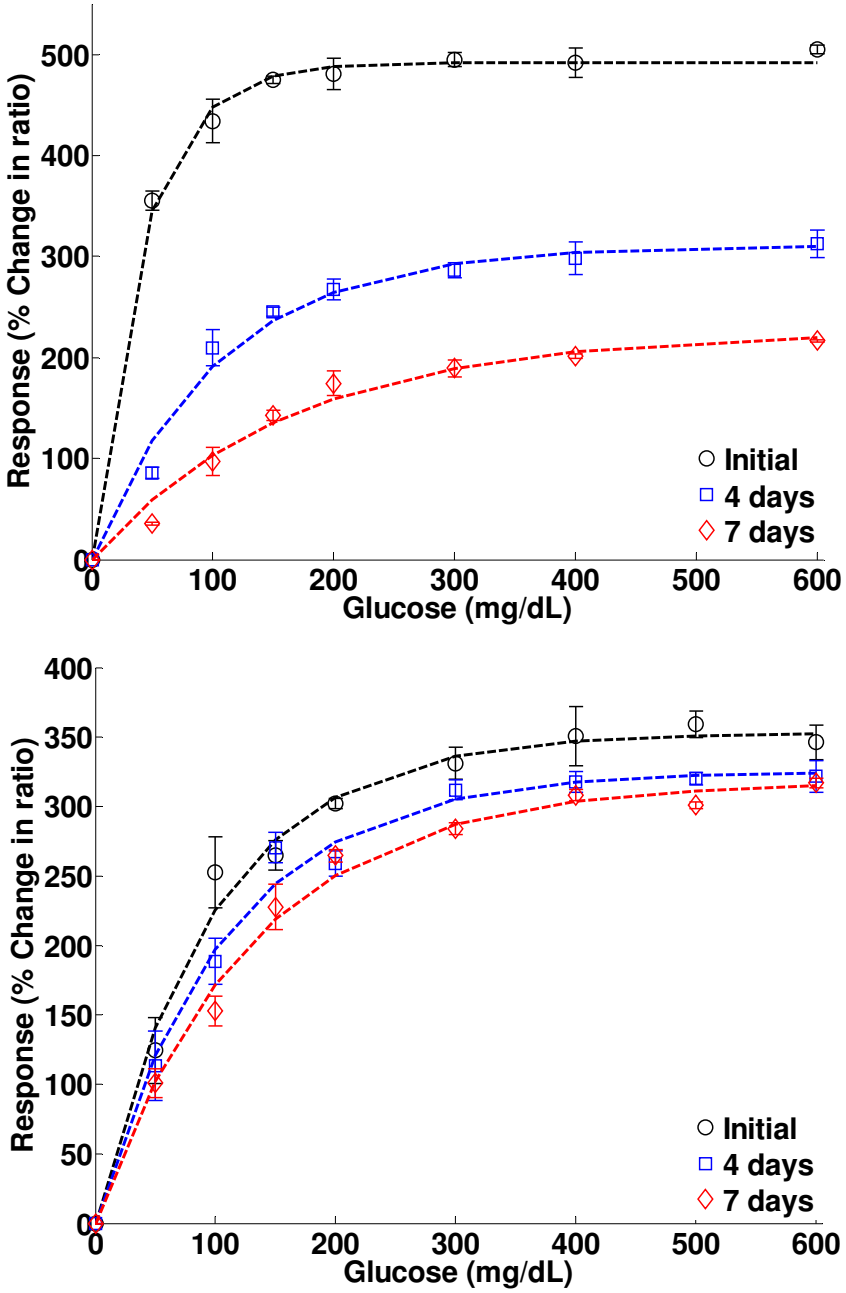

Figure 7.6 Experimentally-determined response of both types of sensors that were continuously exposed to 5.5 mM glucose and 140 µM O_2 at 37 °C. (A) response of sensors loaded with 0.2 mM GOx and (B) response of sensors loaded with 0.1 mM GOx and 0.1 mM CAT

7.3.5 Variation of *k* with time

Evaluation of the change in response over time was performed to more clearly understand the magnitude of calibration shifts with time. Equation 4.1 was used as a model equation to fit the response of sensors using nonlinear least-square analysis. The shape of the response profile and range primarily depend on *k*. Although sensitivity is directly related to R_{max}, it is difficult to draw conclusions based on R_{max} variation in luminescent sensors, as it is strongly affected by photobleaching. In contrast, *k* will only be affected by the enzyme concentration and distribution. Therefore, models were solved to predict the variation in *k* with time for sensors consisting of different GOx and CAT loadings. Figure 7.7 contains plots of *k* versus time for such sensors, wherein a decrease in *k* is understood to be an increase in the response range of the sensors due to the decreased overall reaction rate from less enzyme available for catalysis. A close correspondence between *k* and its decay trend can be observed between the experimental data and models for sensors loaded with 0.02 mM GOx (without CAT). This matches the previous discussion, and further supports the inference that almost 90% of the total enzyme activity was lost during the immobilization process. These curves further illustrate that a noticeable change in *k* would not be expected for sensors loaded with 0.1 mM GOx and CAT. However, a linear decay in *k* is expected if the loaded concentration for each enzyme is 0.01 mM or less. The decay rate of *k* that we observed experimentally was in between the one predicted for 0.01 mM and 0.005 mM (GOx and CAT), suggesting the loss in active enzyme is perhaps 90-95% in this case. While these results highlight a major inefficiency in immobilization of enzymes, the experimental *k*

decay rates reveal a reduction in the decay rate of k by five times due to the incorporation of CAT.

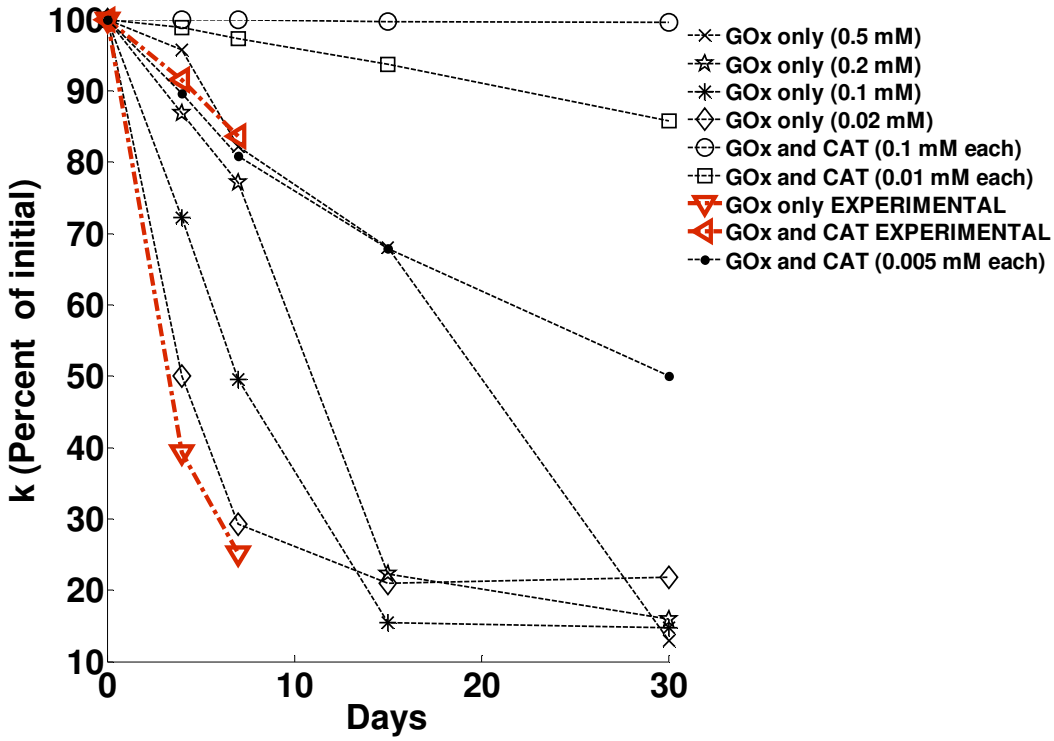

Figure 7.7 Theoretically-predicted and experimentally-determined variation in the curve fit parameter, *k*, with respect to time.

7.4 Conclusion

Considering the rate of change of k as a parameter defining the response stability of a sensor, the sensors obtained by the incorporation of 0.1 mM CAT can be considered as five times more stable than sensors having no CAT, despite undergoing an estimated 90% loss in enzyme activity upon immobilization. Increasing the concentration of both active GOx and CAT to ≥0.1 mM is expected to result in a very stable response –only

2% decrease in *k* value over a one month period, which translates to less than 5% drift in sensitivity and range. Increased enzyme loading can be attained by using microparticles with higher porosity than the particles employed here, which had a rather low porosity of 0.005. Mesoporous microparticles with porosity exceeding 0.5 can be synthesized,[70] and we have already observed major improvements in Section 6 where mesoporous silica substrates were used for immobilization. By employing such materials, it is reasonable to believe that microsphere-based sensors exhibiting less than 10% deviation in sensitivity and range over a 3-month period can be fabricated. Such an approach could overcome one of the primary obstacles for deployment of enzymatic systems in minimally-invasive continuous glucose monitoring.

8 LONG-TERM RESPONSE UNDER SIMULATED *IN VIVO* CONDITIONS

8.1 Introduction

It was predicted through modeling that sensors with increased GOx loading will have an improved longevity. High GOx loading cannot be achieved for algilica microparticles, due to their low porosity. Therefore, to construct stable sensors, there is a need to use microparticles that are highly porous. In Section 6, highly-porous Zorbax® microparticles were used to increase the response range of sensors. Due to their high porosity, it is also possible to obtain higher enzyme loading in these microparticles. However, there is some concern that these smaller particles are more likely to be endocytosed after being deployed in the tissue due to their small size.[80] Therefore, we used amine-functionalized silica microparticles with average size of ~20 μm, a safer choice for *in vivo* application.

In the work described thus far, the response of sensors was investigated by immobilizing particles on a pressure-sensitive adhesive attached to a glass slide. The response was then recorded by exposing them to step changes in glucose concentrations. In this situation, there was no additional barrier other than the NF that could reduce the influx of glucose and oxygen into the sensor matrix. Because of the absence of any other transport barrier, the response of each sensor is expected to be minimally affected by the presence of other sensors in close proximity.

However, the scenario could be very different when the sensors are deployed in tissue, where tissue will present an additional barrier to the influx of glucose and oxygen reaching the sensors. It must be noted that the oxygen and glucose supplied to the dermis come from the capillaries, and even in the highly-vascularized dermis the intercapillary distance is 120-220 μm.[81] It is expected that the transport resistance of tissue will alter the measured response range and the sensitivity of microparticle-based sensors. Furthermore, outflux of the hydrogen-peroxide will be reduced. The reduced outflux will result in increased peroxide concentrations inside the microparticles, thereby resulting in less stable sensors.

The goal of this phase of the research was to study the long-term response of microparticle-based sensors under simulated tissue conditions. For this, sensors were immobilized in a hydrogel attached to a glass slide, which will present an additional barrier to the diffusion of substrates and byproducts. Highly porous (porosity = 0.65, pore size = 8 nm) amine-functionalized silica microparticles were used, as they enabled increased enzyme loading. Sensors with increased enzyme loading were constructed and tested for a period of two months.

8.2 Experimental

8.2.1 Chemicals

Amine-functionalized microparticles with average diameter and porosity of ~20 μm and 0.65, respectively, were obtained from Supelco®. Ethanol with a purity of 99.5% was obtained from Sigma. Pt(II) meso-tetra (4-carboxyphenyl) porphine (PtP, Frontier Scientific), dimethyl sulfoxide (DMSO, Aldrich), glucose oxidase (GOx, EC

232-601-0, Sigma), *N*-(3-dimethylaminopropyl)-*N´*-ethylcarbodiimide hydrochloride (EDC, Fluka), *N*-hydroxysulfosuccinimide sodium salt (NHSS, Toronto Research Chemicals Inc.), and sodium acetate (Sigma) were used to prepare PtP/GOx-doped microparticles. Poly(allylamine hydrochloride) (PAH, MW 70 kDa, Aldrich), poly(sodium 4-styrenesulfonate) (PSS, MW 70 kDa, Aldrich), poly(acrylic acid) (PAA, MW 100 kDa, Aldrich) and sodium chloride (Sigma) were used during the deposition of multilayer thin films. Additionally, rhodamine B isothiocyanate (RITC, Aldrich) was conjugated to PAH (PAH-RITC), which was also used in LbL NF deposition. β-D-glucose (MP Biomedicals, Inc.), oxygen and nitrogen gas (PraxAir), and PBS (Sigma) were used during dynamic testing. Poly(ethylene glycol)1000 monomethacrylate (PEG-A Polysciences Inc.) and poly(ethylene glycol)4000 diacrylate (PEG-DA Polysciences Inc.) were used to form PEG gels for sensor immobilization. Irgacure 184 (Ciba) was used as a UV initiator to cross-link PEG. 3-(Trimethoxysilyl)propyl methacrylate (TPM, Sigma) was used to activate microscope slide for attaching PEG gels to the glass. All necessary pH adjustments were performed using titrations of 1.0 M HCl and 1.0 M NaOH (Fluka). Chemicals listed above were reagent grade and used as received. Ultrapure water with a resistivity greater than 18 MΩ-cm was used to prepare all aqueous solutions. All experiments were conducted at room temperature and the oxygen concentration in the glucose and buffer reservoirs was maintained at 277 μM (air saturated) by aeration.

8.2.2 Sensor preparation and characterization

Dried microparticles were sent to an external lab for surface area and pore size analysis (Delta Lab, North Huntingdon, PA). A particle size analyzer (ElZone 540, Micromeritics®) was used to measure the concentration and size distribution of the microparticles.

Three batches of sensors were prepared, consisting of varying enzyme concentrations to study the role of CAT in sensor stabilization. The first enzyme loading solution consisted of GOx (35 mg/mL) dissolved in bicarbonate buffer. The second loading solution consisted of a mixture of GOx (30 mg/mL) and CAT (5 mg/mL) in phosphate buffer. The third loading solution was a mixture of GOx (10 mg/mL) and CAT (5 mg/mL). The purpose of choosing three different concentrations was to construct three sets of sensors that have fixed amount of total enzyme (GOx + CAT) immobilized within the microparticles, but different ratio of GOx and CAT.

To prepare sensors, amine-functionalized microparticles were suspended in a phosphate-buffered solution (pH = 9.0) containing 50 mg/mL of both EDC and NHSS. PtP in DMSO was added to a final concentration of 50 μM and the mixture was vortexed for ~2 hours. Dye-labeled microparticles were rinsed twice in deionized (DI) water, and then suspended in EDC/NHS solution (50 mg/mL) in acetate buffer (pH = 5) to activate the free caboxylate moieties of immobilized PtP. Subsequently, enzymes dissolved in bicarbonate buffer were added to the dye-labeled microspheres and the solution was vortexed for four hour, which led to the coupling of amine moieties of enzyme to the activated carboxylate moieties of PtP. Finally, the microparticles were rinsed with DI

water and coated with $[PAH\text{-}RITC/PSS]_3$-$[PAH/PAA]_{12}$ NFs using LbL technique. PAA is more hydrophobic than PAH and PSS and, therefore, it expected that this will further decrease the transport of glucose, thereby increasing the range of sensors.[30]

PtP labeled microparticles were also separately loaded with RITC-GOx and FITC-CAT, and were imaged using confocal microscopy (Leica TCS SP5) to determine the homogeneity of PtP, GOx, and CAT distribution inside the microparticles. A 63X oil objective with pinhole set to 1 Airy was used for imaging. The enzyme loading was determined using UV-Vis on the supernatant loading solution.[78]

A mold for hydrogel fabrication was created by attaching a ~2 mm thick poly(dimethylsiloxane) (PDMS) membrane to the glass slide. A 2.5 millimeter diameter hole was created in the membrane using a biopsy punch (Acu·Punch, Acuderm inc.). The PDMS membrane was bonded to the glass to prevent leaks; bonding was performed by treating the glass and PDMS surface with plasma prior to contact.[82]

The glass slide was rinsed with ethanol and water after the mold was created. Subsequently, a mixture containing a silane precursor (2% TPM, 97% ethanol, and 1 % DI water) was dropped into the mold to activate the glass surface. After 5 minutes, weakly-bound silane precursor was removed by an ethanol rinse. A mixture of PEG-A (1 g/mL), PEG-DA (0.1 g/mL), Irgacure 184 (20 mg/mL), and sensors was then prepared, with the concentration of microparticles in the mixture was at ~10^7 particles/mL. A 10 μL aliquot of this mixture was dropped on the activated surface of the glass slide and subsequently exposed to UV light for *ca.* 10 minutes. Finally, the PDMS was peeled off from the glass surface, leaving behind the cross-linked gel with microparticles entrapped

within the gel. Sensors were immobilized using this method each time the response was to be measured.

The sensor response was experimentally determined using the flow-through system described in Section 4.[18] Measurements of response were performed in a similar fashion and under same conditions that were described in Section 3. The data were processed to calculate response range and sensitivity using Method 2 described in Section 4 (sigmoidal fit).

After recording the initial response of sensors, they were incubated in glucose reservoirs (100 mg/dL) at 37 °C. The solution in the glucose reservoir was replaced with a fresh solution every 24 hours to minimize bacterial growth and to avoid depletion of glucose level; under these conditions, glucose and oxygen were continuously consumed by the sensors during incubation. In addition, the glucose solution was continuously aerated by leaving the lid of the glucose reservoir open, preventing the depletion of oxygen levels in the reservoir. The response was then recorded after 9, 18, and 30 days of continuous exposure to glucose at 100 mg/dL.

8.3 Results and Discussion

8.3.1 Sensor characterization

The mean volume-weighted size of the microparticles was determined to be *ca.* 21 μm using the Coulter method (Figure 8.1). Using BET method, the average porosity and pore size were found to be 0.65 and 8 nm, respectively. The porosity and pore size of algilica were determined to be 0.005 and 18 nm, respectively.

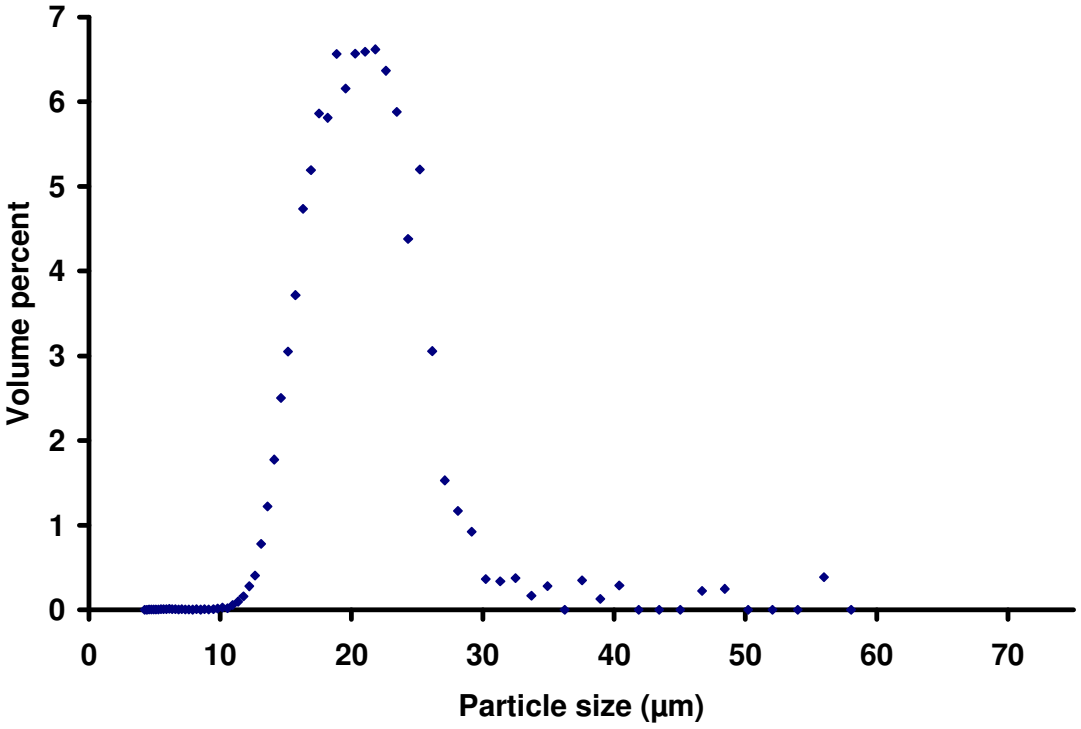

Figure 8.1 Size distribution of commercial microparticles, as measured with electrical sensing zone analysis.

Confocal microscopy was performed on microparticles loaded with FITC-CAT and RITC-GOx (Figure 8.2). It was observed that, unlike other microparticles used in this research, these particles are not spherical. Images indicated that both GOx and CAT penetrate through the pores of the microparticles and are present throughout the interior.

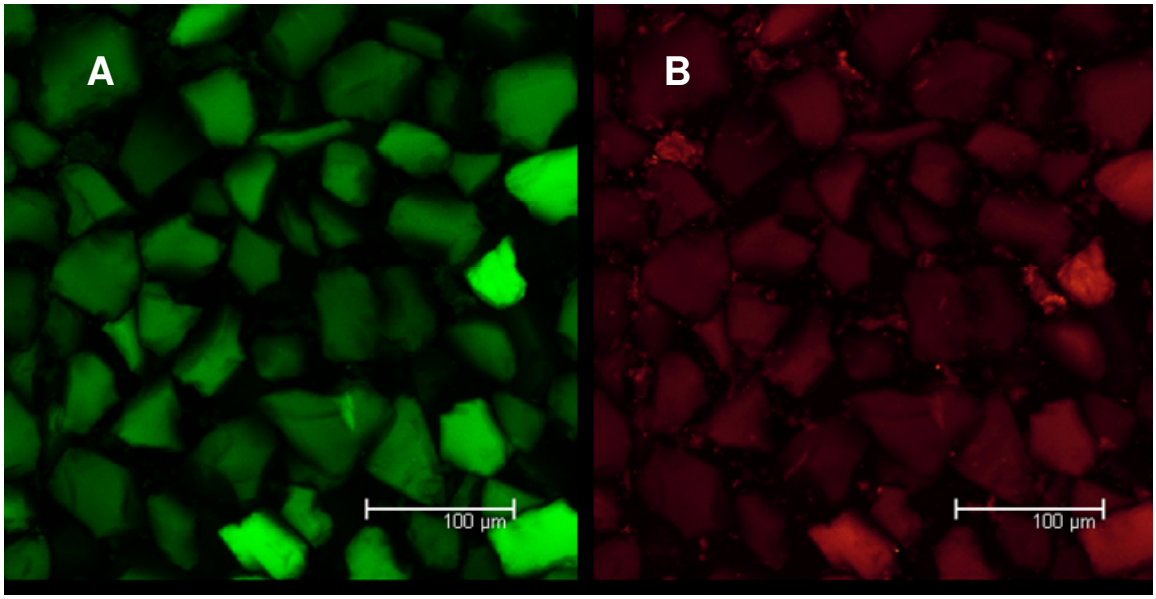

Figure 8.2 Confocal images depicting the distribution of RITC-GOx (A) and FITC-CAT (B) within commercial microparticles, obtained with sequential excitation at 543 and 488 nm.

8.3.2 Enzyme loading

The GOx and CAT loading in the three different types of sensors is shown in Figure 8.3. The immobilized GOx concentration for the 35 mg/mL loading solution (no CAT) was *ca.* 1.2 mM, much higher than the loading for algilica sensors (0.1 mM) and similar to what was measured for 6 µm spherical particles. This increased loading can be attributed to the higher porosity of these microparticles as compared to algilica (porosity of Supelco® and algilica are 0.65 and 0.005).

The concentration of GOx and CAT in the loading solution used to prepare second type of sensors was 30 mg/mL and 5 mg/mL, respectively. For the second type of sensors the concentration of immobilized GOx and CAT was determined to be 0.04 and

0.25 mM, respectively. Due to the higher GOx in the loading solution, it was expected that the concentration of the immobilized GOx within microparticles would be higher than CAT. Furthermore, the smaller size of GOx (M.W. 160 kDa) compared to CAT (M.W. 250 kDa) was expected to improve diffusion into the pores of the microparticles. However, experimentally determined GOx loading was found to be much lower than CAT loading. This odd observation can potentially be explained by Vroman effect, which described the time-dependent nature of protein adsorption to a surface.[83] Vroman investigated adsorption of serum proteins on a surface and found that high concentration and high mobility (small size) proteins arrive first to the surface; however, they are later replaced by less motile proteins (large size proteins) that have higher affinity of the surface. It is possible that, with time, GOx that was initially adsorbed on the surface was subsequently replaced by CAT.

The concentration of GOx and CAT in the loading solution that was used to prepare third type of sensors was 10 and 25 mg/mL, respectively. The immobilized GOx concentration in the third type of sensors was found to 0.002 mM, which is negligible in comparison to the GOx-only sensors. Concentration of immobilized CAT was found to be 0.277 mM, which again suggests that CAT has higher affinity for the microparticle surface. Even though the concentration of CAT in the third solution was higher than the second solution, the concentration of immobilized CAT was same, which also suggest that the attachment of the CAT to the surface is highly affinity-driven. Three types of loading solutions were chosen such that if the enzyme loading was concentration-driven, they would have resulted in sensors with no CAT, a small amount of CAT, and a very

large amount of CAT. The long-term response testing of such sensors would have been very useful in better understanding the role of CAT in enhancing the longevity of sensors.

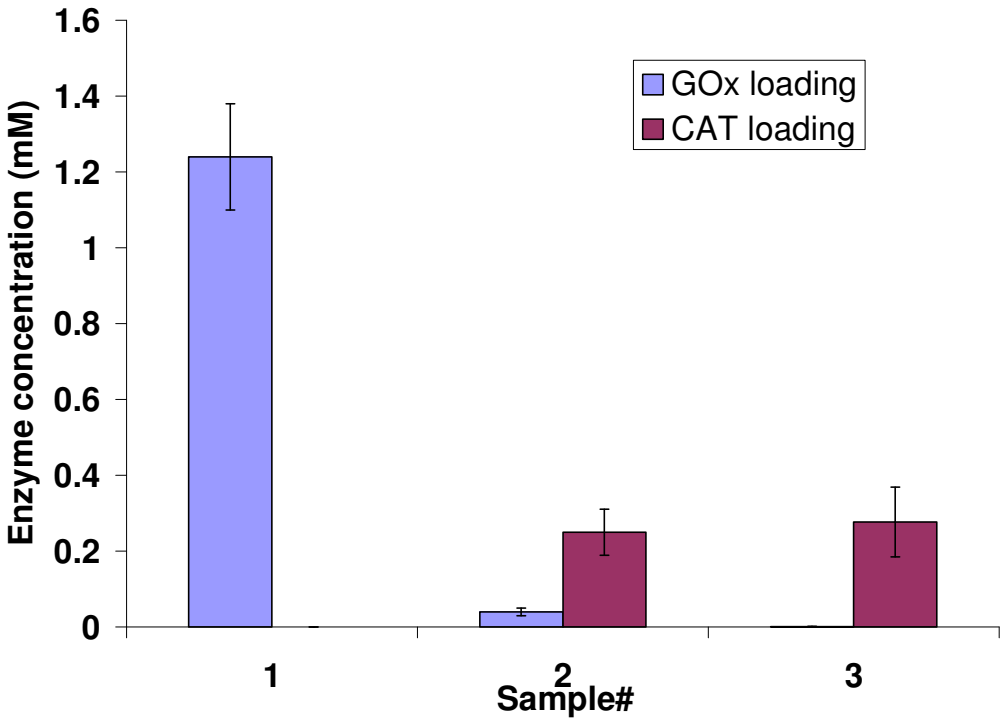

Figure 8.3 Concentration of immobilized GOx and CAT within three types of sensors determined using absorbance measurements on the supernatant loading solution. Error bars indicate the standard deviations from three replicates.

8.3.3 Response stability

It was only possible to obtain an initial response from the first and second type of sensors. The third type was found to be unresponsive to glucose, due to the absence of GOx within the microparticles. Figure 8.4 contains a plot of the response profile obtained from the first type of sensors (GOx-only). Initially, the response range was

determined to be 192 mg/dL. After 9, 18, and 30 days the range was found to be 239, 171, and 228 mg/dL, respectively. As there is no evidence of extension of response range, it can be concluded that even after 30 days of continuous operation, the reaction is still diffusion-limited.

These sensors were also tested after 60 days of continuous operation. Unfortunately, no response was observed this time. From this, we must infer that somewhere between 30 and 60 days of continuous operation, the active GOx concentration became so small that the sensing scheme shifted from diffusion-limited to reaction-limited regime. Subsequently, the sensors must have stopped responding once the GOx concentration dropped below a point where significant oxygen could be depleted.

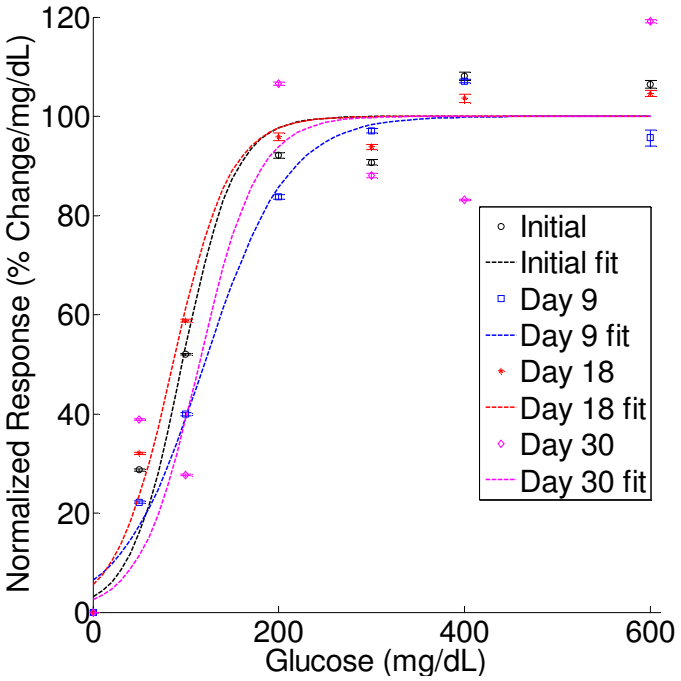

Figure 8.4 Thirty day response of sensors loaded with GOx (1.2 mM) only. Error bars indicate the standard deviation obtained from twenty data points for a single step change in glucose concentration.

It must be noted that several variables are added into the response measurement process when the sensors are immobilized within a hydrogel. Although, a mold is used to reproducibly a hydrogel of definite shape and size, the final shape of the hydrogel after swelling is very much different from the initial shape. An altered shape and size of the hydrogel can change the dynamics of the reaction-diffusion system, thereby resulting in an altered response profile. It is important to note that, the data presented in Figure 8.4 come from a single set of experiments. As the sensors were immobilized in a hydrogel, which can further add to the variability in the observed response, experiment was repeated to obtain an estimate of gel-to-gel variability in the response. The response range of first type of sensors obtained from two gels is tabulated in Table 8.1. Initial, 9 day, 18 day, and 30 day response range were compared using t-test and in each case the P-value was determined to be greater than 0.11, which implies that there was no significant variation in the response range with time (Figure 8.5). This finding suggests that, even after 30 days of continuous operation, there was sufficient amount of active GOx still present within the microparticles to make the sensing scheme diffusion-limited.

Table 8.1 Response range of first type of sensors obtained from two gels

Time	Range (gel-1) mg/dL	Range (gel-2) mg/dL	Mean Range mg/dL	Standard Deviation
Initial	192	218	205	18
Day 9	239	254	246	11
Day 18	171	247	209	54
Day 30	228	262	245	24

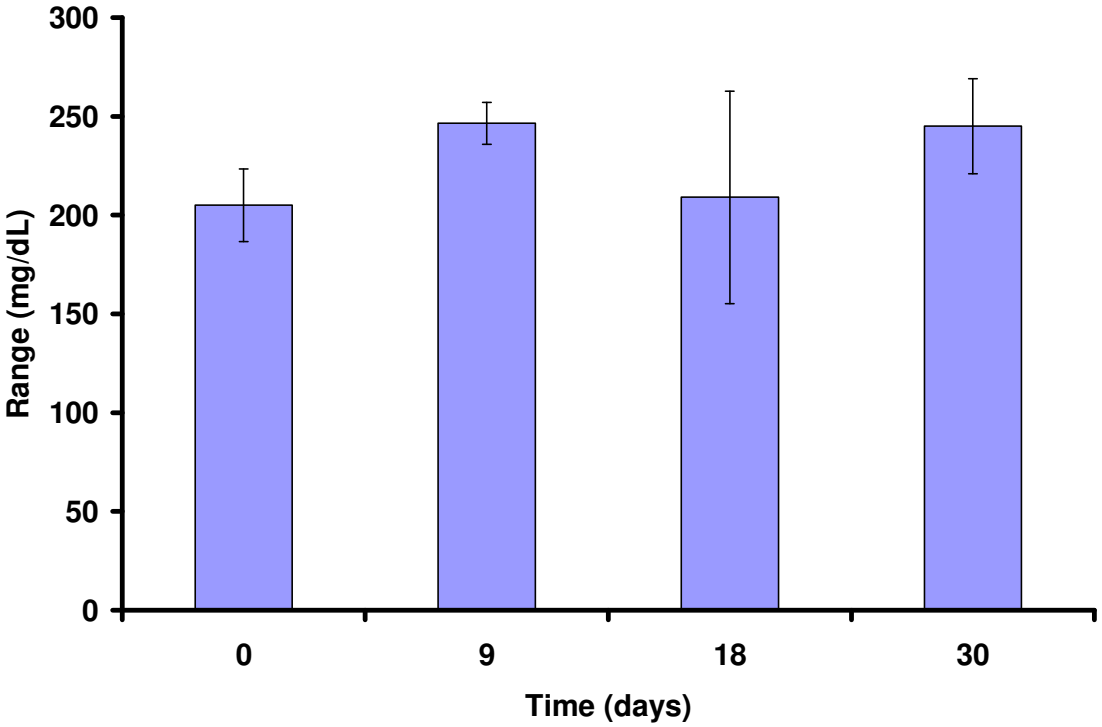

Figure 8.5 Average response range of first type of sensors. Error bars indicate the standard deviation obtained from two replicates.

The measured response for the second type of sensors (with 0.04 mM GOx and 0.25 mM CAT) is shown in Figure 8.6. The initial range observed in this case was 364 mg/dL, much higher than the sensors made from GOx only. This is similar to what we previously observed with algilica-based sensors: inclusion of CAT results in extended response range (Figure 7.6). The range after the 9^{th} and 18^{th} days was found to be 376 and 564 mg/dL, respectively. However, after 30 days of continuous exposure to glucose (100 mg/dL) and oxygen (277 μM), no measurable response was observed. This indicates the complete loss of active GOx in 30 days, and the trend of increasing range follows the expected behavior; due to a very low concentration of the immobilized GOx, the sensing scheme was reaction-limited from the initial time point and, therefore, with the loss of active enzyme over time an increase in the response range was observed. Although the purpose of incorporating CAT within the microparticles was to extend the longevity of sensors, minimal adsorption of GOx into the microparticles is the reason for this unintended result. If the amount of GOx immobilized in the second type of sensors was close to the first type, we would have expected a very stable response.

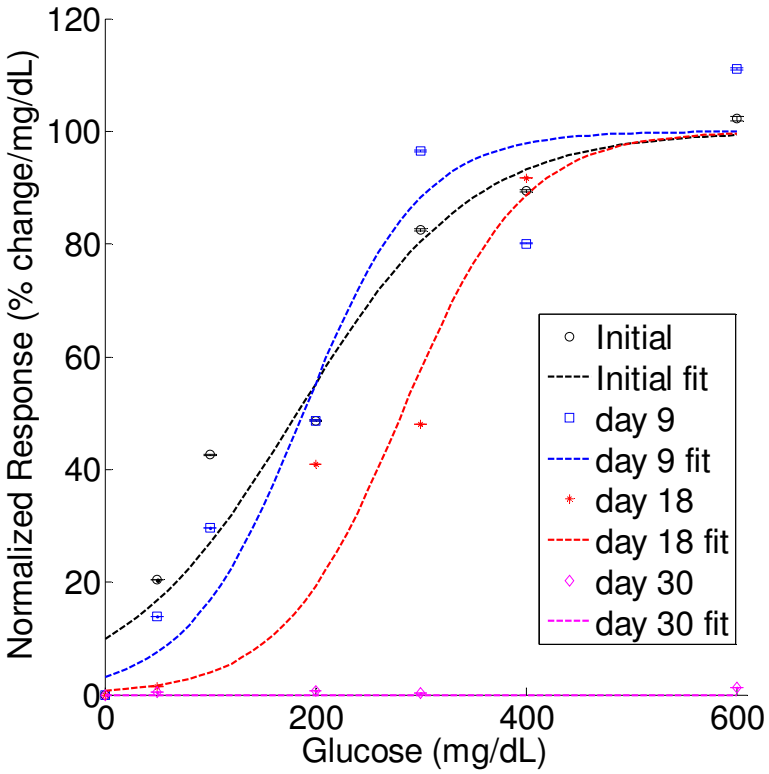

Figure 8.6 Thirty day response of sensors loaded with GOx (0.04 mM) and CAT (0.25). Error bars indicate the standard deviations obtained from twenty data points for a single step change in glucose concentration.

As before, the same experiment was repeated to obtain an estimate of gel-to-gel variability in the response. The response range values for the second type of sensors obtained from two gels are tabulated in Table 8.2. Using t-test, the initial and 18th day response of sensors were found to be significantly different (P-value = 0.02). Also, the 9th and 18th day response were found to be significantly different (P-value = 0.01). However, the initial and 9th day responses were not significantly different. Unlike GOx-only sensors, a substantial drift in the response was observed for these sensors after nine days of operation (Figure 8.7).

Table 8.2 Response range of second type of Supelco®-based sensors obtained from two gels

Time	Range (gel-1) mg/dL	Range (gel-2) mg/dL	Mean Range mg/dL	Standard Deviation
Initial	364	292	328	51
Day 9	376	398	387	15
Day 18	564	594	579	21
Day 30	No response	No response		

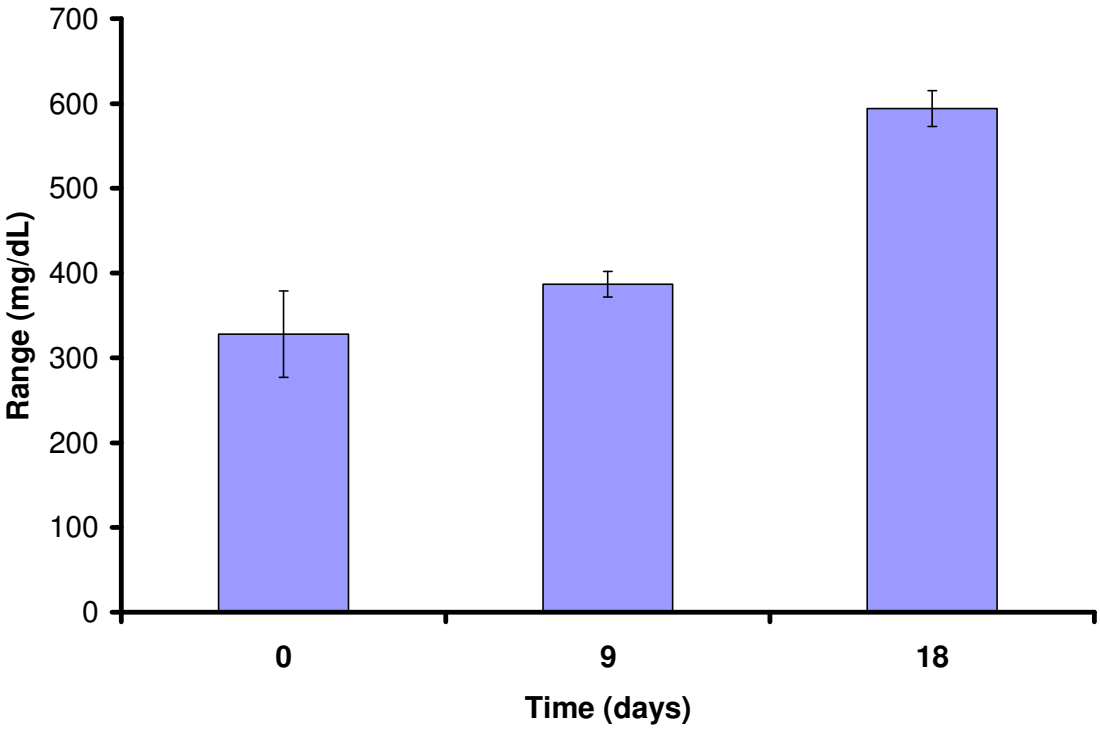

Figure 8.7 Average response range of second type of sensors. Error bars indicate the standard deviations obtained from two replicates.

8.4 Conclusion

In this work, highly porous amine-functionalized microparticles were used to prepare sensors. Due to the high porosity of the particles, very high enzyme loading was observed; approximately six times more enzyme was loaded than what was achieved for the low-porosity algilica microparticles. Even after continuous operation for one month, the sensors incorporating GOx (without CAT) were found to exhibit a stable response, with no apparent drift in the range over that period. In contrast, the response range of sensors incorporating GOx and CAT was observed to increase drastically after 9 days of continuous operation due to low GOx loading. Moreover, sensors were found to be unresponsive after 30 days, which indicates a complete loss of active GOx. This early failure of sensors incorporating GOx and CAT was due to the poor loading of GOx within the microparticles, which we believe may be explained by the Vroman effect.

Sensors made from algilica microparticles (without CAT) exhibit two times increase in the response range after 7 days of continuous operation (Figure 7.6). In contrast, the sensors constructed using microparticles maintained a very robust response even after 30 days of continuous operation; no significant change in the response range was observed (Figure 8.4). From these results, it can be concluded that the work presented in this dissertation is a significant step towards the realization of highly stable sensors.

It has been shown that after the deployment of microparticles into the quadriceps muscles of rats, less than 20 μm in diameter, the healing process is complete within seven days.[84] From this, it can be expected that the response of microparticle-based

sensors would stabilize within seven days of their deployment into the dermis. Therefore, the current sensor prototypes can be used to continuously track glucose levels for more than 23 days; this can be considered as a significant advancement in the field of enzymatic glucose sensors.

9 CONCLUSION AND FUTURE WORK

In the work presented in this dissertation, enzymatic microparticle-based sensors were considered for glucose monitoring. Such sensors are comprised of five essential components: (1) GOx, the enzyme used to drive a glucose-dependent depletion of oxygen; (2) an oxygen-sensitive indicator used to transduce glucose-dependent oxygen levels to luminescence intensity; (3) a reference dye to account for nonspecific light intensity modulations; (4) mesoporous microparticles used as a containers for the sensing chemistry (GOx, indicator, and reference); and (5) nanofilm coatings employed to tailor the mass transport of substrates. A sixth component, catalase, may also be used to extend the stability of sensors.

The goal of this research was to design and fabricate sensors that exhibit a linear response in the 0-600 mg/dL range, and exhibit a stable response for at least one month, when operated continuously. Towards the goal of extending the response range, the effect of NF thickness, deposition condition, capping layer, and most importantly, the role of microparticle porosity were investigated.

A key finding was that by simply adjusting film assembly conditions of the microparticles, device sensitivity could be fine-tuned to pinpoint hypo- (0-80 mg/dL), normo- (80-120 mg/dL), and hyperglycemic levels (>120 mg/dL). However, these studies also revealed that in order to achieve range up to 600 mg/dL, more than 60 bilayers of PAH/PSS (0.2 M NaCl) would be required; this will require an impractical number of polyelectrolyte deposition cycles. An alternative for reducing the number of polyelectrolyte deposition cycle will be to use PAA instead of PSS as a polyanion.

However, particles coated with PAA often exhibit aggregation, because PAA is a weak polyelectrolyte.

Use of microparticles with higher porosity was proposed as a more effective way of increasing the response range of sensors. Sensors fabricated using high-porosity (0.6) microparticles with 25 bilayers of PAH/PSS (0.2 M NaCl) were shown to exhibit a linear response up to 600 mg/dL. From modeling, it was predicted that with an increase in the porosity of the microparticles, we would expect an increase in the response range and a consequential decrease in the sensitivity. Also, particles with increased size are expected to exhibit a significantly higher sensitivity and a slightly increased response range in comparison to smaller particles. In addition, it was predicted that sensors constructed from ~12 μm microspheres, loaded with 0.2 mM GOx, having an effective porosity somewhere in between 0.01 and 0.1 with 65 nm PAH/PSS coating (0.2 M NaCl) would respond over the entire physiological (0-600 mg/dL) glucose range with maximized sensitivity.

Towards the goal of increasing the longevity of sensors, algilica-based sensors were prepared with GOx and CAT coimmobilized within the microparticles. Sensors were continuously operated for seven days under *in vivo* substrate (100 mg/dL glucose and 140 μM oxygen) concentrations and physiological conditions (37 °C and pH 7.4), and change in response was measured. Sensors incorporating CAT were found to be five times more stable than sensors having no CAT. Unfortunately, very poor enzyme loading was attained (0.1 mM GOx and 0.1 mM CAT) due to the low porosity of algilica. In addition, with the combination of modeling and experimental results it was

estimated that only ~10% of the loaded enzyme was active. It was realized that increasing the concentration of both active GOx and CAT by ten times (to ~0.1 mM each) could result in a very stable response: only ~2% decrease in the response-curve fit parameter (*k*) value over a one month period. This would translate to less than 5% increase in the response range. Increase in the response range will result in an under estimation of glucose levels if the sensors are not recalibrated over time. Nevertheless, even without recalibrating the sensors, the error in the prediction would be ~5%, and the measurements would still fall within the region A in the Clarke's error grid.[31] Therefore, even after one month of continuous operation, readings obtained from such sensors will be "clinically-acceptable."

In order to make more stable sensors, highly-porous 20 μm microparticles were used. The concentration of immobilized GOx was approximately six times higher in these microparticles. Response r*ange was found to be very stable during the entire test period with no significant drift observed for 30 days of continuous operation.* These results are very promising for long-term in vivo glucose monitoring.

It is logical that the stability of such sensors can further be improved by incorporating CAT in to the microparticles. Unfortunately, the coimmobilization of GOx and CAT into the microparticles was not very successful. Even for the loading solution containing GOx in excess (30 mg/mL GOx and 5 mg/mL CAT), the concentration of the immobilized GOx was very low in comparison to CAT (0.04 mM GOx and 0.25 mM CAT). Not surprisingly, the sensors incorporating CAT were found to be less stable than

GOx-only sensors. To further improve the stability of such sensors, the effort must be to incorporate CAT in to the matrix without a substantial reduction in GOx loading.

By modeling and experiments, we have gained a better insight into the performance of these complex systems. Although response range and stability were separately investigated, we have learned that they are higly interrelated. Increasing the response range often involves reducing the flux of glucose, which decreases the rate of reaction for the same bulk glucose concentration; this results in decreased peroxide production inside the microparticles. This eventually will decrease the peroxide-mediated enzyme deactivation and result in more stable sensors. Thus, the increase in response range by reducing the NF permeability also results in more stable sensors. Also, we have learned that as long as the sensing scheme is diffusion-limited rather than reaction-limited, the effect of enzyme deactivation will not be reflected in the measure response of sensors. After reaching the reaction-limited regime, we expect to observe a continuous and fast change in the response. Therefore, to maximize the response stability of enzymatic sensors, the time at which the sensing scheme will shift from diffusion-limited to reaction-limited regime must be extended. This dissertation has shown that, this time can be extended by: (1) increasing the transport barrier to glucose diffusion, (2) maximizing the loading of GOx into the microparticles, and (3) incorporating CAT to protect GOx from peroxide-mediated deactivation.

The experimental validation of modeling predictions was performed in most aspects of this research. Throughout, strong agreement between the modeling predictions and experimental observations, at least in terms of general trends, was

noticed. As there are several figure of merits (FOMs) that have to be considered in the design of sensors, having a reliable mathematical model will be very helpful for future design optimizations.

It has been shown that after the deployment of microparticles into the quadriceps muscles of rats, less than 20 μm in diameter, the healing process is complete within seven days.[84] From this, it can be expected that the response of microparticle-based sensors would stabilize within seven days of their deployment into the dermis. Therefore, *the current sensor prototypes can be used to continuously track glucose levels for more than 23 days*; this can be considered as a significant advancement in the field of enzymatic glucose sensors.

In this dissertation, sensors demonstrating a stable response up to one month were constructed. Sensors were also tested after two months of continuous operation and were found to be unresponsive to glucose. Somewhere between 30 and 60 days, the sensing scheme shifted from diffusion-limited to a reaction-limited regime due to the deactivation of GOx. It is desirable to improve this further to make clinical use as implants more attractive. To increase the time of this shift, CAT must be incorporated within the microparticles, without substantially reducing the concentration of immobilized GOx. For this, other enzyme immobilization strategies must be investigated. One possibility is to perform the sequential immobilization of GOx and CAT, rather than the simultaneous immobilization. First, GOx can be immobilized using the same protocol that was described earlier, followed by which CAT immobilization can be performed. The other possibility is to perform simultaneous coimmbolization of

GOx and CAT, but rather have a very small amount of CAT in the loading solution so that it does not occupy all the attachment sites available within a microparticle.

A design for an ideal sensor is proposed that can be used to continuously monitor *in vivo* glucose without a significant drift in the response over a period of three months. The sensor will be constructed using amine-functionalized 12 μm particles with a porosity of 0.1 (*ca.* 20 times more porous than algilica). Microparticles will be doped with PtP using the method described in Sections 6 and 8. Following this, GOx and CAT will be loaded such that the concentration of the immobilized GOx and CAT are 1 mM and 0.1 mM, respectively. Subsequently, a $[PSS/PAH\text{-}RITC]_2$-$[PSS/PAH]_{23}$-PSS nanofilm will be deposited on the microparticles using LbL assembly technique, which will serve the purpose of a transport barrier. Lastly, a final layer of poly(L-lysine) grafted with PEG (PLL-*g*-PEG) will be deposited using LbL method. PEG is highly biocompatible and is widely known as a "stealth" polymer.[85] Therefore, microparticles with PEG on their surface are expected to undergo minimal protein adhesion, which may also minimize the consequential fibrotic encapsulation. In addition, a biocompatible surface will also minimize the inflammation that could occur due to a foreign body invasion.

It is noteworthy that, protein adhesion and fibrotic encapsulation will present an added barrier to the transport of substrates into the microparticles, which can significantly change the response of a sensor. Also, if there is a severe inflammation occurring after sensor implantation, we might not be able to observe any glucose

response because it will be consumed by the leukocytes surrounding a sensor before it ever reaches the sensor.

Figure 9.1 contains the response of the ideal sensor over a period of three months. No significant drift in the response is expected over the period of three months of continuous operation. Sigmoidal fit was performed as discussed in Section 4 to obtain the response range of such sensors.

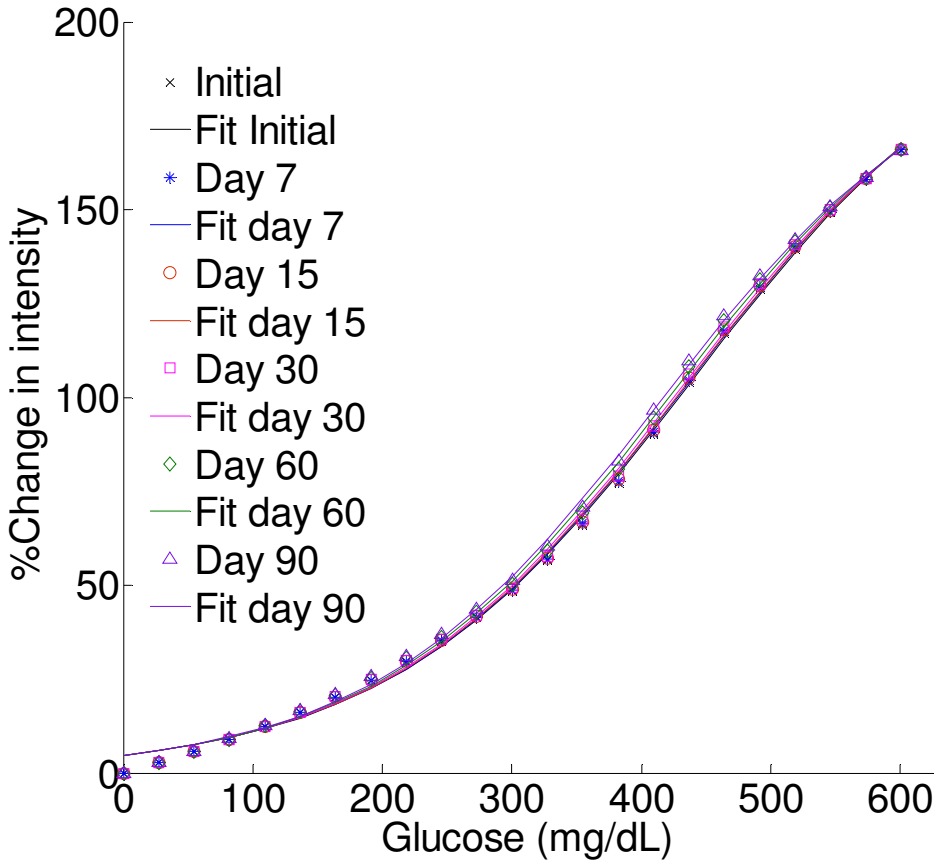

Figure 9.1 Theoretically predicted 3 month response of an ideal sensor.

Figure 9.2 contains the theoretically predicted response range of the ideal sensor under continuous operation for three months. A slight decrease in the response range is predicted over the entire period. It is contrary to what was observed in Section 7; an increase in the response range is expected over time. In this case, even after 3 months, the concentration of GOx is such that the sensing scheme is diffusion-limited. Therefore, the deactivation of GOx does not result in the extension of response range during this period. It must be recalled that CAT extends the response range as it produces oxygen in its catalytic reaction. This effect of CAT weakens over time due to its higher degradation rates than GOx, thereby resulting in the reduced response range.

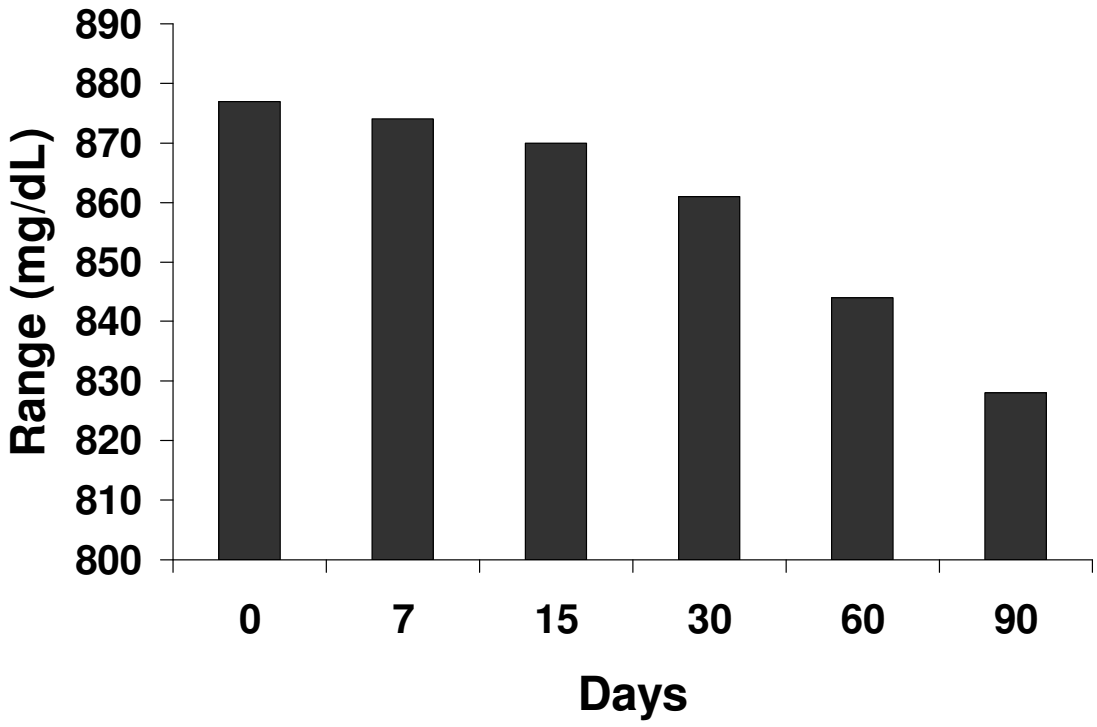

Figure 9.2 Theoretically predicted range of an ideal sensor over 3 month.

REFERENCES

(1) Anzai, J.-i.; Kobayashi, Y.; Suzuki, Y.; Takeshita, H.; Chen, Q.; Osa, T.; Hoshi, T.; Du, X. *Sensors and Actuators B*: *Chemical* **1998,** 52, 3-9.

(2) Basu, A. K.; Chattopadhyay, P.; Roychoudhuri, U.; Chakraborty, R. *Bioelectrochemistry* **2007,** 70, 375-379.

(3) Gough, D. A.; Lucisano, J. Y.; Tse, P. H. S. *Analytical Chemistry* **1985**, *57*, 2351-2357.

(4) http://www.cdc.gov/diabetes/pubs/estimates05.htm; CDC: 2009; Access date 09/21/2009.

(5) http://www.diabetes.org/diabetes-statistics/prevalence.jsp; American Diabetes Association: 2010; Access date 09/22/2009.

(6) Klonoff, D. C. *Diabetes Care* **2005**, *28*, 1231-1239.

(7) Pickup, J. C.; Hussain, F.; Evans, N. D.; Sachedina, N. *Biosensors and Bioelectronics* **2005**, *20*, 1897-1902.

(8) Pickup, J. C.; Hussain, F.; Evans, N. D.; Rolinski, O. J.; Birch, D. J. S. *Biosensors & Bioelectronics* **2005**, *20*, 2555-2565.

(9) Amerov, A. K.; Chen, J.; Small, G. W.; Arnold, M. A. *Analytical Chemistry* **2005**, *77*, 4587-4594.

(10) Stuart, D. A.; Yonzon, C. R.; Zhang, X.; Lyandres, O.; Shah, N. C.; Glucksberg, M. R.; Walsh, J. T.; Van Duyne, R. P. *Analytical Chemistry* **2005**, *77*, 4013-4019.

(11) Wan, Q.; Cote, G. L.; Dixon, J. B. *Journal of Biomedical Optics* **2005**, *10*, 024029-024038.

(12) Russell, R. J.; Pishko, M. V.; Gefrides, C. C.; McShane, M. J.; Cote, G. L. *Analytical Chemistry* **1999**, *71*, 3126-3132.

(13) Chinnayelka, S.; McShane, M. J. *Biomacromolecules* **2004**, *5*, 1657-1661.

(14) Chinnayelka, S.; McShane, M. J. *Diabetes Technology & Therapeutics* **2006**, *8*, 269-278.

(15) Brown, J. Q.; Chopra, S.; Grant, P. S.; McShane, M. J. *Proceedings of SPIE-The International Society for Optical Engineering* **2004**, *5325*, 21-30.

(16) Brown, J. Q.; McShane, M. J. *Biosensors & Bioelectronics* **2006**, *21*, 1760-9.

(17) Brown, J. Q.; Srivastava, R.; Zhu, H.; McShane, M., J. *Diabetes Technology & Therapeutics* **2006**, *8*, 288-95.

(18) Stein, E. W.; Grant, P. S.; Zhu, H.; McShane, M. J. *Analytical Chemistry* **2007**, *79*, 1339-1348.

(19) Stein, E. W.; Singh, S.; McShane, M. J. *Analytical Chemistry* **2008**, *80*, 1408-1417.

(20) McShane, M. J. *Topics in Fluorescence Spectroscopy*; Springer: New York, 2006; Vol. 11.

(21) Singh, S.; McShane, M. *Biosensors and Bioelectronics* **2010**, *25*, 1075-1081.

(22) Wolfbeis, O. S.; Narayanaswamy, R. *Optical Sensors*; Springer, 2004; Vol. 1.

(23) Papkovsky, D.; O'Riordan, T. *Journal of Fluorescence* **2005**, *15*, 569-584.

(24) Lakowicz, J. R. *Principles of Fluorescence Spectroscopy*; Plenum Press: New York.

(25) Mills, A.; Lepre, A. *Analytical Chemistry* **1997**, *69*, 4653-4659.

(26) Wolfbeis, O. S.; Weis, L. J.; Leiner, M. J. P.; Ziegler, W. E. *Analytical Chemistry* **2002**, *60*, 2028-2030.

(27) Brown, J. Q.; Srivastava, R.; McShane, M. J. *Biosensors and Bioelectronics* **2005**, *21*, 212-216.

(28) Wan, L. S. C.; Heng, P. W. S.; Chan, L. W. *Journal of Microencapsulation* **1992**, *9*, 309 - 316.

(29) Szmacinski, H.; Castellano, F. N.; Terpetschnig, E.; Dattelbaum, J. D.; Lakowicz, J. R.; Meyer, G. J. *Biochimica et Biophysica Acta (BBA) - Protein Structure and Molecular Enzymology* **1998**, *1383*, 151-159.

(30) Liu, X.; Bruening, M. L. *Chem. Mater.* **2004**, *16*, 351-357.

(31) Clarke, W. L.; Cox, D.; Gonder-Frederick, L. A.; Carter, W.; Pohl, S. L. *Diabetes Care* **1987**, *10*, 622-628.

(32) Naka, T.; Sakamoto, N. *Journal of Membrane Science* **1992**, *74*, 11.

(33) Kulcu, E.; Tamada, J. A.; Reach, G.; Potts, R. O.; Lesho, M. J. *Diabetes Care* **2003**, *26*, 2405-2409.

(34) Brunner, G. A.; Ellmerer, M.; Sendlhofer, G.; Wutte, A.; Trajanoski, Z.; Schaupp, L.; Quehenberger, F.; Wach, P.; Krejs, G. J.; Pieber, T. R. *Diabetes Care* **1998**, *21*, 585-590.

(35) Decher, G. *Science* **1997**, *277*, 1232-1237.

(36) Johnston, A. P. R.; Cortez, C.; Angelatos, A. S.; Caruso, F. *Current Opinion in Colloid & Interface Science* **2006**, *11*, 203-209.

(37) Campas, M.; O'Sullivan, C. *Analytical Letters* **2003**, *36*, 2551-2569.

(38) Dubas, S. T.; Schlenoff, J. B. *Macromolecules* **1999**, *32*, 8153-8160.

(39) Wang, C.; He, C.; Tong, Z.; Liu, X.; Ren, B.; Zeng, F. *International Journal of Pharmaceutics* **2006**, *308*, 160-167.

(40) Vaddiraju, S.; Burgess, D. J.; Jain, F. C.; Papadimitrakopoulos, F. *Biosensors and Bioelectronics* **2008**, *24*, 1557-1562.

(41) Fang, M.; Grant, P. S.; McShane, M. J.; Sukhorukov, G. B.; Golub, V. O.; Lvov, Y. M. *Langmuir* **2002**, *18*, 6338-6344.

(42) Klitzing, R. V.; Mohwald, H. *Macromolecules* **1996**, *29*, 6901-6906.

(43) Stroeve, P.; Vasquez, V.; Coelho, M. A. N.; Rabolt, J. F. *Thin Solid Films* **1996**, *284-285*, 708-712.

(44) Kotov, N. A.; Magonov, S.; Tropsha, E. *Chemistry of Materials* **1998**, *10*, 886-895.

(45) Levasalmi, J.-M.; McCarthy, T. J. *Macromolecules* **1997**, *30*, 1752-1757.

(46) Klitzing, R. V.; Möhwald, H. *Thin Solid Films* **1996**, *284-285*, 352-356.

(47) Wong, C.; Wong, K.; Chen, X. *Applied Microbiology and Biotechnology* **2008**, *78*, 927-938.

(48) Wilson, R.; Turner, A. P. F. *Biosensors and Bioelectronics* **1992**, *7*, 165-185.

(49) Gibson, Q. H.; Swoboda, B. E. P.; Massey, V. *The Journal of Bioligical Chemistry* **1964**, *239*, 3927-3934.

(50) Bright, H. J.; Gibson, Q. H. *The Journal of Bioligical Chemistry* **1967**, *242*, 994-1003.

(51) Lardinois, O. M.; Mestdagh, M. M.; Rouxhet, P. G. *Biochimica et Biophysica Acta (BBA) - Protein Structure and Molecular Enzymology* **1996**, *1295*, 222-238.

(52) Roger , A. S. *Advanced Synthesis & Catalysis* **2007**, *349*, 1289-1307.

(53) Tse, P. H. S.; Gough, D. A. *Biotechnology and Bioengineering* **1987**, *29*, 705-713.

(54) Kim, J.; Grate, J. W.; Wang, P. *Chemical Engineering Science* **2005**, *61*, 1017-1026.

(55) Zhou, H. X.; Dill, K. A. *Biochemistry* **2001**, *40*, 11289-11293.

(56) Vamvakaki, V.; Chaniotakis, N. A. *Biosensors and Bioelectronics* **2007**, *22*, 2650-2655.

(57) Kleppe, K. *Biochemistry* **1966**, *5*, 139-143.

(58) Pao, C. V. *Nonlinear Parabolic and Elliptic equations*; Springer, 1993.

(59) Polyanin, A. D. *Handbook of Linear Partial Differential Equations for Engineers and Scientists* CRC Press: Moscow, 2001.

(60) http://www.comsol.com/; COMSOL: 2010; Access date 10/20/2009.

(61) Stein, E. W. Dissertation, Louisiana Tech University, 2007.

(62) Stucker, M.; Struk, A.; Altmeyer, P.; Herde, M.; Baumgartl, H.; Lubbers, D. W. *J Physiol (Lond)* **2002**, *538*, 985-994.

(63) Liu, G.; Zhao, J.; Sun, Q.; Zhang, G. *J. Phys. Chem. B* **2008**, *112*, 3333-3338.

(64) Crank, J. *The Mathematics of Diffusion*; Oxford University Press: New York, 1980.

(65) Smith, P. K.; Krohn, R. I.; Hermanson, G. T.; Mallia, A. K.; Gartner, F. H.; Provenzano, M. D.; Fujimoto, E. K.; Goeke, N. M.; Olson, B. J.; Klenk, D. C. *Analytical Biochemistry* **1985**, *150*, 76-85.

(66) Wilke, C. R.; Chang, P. *AIChE Journal* **1955**, *1*, 264-270.

(67) Mu, D.; Liu, Z.-S.; Huang, C.; Djilali, N. *Microfluidics and Nanofluidics* **2008**, *4*, 257-260.

(68) Harold, L. W. *Journal of Applied Physics* **1963**, *34*, 2636-2639.

(69) Steitz, R.; Leiner, V.; Siebrecht, R.; von Klitzing, R. *Colloids and Surfaces a-Physicochemical and Engineering Aspects* **2000**, *163*, 63-70.

(70) Katiyar, A.; Yadav, S.; Smirniotis, P. G.; Pinto, N. G. *Journal of Chromatography A* **2006**, *1122*, 13-20.

(71) Decher, G. *Nature* **1997**, *277*, 1232-1237.

(72) Leypoldt, J. K.; Gough, D. A. *Analytical Chemistry* **1984**, *56*, 2896-2904.

(73) Baker, D. A.; Gough, D. A. *Analytical Chemistry* **1996**, *68*, 1292-1297.

(74) Sha, X.; Jablecki, M.; Gough, D. A. *Proceedings of SPIE-The International Society for Optical Engineering* **2001**, *4414*, 77-81.

(75) Gough, D. A.; Bremer, T. *Diabetes Technology and Therapeutics* **2000**, *2*, 377-380.

(76) Baker, D. A.; Gough, D. A. *Biosensors and Bioelectronics* **1993**, *8*, 433-441.

(77) Jablecki, M.; Gough, D. A. *Analytical Chemistry* **2000**, *72*, 1853-1859.

(78) Ozyilmaz, G.; Tukel, S. S. *Applied Biochemistry and Microbiology* **2007**, *43*, 29-35.

(79) Sha, X.; Jablecki, M.; Gough, D. A. *Proceedings of SPIE-The International Society for Optical Engineering* **2001**, *4414*, 77-81.

(80) Yin Win, K.; Feng, S.-S. *Biomaterials* **2005**, *26*, 2713-2722.

(81) Yum, S. I.; Roe, J. *Diabetes Technology & Therapeutics* **1999**, *1*, 29-37.

(82) Haubert, K.; Drier, T.; Beebe, D. In *Lab on a Chip*; RSC: 2006; Vol. 6, p 1548-1549.

(83) Vroman, L. *Nature* **1962**, *196*, 476-477.

(84) Fellah, B.; Josselin, N.; Chappard, D.; Weiss, P.; Layrolle, P. *Journal of Materials Science: Materials in Medicine* **2007**, *18*, 287-294.

(85) Hermansky, S. J.; Neptun, D. A.; Loughran, K. A.; Leung, H. W. *Food and Chemical Toxicology* **1995**, *33*, 139-149.

VITA

Name:	Saurabh Singh
Address:	c/o Mike McShane, 337 Zachry Engineering Center, College Station, TX – 77843-3120
Email Address:	saurabh1913@gmail.com
Education:	B.E., Chemical Engineering, Government Engineering College, Raipur, affiliated to Pt. Ravishankar Shukla University, Raipur, INDIA, 2002 The institution is currently know as "National Institute of Technology, Raipur," which is a deemed university. M.S., Chemical Engineering, Louisiana Tech University, Ruston, Louisiana, 2006